12-2012

Evaluation of Polymer Gel Dosimeters for Measurements of Dose and LET in Proton Beams

Kevin M. Vredevoogd

Evaluation of Polymer Gel Dosimeters for Measurements of Dose and LET in Proton Beams

by

Kevin Michael Vredevoogd, B.S.

APPROVED:

_____

Geoffrey Ibbott, Ph.D.
Supervisory Professor

_____

Kent Gifford, Ph.D.

_____

Kenneth Hess, Ph.D.

_____

Stephen Kry, Ph.D.

_____

Narayan Sahoo, Ph.D.

APPROVED:

_____

Dean, The University of Texas
Health Science Center at Houston
Graduate School of Biomedical Sciences at Houston

Evaluation of Polymer Gel Dosimeters for Measurements of Dose and LET in Proton Beams

A

THESIS

Presented to the Faculties of
The University of Texas
Health Science Center at Houston
and
The University of Texas
M. D. Anderson Cancer Center
Graduate School of Biomedical Sciences
in Partial Fulfillment

of the Requirements

for the Degree of

MASTER OF SCIENCE

by

Kevin Michael Vredevoogd, B.S.
Houston, Texas

December, 2012

Dedication

Dedicated to Mom and Dad

for, you know, raising me and stuff.

Acknowledgements

I would like to thank my advisor, Dr. Geoffrey Ibbott, for his guidance and support throughout the course of this project. I would like to thank the other members of my supervisory committee, Dr. Kent Gifford, Dr. Kenneth Hess, Dr. Stephen Kry, and Dr. Narayan Sahoo, for their time and advice. The staff at the Radiological Physics Center helped me time and time again in the year and half I spent with them and I thank everyone there for making my life easier. I would also like to thank Dr. Marek Maryanski and the staff at MGS Research, Inc., for answering the plethora of questions I had about OCT and gel dosimeters.

I would like to give special thanks to those who helped me to plan and execute the proton irradiations performed in this project. In particular, a big thanks to Dr. Michael Gillin for delivering proton treatments and to Paige Summers for allowing me to steal her water phantom on occasion and answering many proton therapy questions over the course of the project. Additionally, I want to thank the other members of the 3D dosimetry lab group for their advice and friendship. I will miss the lab meetings and scanner room cleanup sessions.

I want to thank my family for their help and support over the course of my studies. Their love and encouragement have helped me endlessly during this project and over my life in general. A final thanks to two groups: my former roommates (Chris MacLellan, Chris Walker, and Matt Pearce), whose company gave me a wonderful reason to get away from the office on occasion, and the RPC crew (Kevin Casey, Jennelle Bergene, Mitchell Carroll, and Jessie Huang), without whom I would likely have set fire to the scanner room and fled to Mexico months ago.

I cannot thank you all enough.

Evaluation of Polymer Gel Dosimeters for Measurements of Dose and LET in Proton Beams

Publication Number: _____

Kevin M. Vredevoogd, B.S.

Supervisory Processor: Geoffrey S. Ibbott, Ph.D.

This project assessed the effectiveness of polymer gel dosimeters as tools for measuring the dose deposited by and LET of a proton beam. A total of three BANG® dosimeter formulations were evaluated: BANG®-3-Pro-2 BANGkits™ for dose measurement and two BANG®-3 variants, the LET-Baseline and LET-Meter dosimeters, for LET measurement. All dosimeters were read out using an OCT scanner. The basic characteristics of the BANGkits™ were assessed in a series of photon and electron irradiations. The dose-response relationship was found to be sigmoidal with a threshold for response of approximately 15 cGy. The active region of the dosimeter, the volume in which dosimeter response is not inhibited by oxygen, was found to make up roughly one fourth of the total dosimeter volume. Delivering a dose across multiple fractions was found to yield a greater response than delivering the same dose in a single irradiation. The dosimeter was found to accurately measure a dose distribution produced by overlapping photon fields, yielding gamma pass rates of 95.4% and 93.1% from two planar gamma analyses.

Proton irradiations were performed for measurements of proton dose and LET. Initial irradiations performed through the side of a dosimeter led to OCT artifacts. Gamma pass rates of 85.7% and 89.9% were observed in two planar gamma analyses. In irradiations performed through the base of a dosimeter, gel response was found to increase with height in

the dosimeter, even in areas of constant dose. After a correction was applied, gamma pass rates of 94.6% and 99.3% were observed in two planar gamma analyses. Absolute dose measurements were substantially higher (33%-100%) than the delivered doses for proton irradiations. Issues encountered while calibrating the LET-Meter gel restricted analysis of the LET measurement data to the SOBP of a proton beam. LET-Meter overresponse was found to increase linearly with track-average LET across the LET range that could be investigated (1.5 keV/micron – 3.5 keV/micron).

Table of Contents

List of Figures

List of Tables

Chapter 1

Introduction and Background

1.1 Statement of the Problem

As the complexity and conformality of radiation therapy procedures have increased, the need for a three-dimensional dosimeter has arisen. Accurate dosimetry is integral for the administration of safe and effective treatments in modern radiation therapy. This is particularly true in proton therapy, where the high dose region and rapid dose falloff at the end of the range of a proton beam allow for extremely conformal treatments and low doses to surrounding normal tissue. The nature of a proton beam dose distribution gives it a substantial advantage over those produced by photons and electrons.

In addition to the benefits of the dose distribution shape, an increase in linear energy transfer (LET) near the end of the range of a proton beam leads to an increased relative biological effectiveness (RBE) in that region. This increase in RBE results in a biological dose (the product of RBE and physical dose) that is higher than the physical dose and that extends as much as a few millimeters beyond the physical dose. While the clinical significance of this difference is still under investigation, a 2012 study found correlations between areas of high biological dose and radiation induced necrosis for a postoperative IMPT patient being treated for malignant meningioma [1]. An accurate biological dose model could potentially be used to predict these kinds of toxicity risks and may be necessary in order to avoid overdosing normal tissue or critical structures located directly next to targets.

While proton therapy shows great potential, some challenges still exist. With treatments conforming to three dimensional target volumes, a dosimeter capable of taking measurements in three dimensions is required to completely characterize the delivered dose distribution. Additionally, if it is determined that an accurate model of biological dose is necessary for the safe and effective treatment of patients, dosimeters capable of measuring the LET of a proton beam could be useful tools for creating this model. The aim of this study is to assess the ability of polymer gel dosimeters to measure the dose deposited by and LET of a proton beam.

1.2 Proton Therapy

The primary advantage proton therapy holds over the more commonly used photon and electron treatment modalities lies in the dose deposition characteristics of a proton. As was touched upon in section 1.1, the majority of the dose deposited by a proton beam is deposited near the end of the range of the beam in a region called the Bragg peak. Compared to the dose distributions obtained from photon and electron beams, substantial dose sparing can be achieved both at shallow depths, where photons and electrons deposit a substantial amount of their energy, and distal to the target, beyond the range of the beam. While electrons also possess a finite range, their low mass allows for substantial amounts of lateral scatter, preventing the electron beam dose distribution from exhibiting the Bragg peak seen in proton beams. A comparison of the depth dose curves produced by photons, electrons, and protons is shown in Figure 1.1.

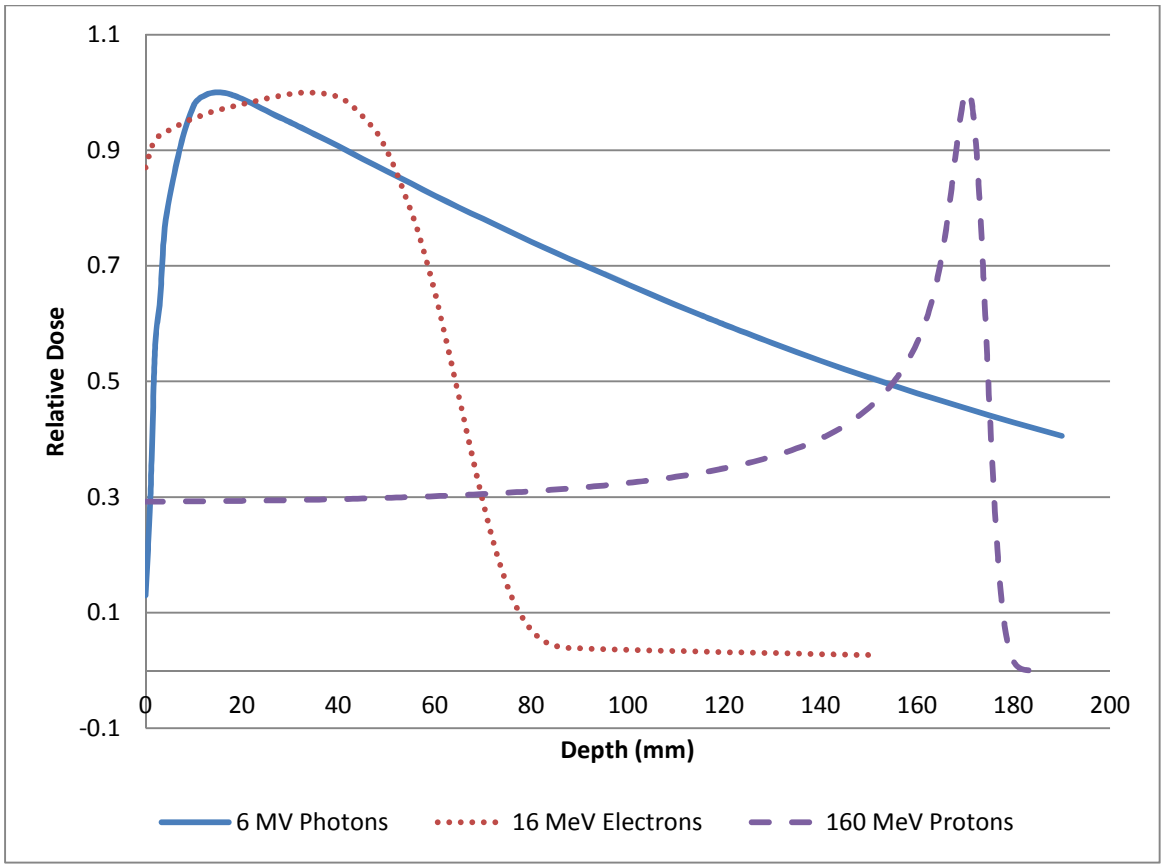

Figure 1.1: Depth dose distributions for 6 MV photons, 16 MeV electrons, and 160 MeV protons.

1.2.1 History

Therapeutic uses for protons were first suggested in 1946 by Robert Wilson. Before this time, electrons were the only particles capable of being accelerated to therapeutically relevant energies. Wilson noted that modern accelerator technology had progressed to a point where protons with medically relevant ranges (12-27 cm, corresponding to 125-200 MeV) could be produced. The relatively massive protons would travel through tissue in a nearly straight line, exhibiting far less lateral spreading than electrons. Further, he noted absorbed dose would be many times less at the proton beam entrance than at the end of the proton range, where the particle comes to a rest (to say nothing of biological enhancement due to the high ionization density in this region). These dose deposition characteristics

would allow high doses to be delivered to minute targets while substantially lower doses were maintained in neighboring normal tissue. Wilson also noted the effects that range straggling would have on the final dose distribution and proposed what would ultimately become the range modulator wheel (RMW) [2].

The first proton therapy treatment of a human patient occurred at the University of California at Berkeley in 1954. In an early study, the pituitary glands of 26 patients with metastatic breast cancer were irradiated using a 340 MeV proton beam produced by a 184 inch cyclotron, administering doses ranging between 140 and 300 Gy. Clinical improvement was noted in several of the patients [3]. When the Berkeley lab switched their focus to helium ions in 1957, proton therapy did not reappear in the United States until 1961, when physicians from Massachusetts General Hospital (MGH) used the 160 MeV cyclotron at the Harvard Cyclotron Laboratory for the treatment of intracranial lesions [4]. MGH would go on to receive the first National Cancer Institute (NCI) grant for proton therapy in 1972 [5]. The first hospital-based proton therapy center, the James M. Slater Proton Therapy and Research Center at Loma Linda University Medical Center (LLUMC), opened in 1990. As of January 2011, over 15,000 patients have received proton treatments at LLUMC [6].

In recent decades, proton therapy has continued to spread both nationally and internationally. As of July 2012, there were 11 proton centers currently operating and another 7 centers in development in the United States. Worldwide, there were 35 operational proton therapy centers that had collectively treated tens of thousands of patients [6].

1.2.2 Physical Properties of Protons

1.2.2.1 Energy Loss and Range

Protons are charged particles, with a charge equal in magnitude but opposite to that of an electron (~1.6×10^{-19} C). As a result, a proton traveling through a medium interacts with its surroundings primarily through Coulombic interactions. Each interaction causes the proton to lose a small amount of its total energy. The average energy that a proton loses in traversing a unit path length through a medium is referred to as the stopping power of that medium. As the density of the medium affects the stopping power, mass stopping power, a quantity equal to the stopping power divided by density, is typically used to characterize the rate of energy loss of a proton [7].

The mass collision stopping power, the component of mass stopping power due to inelastic collisions with electrons, is the predominant component of the total stopping power for protons. According to Bethe theory, the mass collision stopping power for a heavy charged particle passing through a medium can be calculated using the following equation:

$$\frac{1}{\rho} S_{col} = \frac{4\pi r_e^2 m_0 c^2}{\beta^2} \frac{1}{u} \frac{Z}{A} z^2 L(\beta)$$

where ρ is the density of the medium, r_e is the classical radius of the electron, m_0c^2 is the rest energy of an electron, β is the velocity of the particle divided by the speed of light, u is the atomic mass unit, Z is the is the atomic number of the medium, A is the atomic mass of the medium, z is the charge of the particle, and L(β) is the stopping number. All terms preceding L(β) determine the gross shape of the function, while L(β) takes fine details into account. L(β) is, in turn, dependent on several factors, including:

1. The mean excitation energy of the medium, a measure of how tightly bound the electrons in the medium are to the atoms/molecules making up the medium.
2. The shell correction, which accounts for changes in electronic interactions as the speed of the particle decreases.
3. The density effect correction, which takes into account changes in stopping power caused by the particle polarizing the medium during transit [7].

The form of the Bethe equation provides some insight into the dose deposition characteristics of a proton beam. As mass collision stopping power is inversely proportional to the velocity and, hence, the energy of a proton, it will increase substantially at the end of the range of a proton beam. As a result, a proton beam deposits a large amount of energy at the end of its range, resulting in the pristine proton beam dose distribution shown in Figure 1.1. Additionally, mass collision stopping power increases with increasing Z/A, implying that a medium with a higher fractional composition of protons will have a higher stopping power, resulting in a shorter range for the proton beam (assuming all other factors are held constant).

While the rate at which a proton loses its energy fluctuates across its path due to the stochastic nature of Coulomb collisions, the rate of energy loss can be approximated as constant. Using this approximation, termed the continuous-slowing-down approximation (CSDA), it is possible to determine the range of a proton simply by integrating the reciprocal of total stopping power with respect to energy. This "CSDA range" yields a reasonable approximation of the true range of a proton [7].

1.2.2.2 LET and RBE

LET is a fundamental characteristic of particles traveling through matter that describes the ionization density produced along the path of the particle. LET was defined by the International Commission of Radiological Units (ICRU) in 1962 as:

$$LET = \frac{dE}{dl}$$

where dE is the average energy deposited locally by a particle as it travels an incremental distance, dl, through a medium. Typically, this quantity is calculated by averaging the energy deposited by a particle across equal lengths of its track – this is known as the track-average LET. The LET of a particle may also be evaluated by averaging the lengths across which the particle deposits a fixed amount of dose – this quantity is called the dose-average LET. These quantities are roughly equal for photons and electrons, but can differ substantially from one another for neutrons and near the end of the range of a proton [8]. Unless otherwise stated, the term LET in this thesis will refer to the track-average LET.

The LET of a proton beam varies substantially with depth. As stopping power is inversely proportional to β^2, the stopping power of a medium increases sharply as a proton slows to a halt near the end of its range. As a result, the amount of energy a proton deposits in a given length in this region is much higher than at shallower depths. This, in turn, causes an increase in LET in and around the Bragg peak. A comparison of the dose and LET distributions for a pristine proton beam is shown in Figure 1.2.

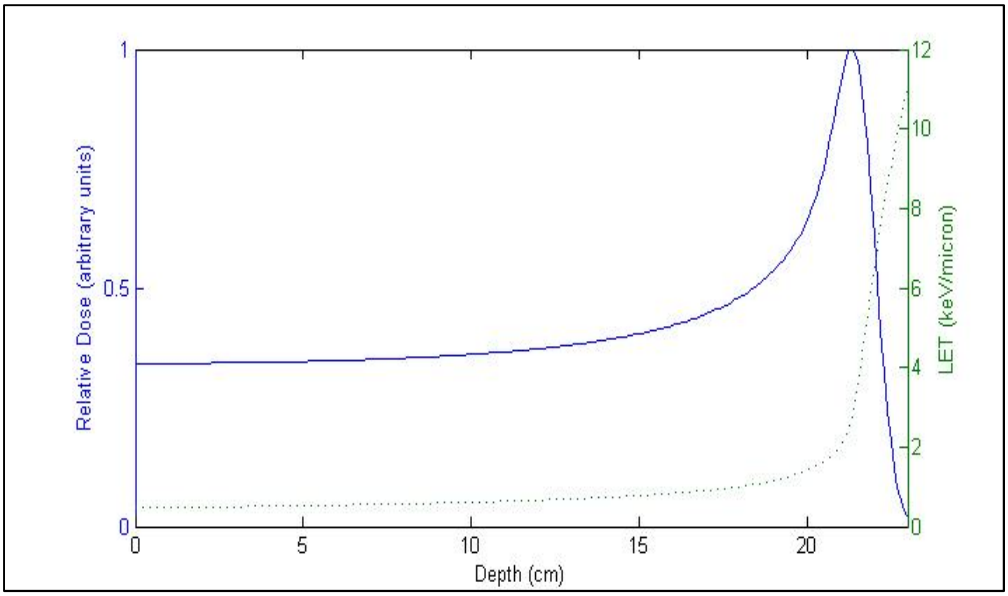

Figure 1.2: The dose and LET distributions for a pristine proton beam.

While LET is an important concept in itself, the RBE of a beam is of more direct relevance to clinical radiation therapy. RBE was defined in 1953 by the National Bureau of Standards as:

$$RBE = \frac{D_{250}}{D_r}$$

where D_{250} and D_r are, respectively, the dose of 250 kV x-rays and the dose of a test radiation required to reach the same biological endpoint [9]. RBE is dependent on several variables, including LET, dose rate, total dose, and the biological endpoint being examined [8].

Biological dose (D_{RBE}) is defined by the ICRU as the product of physical dose and RBE [10]. The ICRU recommends that D_{RBE} be used in selecting appropriate proton doses for treatment, comparing the effects of proton and photon therapy, and in predicting therapeutic outcomes based on photon data. Across years of research, studies have produced a range of proton RBE values to be used for the calculation of $D_{RBE.}$ Across all in vivo and in vitro studies, values have ranged from as low as 0.7 to as high as 2.1. The variation in these

values can be attributed to a variety of sources, including variations in beam energy, cell type, endpoint definition, and dose level across the studies performed. As a result, the ICRU recommends that that a constant, generic RBE of 1.1 (the average in vivo value of RBE these studies) be used for calculations of D_{RBE} [10, 11].

Assuming all other variables are held constant, changes in RBE are generally accepted to be due to changes in LET. Across the range of LETs relevant to proton therapy, RBE increases with increasing LET [11]. As a result, the RBE of a proton beam is highest in the distal falloff of the Bragg peak. This leads to a biological dose distribution that is shifted to a somewhat deeper depth than the physical dose distribution. This shift can be by as much as a few millimeters [12].

1.2.3 The Proton Therapy Treatment-Delivery System

There are two primary proton beam treatment delivery techniques: passive scattering and spot scanning. In a passive scattering beamline, a proton beam is incident upon a series of scatterers and beam degraders that shape a pristine beam into one that will appropriately cover a target volume. This beamline will be discussed in greater detail below. In a spot scanning beamline, pristine beams of varying energies are magnetically steered across a target to conformally irradiate a target volume. As all irradiations performed in this study were performed using passively scattered beams, spot scanning beamlines will not be addressed in detail. Thorough write-ups of these beamlines have been published by the ICRU and Smith et al. describing a general case and the MD Anderson Proton Therapy Center at Houston (PTC-H) system, respectively [10, 13].

The PTC-H passive scattering proton therapy treatment-delivery system is described in depth by Smith et al and is summarized below [13]. At the PTC-H, proton beam

production begins with a hydrogen ion source in a 7 MeV linac. Protons accelerated through the linac are injected into a synchrotron, which is capable of further accelerating the protons to treatment energies (70 to 250 MeV). The treatment beam is produced in discrete units called spills. After protons are accelerated to a desired energy, a process that takes approximately one second, they are "spilled" from the synchrotron [14]. For a passive scattering treatment, the spill length can vary between 0.5 and 5 seconds. After a spill, the beam is decelerated, taking about another second, and the process repeats.

Protons extracted from the synchrotron exit into a beam transport line. Here, aided by a series of bending and focusing magnets, the pristine beam is focused and steered into a treatment delivery nozzle. A schematic diagram of a passive scattering nozzle is shown in Figure 1.3 [15]. The proton beam enters through a titanium vacuum window and is incident upon a beam profile monitor. The profile monitor is capable of sending an interlock signal to stop treatment delivery if the beam profile, beam width, or the position of the beam center is too far off from baseline. The reference chamber and dose monitors are responsible for monitoring the number of monitor units (MUs) that have been delivered. The dose monitors, comprised of redundant primary and secondary monitors, also monitor the flatness and symmetry of the beam. Interlock signals are sent if any of these parameters vary drastically from specifications.

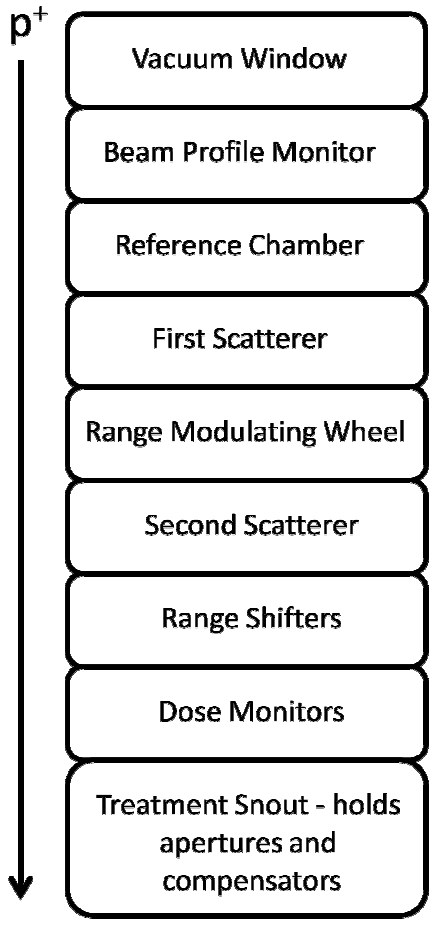

Figure 1.3: A schematic diagram of the passive scattering proton nozzle at the PTC-H. The arrow indicates the direction of travel for the proton beam.

The scatterers and RMW are largely responsible for transforming the pristine beam produced by the synchrotron into the beam desired for treatment. The scatterers spread the beam laterally and are capable of generating flat beams for any of three treatment snout sizes, corresponding to maximum field sizes of 25 × 25 cm^2, 18 × 18 cm^2, and 10 × 10 cm^2, respectively. Meanwhile, the RMW is responsible for varying the range of the beam over time, in effect producing a series of pristine beams that combine to form a spread out Bragg peak (SOBP). A sample SOBP is shown in Figure 1.4. To accomplish this feat, the thickness of the RMW varies about its circumference, producing a series of ascending and descending steps. As the RMW rotates, the amount of material the beam is required to pass

through varies, producing pristine beams with unique ranges. The weighting of each pristine beam depends on the angular extent of the step that produces it. An RMW from the PTC-H is shown in Figure 1.5.

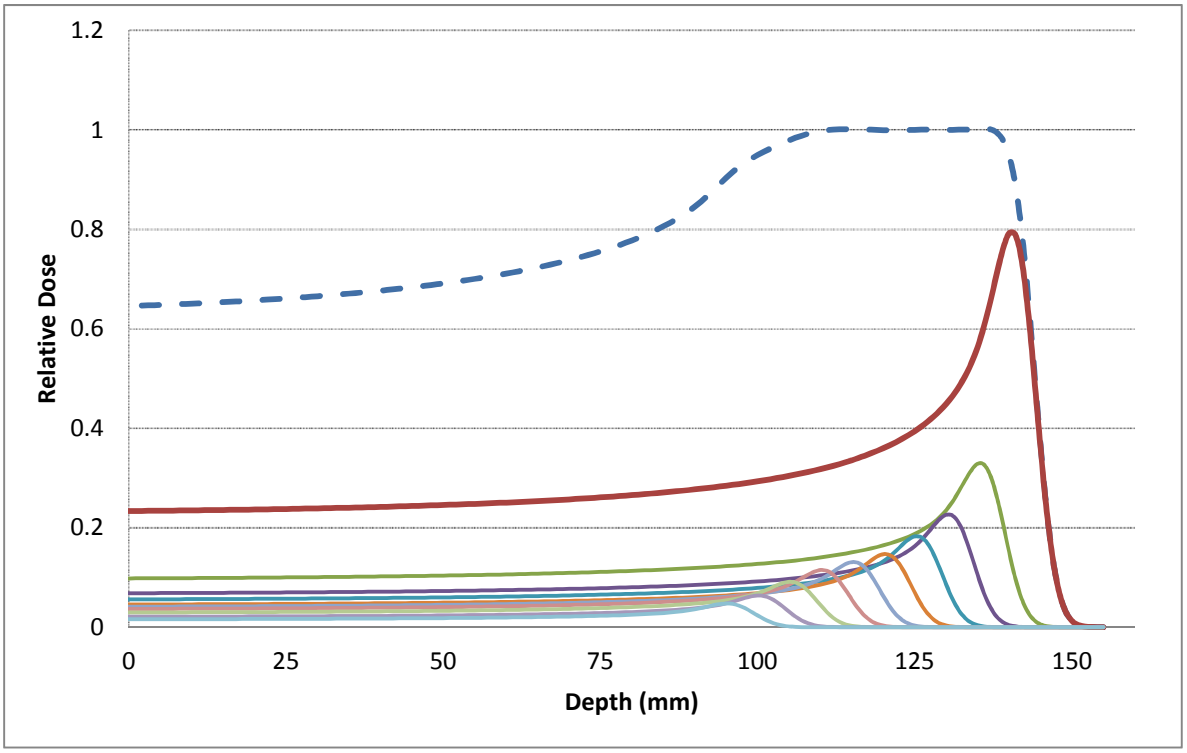

Figure 1.4: A spread-out Bragg peak (dashed line) made up of many pristine beams (solid lines).

Figure 1.5: An RMW used by the PTC-H.

Range shifters, located between the second scatter and the dose monitors, help to adjust the range of the proton beam. In combination, the available beam energies and range shifter thicknesses give the PTC-H passive scattering system a range adjustment resolution of 0.1 g/cm^2. Finally, before reaching the patient, the proton beam passes through the treatment snout. The treatment snout holds both treatment apertures and range compensators. The treatment apertures are made of brass and define the final cross-sectional size and shape of the treatment beam. The range compensator modifies the range of the beam at different points across its cross section so the final beam conforms to the shape of the distal surface of the target.

1.3 Polymer Gel Dosimetry

In a typical polymer gel dosimeter, irradiation induces a polymerization reaction between monomers suspended in a gel matrix, altering the physical characteristics (e.g.

optical density, paramagnetic relaxation time) of the irradiated volume. As the extent of the response in the dosimeter is a function of the dose deposited, it is possible to measure the altered state of the gel using a variety of imaging techniques (e.g. optical computed tomography, magnetic resonance imaging) and, after producing a dose-response curve, recreate a three-dimensional dose distribution.

1.3.1 History

While using polymerization reactions as a dosimetric tool was proposed as early as 1954, modern, three-dimensional polymer gel dosimetry did not come about until decades later [16]. In 1992, a dosimeter was produced that utilized the polymerization of N,N'-methylene-bis-acrylamide (bis) and acrylamide monomers held in an aqueous agarose matrix to measure radiation dose [17]. During production of these gels, oxygen was removed from the system by bubbling nitrous oxide gas through the mixture. The dosimeter was named BANANA after its constituent elements (**B**is, **A**crylamide, **N**itrous oxide, **AN**d **A**garose).

The production of this dosimeter was huge step forward for gel dosimetry. Prior attempts at using gel-based dosimeters had involved a combination of Fricke solutions and gelling agents. In a Fricke solution, irradiation causes the oxidation of ferrous ions into ferric ions. It was discovered in 1984 that these solutions could be imaged using magnetic resonance imaging (MRI), as the relaxation rates (spin-lattice and spin-spin) of the solution increased with increasing ferric ion concentration [18]. However, in attempting to collect spatially accurate dose distributions using this method, substantial ionic diffusion was noted, greatly damaging the spatial information produced during irradiation. A variety of gelling and chelating agents were used in an attempt to solve this problem with limited success [19].

Polymerization-based gel dosimeters exhibited no such problem: the polymers could not freely diffuse through a gelatin matrix as easily as ions could.

As the relaxation characteristics of the BANANA dosimeters changed upon irradiation and polymerization, they, like Fricke gels, could be read out using MRI. Later, a new gel formulation replaced the agarose gelling agent with gelatin, which substantially decreased the background spin-spin relaxation rate (R_2) and, as a result, improved the dynamic range of the system. In addition to the increased dynamic range, gelatin is more transparent than agarose, allowing for the polymerized volume to be clearly visible. The name BANG (**B**is, **A**crylamide, **N**itrogen, and **G**elatin) was given to these new dosimeters [20]. This formulation was patented and became commercially available through MGS Research, Inc., as BANG® [19]. With "BANG" trademarked, polyacrylamide gel (PAG) became the term used to describe generic BANG-type gels.

In 1996, Maryanski et al. further refined the BANG® formula and created BANG®-2. In this formulation, acrylamide was replaced with acrylic acid. This gel was used by Maryanski et al. to measure dose distributions from photons beams, electron beams, and an ^{192}Ir high dose rate (HDR) brachytherapy source. Good agreement was noted between the dose distributions obtained from treatment planning calculations and those measured by the gel dosimeter [21]. In 1999, a second refinement of the BANG® formula, BANG®-3, replaced bis and acrylic acid with methacrylic acid monomers. This change, coupled with the addition of proprietary response modifiers, allowed for a much greater dose sensitivity and wider dose range than previous formulations [22].

As mentioned above, oxygen was removed from these gels during the manufacturing process. The presence of oxygen was found to inhibit gel response [17]. In 2001, MAGIC

gel (**M**ethacrylic and **A**scorbic acid in **G**elatin **I**nitiated by **C**opper), a gel dosimeter that could be mixed in a fully oxygenated environment, was developed. In this dosimeter, ascorbic acid and copper sulfate acted as an oxygen scavenger, binding to atmospheric oxygen and preventing response inhibition [23]. MGS Research, Inc., went on to release BANGkit™ gel dosimeters, a form of BANG® gels that utilized the same oxygen scavengers as MAGIC [24]. BANGkits™ will be discussed in more detail in Section 2.1.1. The term "normoxic" has been adopted for gels such as these that can be prepared in fully oxygenated environments.

1.3.2 Applications of Polymer Gel Dosimetry

Polymer gel dosimeters possess several characteristics that give them advantages over more conventional dosimetry systems. Polymer gels have the unique ability to conform to the shape of their container. This allows for their use in anthropomorphic phantoms that mimic human anatomy. Additionally, gel dosimeters are capable of rendering complex dose distributions in three dimensions. While other dosimeters are capable of taking measurements at a point (ion chambers, TLDs) or in a plane (film), only three-dimensional dosimeters are capable of giving a complete picture of the dose being delivered. Three-dimensional dosimeters like polymer gels are necessary to rigorously confirm the accuracy of three-dimensional treatment plans [25].

Polymer gel dosimeters have been used to measure the dose distributions produced in a range of treatment modalities, including intensity modulated radiation therapy (IMRT), HDR brachytherapy, and proton radiotherapy [21, 26, 27]. In early studies using gel dosimeters for measurements in proton beams, a quenching effect was noted in the high LET region at the end of the range of a proton beam, leading to substantial underresponse

compared to ion chamber measurements [27]. Recent studies investigating the response of gel dosimeters in proton beams have shown promising results with new BANG® formulations [28, 29]. One of the aims of this study was to replicate these results using commercially available BANGkits™, rather than gels mixed and shipped out by MGS Research, Inc.

1.3.3 Characteristics of BANG® Dosimeters

As with all dosimetry systems, it is important to understand the basic characteristics of BANG® gels. In 1996, BANG®-2 dosimeters were found to have physical densities, electron densities, and average atomic numbers within a few percent of those of muscle tissue [21]. The tissue equivalence of BANG® dosimeters was further investigated in 2004 in a study that determined the mass attenuation and mass energy absorption coefficients of all BANG® formulations (at that time, BANG®-1, 2, and 3). For energies over 60 keV, all BANG® formulations were found to have mass attenuation coefficients within 1% of the coefficient of water. At energies over 100 keV, all BANG® formulations were found to have mass energy absorption coefficients within 1% of the coefficient of water. Below these energies, the compositional differences between water and gel, coupled with the increased photoelectric cross section, yield larger differences [30].

Previous investigations into the energy and dose rate dependencies of BANG® dosimeters have shown results that vary between formulations. BANG®-2 dosimeters were found to have no dose rate dependence for 15 MeV electrons between 20 and 400 cGy/min, and no differences in dosimeter response were observed in irradiations using 6 MV photons, 15 MeV electrons, and a ^{192}Ir brachytherapy source [21]. For BANG®-3 dosimeters, it was found that dosimeter response to a fixed delivered dose decreased with increasing dose rate

in a series of photon irradiations. The magnitude of the response discrepancy increased with the total dose delivered [31].

The dosimeters used in this study, BANG®-3-Pro-2 BANGkits™, have an effective atomic number of 7.84, slightly higher than the effective atomic number of water, 7.22. The density of the gel is 1.08 g/cm^3 and the relative stopping power was found to be 1.085 across the range of proton energies relevant to this study [29].

1.3.4 Drawbacks of Polymer Gel Dosimeters

While the potential uses of these dosimeters are plentiful, there are also many challenges that arise when dealing with these dosimeters. Polymer gel dosimeters require special care during and after the manufacturing process. Oxygen has been found to have a deleterious effect on gel response. When present, oxygen acts as a free radical scavenger, inhibiting or completely preventing the initiation of polymerization reactions. As a result, gel response can be severely inhibited or completely eliminated when oxygen is present [20]. Historically, this issue has been dealt with either through the addition of oxygen scavengers into the gel matrix or by preparing gels in a nitrogenous environment. In either case, an ideal gel vessel would prevent the diffusion of oxygen into the dosimeter upon exposure to normal atmospheric conditions. Additionally, light sensitivity has been noted in many polymer gel formulations. Light in or near the violet end of the spectrum is energetic enough to initiate polymerization in these dosimeters. As a result, gel vessels must either be opaque or utilize a lightproof cover to protect the gels from photopolymerization when exposed to light [20].

In some cases, gel readout can also present an obstacle. The most commonly used readout modalities for gel dosimeters are MRI and optical computed tomography (OCT, which will be discussed in Section 1.4). MRI is fairly widely available, but as it is first and

foremost a clinical device, dosimeter readout could interfere with clinical use or necessitate use at inconvenient hours. Additionally, time on an MRI can be quite expensive. OCT has the advantage of being a modality dedicated to dosimeter readout, but the initial cost of an OCT scanner can be somewhat high, currently ranging from about $25,000 to $50,000. Research into the feasibility of x-ray CT and ultrasound as alternate readout modalities is ongoing [32].

1.4 Optical Computed Tomography

As noted in Section 1.3.1, the polymerization reaction that occurs in a polymer gel dosimeter upon irradiation leads to an increase in R_2 in the irradiated volume. As the magnitude of this increase is directly related to the dose deposited, for the earliest part of their existence gel dosimeters were primarily read using MRI. However, due to the cost and availability issues associated with MRI, the need for a cheaper, dedicated alternative arose. In 1994, a study performed by Maryanski et al. investigated the relationship between absorbed dose and optical density (OD), which had been qualitatively observed to increase with dose. Reading thin slices of a BANG®-1 dosimeter with a densitometer, it was discovered that dose and OD shared the same linear relationship as dose and R_2 [20]. The potential of this discovery was realized in 1996 when the first OCT scanner capable of imaging a gel dosimeter was produced [33]. The scanner probed dosimeters using a 632 nm diode laser and exploited the light-scattering properties of the polymers present in the gel after irradiation to produce planar OD maps [34].

While the earliest OCT scanners were based on the translate-rotate geometry of first generation x-ray CT scanners, the system used for this study was based, from the reference frame of the dosimeter, on the rotate-rotate geometry of third generation CT scanners. Figure

1.6 contains a diagram of a modern, laser-based OCT scanner and demonstrates the acquisition of a one-dimensional projection from a thin slice of the dosimeter. The acquisition of a data point from one such projection begins with a 785 nm (near infrared) beam from a diode laser impinging upon a mirror. This mirror is positioned at the focal point of a collimating Fresnel lens, so any laser light reflected off the mirror will emerge from the lens parallel to the optical axis of the lens. The laser passes through the lens and enters the sample tank, which contains matching fluid and the dosimeter. The matching fluid is composed of glycol and deionized water mixed in such proportions that its index of refraction is equal to that of the dosimeter. This helps to limit any refraction of the laser beam upon entering and exiting the dosimeter.

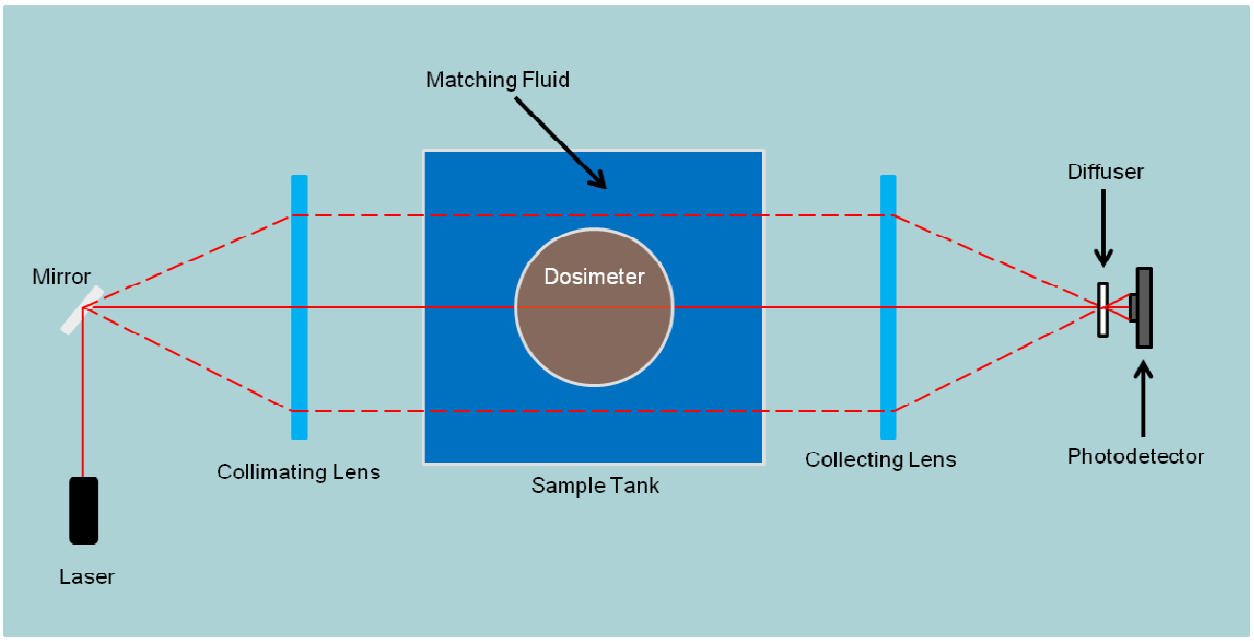

Figure 1.6: A diagram of a modern, laser-based OCT scanner, as viewed from above.

The intensity of the laser is attenuated as it passes through the sample tank. The degree of the attenuation depends on the optical attenuation coefficient, μ, at every point along the path of the laser. Exiting the sample tank, the laser passes through a second,

"collecting" Fresnel lens, which focuses it onto an optical diffuser. The intensity of the light incident upon the diffuser is measured by a photodetector, which outputs a voltage reading to an attached netbook. The intensity read out by the photodetector, I(x), is given by a modified form of Beer's Law in which μ is integrated over the path of the beam:

$$I(x) = I_0 * e^{-\int \mu(x,y)dy}$$

where I_0 is the initial intensity of the beam and x and y are perpendicular to and parallel to the optical axes of the lenses in Figure 1.6, respectively.

Full projection, slice, and volume acquisitions follow fairly simply from the operation described above. To obtain a projection, the mirror is swept across the field of view by a computer-controlled motor. To obtain a slice, a second motor rotates the dosimeter as a user-determined number of projections are recorded. These projections are later reconstructed into axial slices using a reconstruction program. Finally, for volume acquisitions, a third motor translates the laser, mirror, and collimating lens vertically to allow for coverage of the entire gel cylinder.

1.5 Hypothesis and Specific Aims

The hypothesis of this study is that through the use of LET-dependent and -independent polymer gel dosimeters, the LET of a proton beam may be determined and a three-dimensional dose distribution may be obtained with an agreement of 5%/3mm between the measured and expected doses.

The specific aims for testing the hypothesis include the following:

1. Assemble and perform acceptance tests on the optical CT scanner to be used for dosimeter readout.
2. Irradiate LET-independent gels using proton beams; assess dose data.
3. Irradiate LET-dependent gels using proton beams; compare against LET-independent results and analyze response differences.

Chapter 2

Materials and Methods

2.1 Polymer Gel Dosimeters

2.1.1 BANG®-3-Pro-2 BANGkits™

The BANG®-3-Pro-2 dosimeters were shipped from MGS Research, Inc. in the form of BANGkits™. A set of BANGkits™ is shown in Figure 2.1. As shown, BANGkits™ are comprised of four components. The first component, in the five containers on the left side of the image, is made up of methacrylic acid monomers suspended in a gelatin matrix. The characteristics of this gelatin mixture were described in Section 1.3.3. The second, in the vial marked "S," is an oxygen scavenger. The third, in the container marked "M," is a dose response modifier. Finally, in the container marked "C," is a catalyst. While the chemical identities of these last three components were not revealed by the manufacturer, earlier BANGkits™ used copper sulfate and ascorbic acid as additives for oxygen scavenging [24].

Figure 2.1: A set of BANG®-3-Pro-2 BANGkits™.

These gels possess a proprietary high viscosity gelatin matrix, which reduces the mobility of the polymer chains formed in the gel upon irradiation. This reduced mobility in turn lowers the probability of early chain termination in regions containing high free-radical concentrations. As high LET radiation produces these regions of high radical concentration, this gelatin matrix greatly reduces the quenching effects previously noted in regions of high LET. Additionally, a proprietary chain-transfer compound contained in the gelatin matrix lowers the mean molecular weight of the polymer particles produced during irradiation, further reducing the LET-dependence of the dosimeter [29].

BANGkits™ were mixed according to instructions provided by the manufacturer. As these instructions have not been published and some additional details could be beneficial for those trying to reproduce this study, the gel mixture procedure is included below. All work with open gel containers was conducted in the fume hood at the Radiological Physics Center (RPC) to minimize exposure to noxious fumes. A lab coat and gloves were worn throughout the mixing process. Additionally, all mixing sessions were completed in the dark, as several of the gel components, as well as the final product, are sensitive to incandescent light. A head-lamp with a red filter allowed for visibility without having deleterious effects on the gel components.

1. Gel containers were placed, tightly closed, in a 50-60 ºC water bath for 90 minutes. As standard sinks only produce water up to ~50 ºC, a large beaker of water was heated using a hotplate to replenish and increase the temperature of the bath. Water was removed and added as necessary.
2. For each liter of gel being made, 0.2 g of “S” were mixed with 10 mL of deionized water. This solution was stirred using a magnetic stirrer for at least five minutes.

3. For each liter of gel being made, 0.02 g of "M" were mixed with 10 mL of deionized water. This solution was stirred using a magnetic stirrer for at least five minutes.
4. For each liter of gel being made, 5 mL of "C" were measured out.
5. When the gels were fully melted, the containers were wiped dry and their contents were poured into an Erlenmeyer flask one at a time. All gels not actively being poured were allowed to stay in the water bath. The Erlenmeyer flask was placed on a combination hotplate and magnetic stirrer to keep the gel between 45 and 50 ºC and to stir the gel. The gel was stirred relatively slowly – no more than a shallow vortex (< 2 cm) was allowed to form.
6. The "S" solution, "M" solution, and "C" were added to the gel **in that order**. The gel was allowed to stir for at least two minutes after the addition of each additive. Between additions, a coffee filter was placed over the mouth of the flask to prevent dust from entering the system.
7. The gel was allowed to stir for an additional 45 minutes. The temperature of the gel was brought up to ~50 ºC at the end of this time. The gel should be fairly transparent with an amber tint at the end of this stirring period. An image of a nearly completed gel is shown in Figure 2.2.
8. The gel was slowly dispensed into an acrylic cylinder. When possible, the gel was poured on the inner walls of the dosimeter to minimize bubbles. The gel was then covered, but not closed air-tight, for 24 hours.
9. The lid on the acrylic cylinder was sealed. The gel was carefully transferred into a refrigerator and allowed to sit for 72 hours.

It was initially expected that these the gel additives would be shipped out premeasured – that is, that additives would be sent out separated into the quantities necessary for the mixture of a 0.5 L gel dosimeter. However, the additives were all sent in bulk, necessitating the purchase of additional equipment (glassware, primarily) in order to properly measure out the additives. This delayed the mixture of the first gel batch by several weeks.

Figure 2.2: A BANG®-3-Pro-2 BANGkit™ being stirred in a fume hood.

2.1.2 LET Gels

Two gel formulations were purchased from MGS Research, Inc., for the purpose of LET measurement. The first was a BANG®-3-Pro-2 variant that was manufactured to have no dependence on LET. This gel, hereafter referred to as the LET-Baseline gel, was intended to provide an LET-independent measurement of the dose from a proton beam. Initially, it

was thought that the standard BANG®-3-Pro-2 gel formulation would provide this baseline, but a recent study found that there these gels possess a slight overresponse due to LET dependence near the edge of the SOBP [35]. The second gel was also a BANG®-3-Pro-2 variant, but was manufactured to overrespond in areas of high LET. The difference between the responses of this gel, hereafter referred to as the LET-Meter gel, and the LET-Baseline gel was intended to increase as a function of LET. As such, with knowledge of how LET-Meter overresponse related to LET, the LET of a proton beam could be determined.

When conceived, one aim of this study was to do precisely what was stated above: to measure the LET of a proton beam using the LET gels. However, upon further discussion with the manufacturer, it was determined that these gels were still in an early phase of development and, as such, were not yet ready to provide a direct measurement of LET. As such, this goal had to be altered somewhat and, instead, it was decided that the relationship between LET-Meter overresponse and LET would be investigated. Quantifying this relationship will allow future researchers to utilize the gels for their intended purpose.

The physical differences between these gels and the BANG®-3-Pro-2 BANGkits™ are fairly minimal. The proprietary additives added to the LET gels are composed of light elements and were added in low concentrations. The effective atomic number, physical density, and stopping power ratio were unchanged from those reported for the BANG®-3-Pro-2 gels [35].

2.1.3 Storage and Handling

All gels used in this study were contained in acrylic cylinders approximately 14 cm in height and 15 cm in diameter. One of these cylinders is shown in Figure 2.3. The cylinders hold approximately 2.3 L of gel, requiring five BANGkits™ to fill completely. When gels

were not actively in use or planned for future use, they were held in a refrigerator to keep the baseline OD in the active region of the gel from increasing. Due to the light sensitivity of the gels, the acrylic cylinders were wrapped in black, optically opaque paper when not in use.

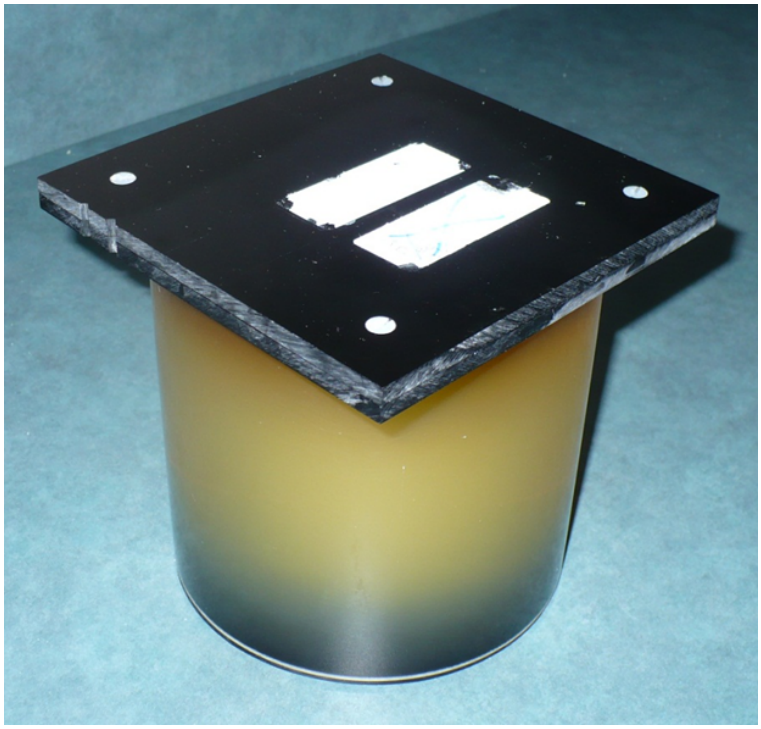

Figure 2.3: An acrylic cylinder holding a BANG®-3-Pro-2 polymer gel dosimeter.

All gel materials were shipped by the manufacturer overnight in an insulated container. Upon arrival, the materials were immediately transferred to a refrigerator to avoid unnecessary warming. BANGkits™ were left in the refrigerator until the day of mixture. Once the kits were mixed, these gels and the LET gels were treated identically. 24 hours prior to irradiation, gels were removed from the refrigerator and placed in an open container. A sheet of black cloth capable of blocking light but not so thick as to be thermally insulating was placed over the open container. The lid of the container was placed upside-down and at an angle relative to its intended orientation to help hold the cloth in place and block light without thermally isolating the system from the room.

2.2 OCT Scanning

Readout of all gel dosimeters was performed using the OCTOPUS™-IQ OCT scanner (MGS Research Inc., Madison, CT), hereafter referred to either as the scanner or the OCTOPUS for simplicity. The scanner was sent in pieces and assembled on arrival. An image of the completed scanner with the case opened is shown in Figure 2.4. The scanner was operated in the dark to prevent light from affecting the gels and to prevent stray light from being measured by the photodiode detector. No formal instruction manual was provided with the scanner, but a full description of the operational procedure has been included in the Section 5.1 and is summarized below.

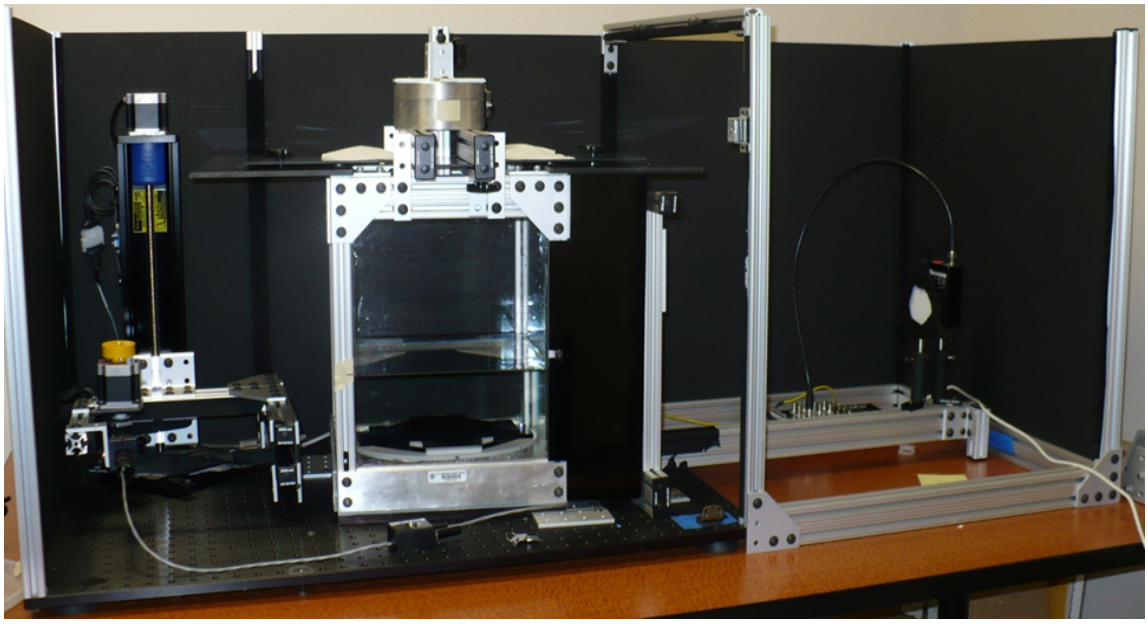

Figure 2.4: The OCTOPUS™-IQ OCT scanner.

2.2.1 Scanner Operation

The gel cylinder to be scanned was clamped into an attachment claw, which affixed to the square lid of the cylinder. The bottom of the cylinder was then secured into a rotational stage in the sample tank. A motor responsible for rotating the gel was connected to

the attachment claw from above the sample tank by a connecting rod. As the motor was built to fit snugly in one position above the sample tank, the connection between the motor and the claw, in combination with the rotational stage, ensured that the position of the gel was reproducible. As both pre- and post-irradiation scans were necessary for a proper reconstruction of the gel data, this reproducibility was integral.

Once a gel was in place, the scanner was operated using an attached netbook containing software created by MGS Research, Inc. First, single projections of the dosimeter were obtained to assess that the gel was well positioned inside the sample tank and to ensure that no major artifacts were present. Next, a full slice was acquired to ensure all motors were plugged in and working properly. Finally, assuming no problems were found earlier, full gel volumes were obtained.

2.2.2 Data Reconstruction

Data collected by the scanner were transferred from the netbook to a desktop computer for reconstruction. The reconstruction program, ReconIQ360, was developed by MGS Research, Inc. ReconIQ360 uses a filtered back projection algorithm to produce planar images from the projection data obtained by the scanner. To reconstruct a dosimeter, it was first necessary to view the sinogram from a slice of the dosimeter. Upon creation of the sinogram, the user is prompted to determine the necessary sinogram centering shift. This procedure is discussed in greater detail in Chapter 5.1. After determining this shift, a full gel reconstruction could be completed. As proper readout of OD data required that a prescan be subtracted from the postscan, the program includes a feature that performs this task. The reconstructed scans were output as raw data files and/or TIFF files. A sample reconstructed

gel slice is shown in Figure 2.5. The pixel values in these reconstructed images were optical density coefficients, or OD/cm.

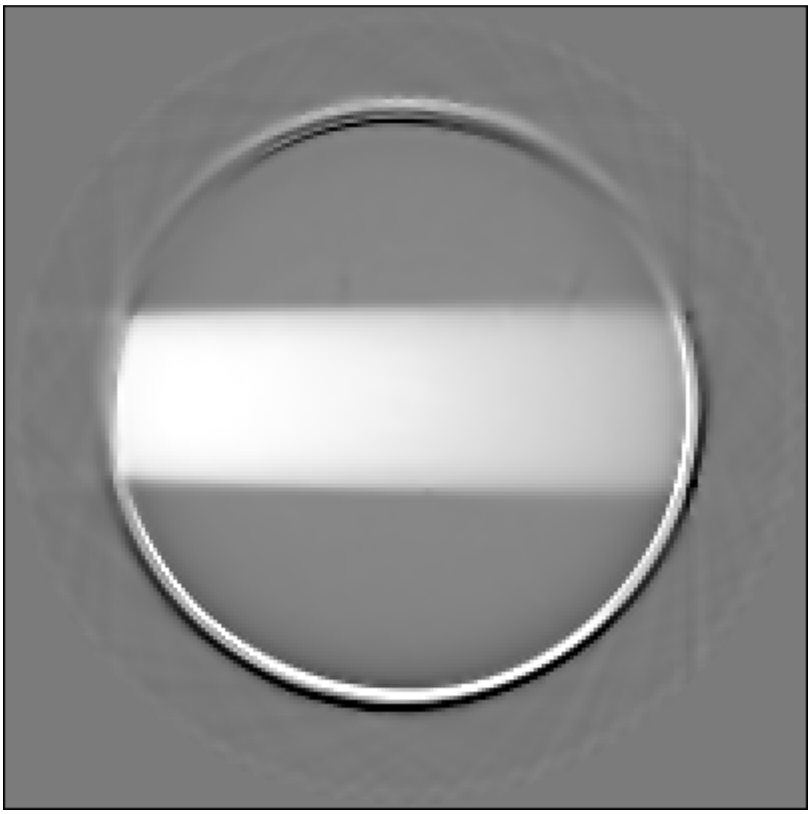

Figure 2.5: A sample reconstructed gel slice from a photon irradiation through the side of a dosimeter.

2.3 Gel Dosimetry Workflow

Once a gel dosimeter was complete and had been allowed to warm up, a prescan was performed using the OCTOPUS. This provided a baseline image of the gel prior to irradiation. The prescan was performed as close to the time of irradiation as possible, typically in the range of one to two hours before. In certain extreme cases (e.g. when more than two gels were being irradiated and all needed to be scanned) the prescan may have been performed as much as four hours prior to irradiation. After the prescan was complete, the gel was carefully transported to either the main campus of the MD Anderson Cancer Center or

the PTC-H for irradiation. After irradiation, the gel was allowed to sit for 24 hours while the radiation-induced polymerization reaction propagated. After this waiting period, the gel was again scanned using the OCTOPUS. The gel volume was then reconstructed using the software discussed in Section 2.2.2. During reconstruction, the prescan image was subtracted from the post-irradiation image. The specifics of the analysis performed on the reconstructed gel dosimeter images will be discussed in full in the relevant sections below.

2.4 Dosimeter Characterization

Prior to any attempts to measure dose or LET from a proton beam, it was desired that several basic features of the BANG®-3-Pro-2-OCTOPUS dosimetry system be characterized. For the purposes of this study, four key characteristics were chosen. These are listed below with brief explanations for their selection. A description of the irradiations performed to assess these characteristics will be discussed in the sections below.

1. Dose-Response Relationship: Understanding the relationship between absorbed dose and dosimeter response is integral for any dosimeter. It was desired that this relationship be studied across a range of clinically relevant doses and the linearity or nonlinearity of the relationship be assessed.
2. Active Region Boundaries: Due to the effects of oxygen inhibition, response near the walls, base, and top of the dosimeter show suppressed response to radiation compared to the center of the gel. As this central region was the only area where useful, reproducible data could be obtained, it was important that the boundaries of this region be characterized.
3. Fractionation Effects: Previous gel dosimetry studies have shown response variations when a dose was delivered with a single beam compared to the same dose delivered

in multiple fractions (e.g. delivering 4 Gy to d_{max} in one beam versus delivering 1 Gy to d_{max} four times) to the same batch of gels [22, 36]. The presence of such effects could yield substantial problems if gels were intended for taking measurements in any treatment plans utilizing multiple fields. As such, it was desired that the existence or nonexistence of these effects be assessed.

4. Overlapping Field Effects: This irradiation was chosen to assess the ability of the dosimeter to reproduce a dose distribution containing sharp gradients and plateaus - characteristics shared by the proton beam dose distribution. Additionally, this served as a secondary evaluation of the dose-response characteristics of a gel, as, assuming a linear dose-response relationship, the OD at the center of the overlapped fields should be approximately equal to the sum of the ODs from the individual fields.

To assess these characteristics, a series of gel dosimeters were irradiated using photons and electrons. These particles were chosen over protons for these irradiations due to the increased availability of the M.D. Anderson linear accelerators (linacs) compared against proton gantries at the PTC-H and the assurance from the manufacturer that the gels were equally effective for photons, electrons, and protons. All irradiations were performed on Varian linacs, with the specific unit used depending on the intended irradiation and machine availability. When electrons were required, a Varian Clinac 2100 was used. Otherwise, for irradiations requiring only low energy photons, a Varian Clinac 6EX was appropriate. Unless otherwise noted, photon irradiations were performed using 6 MV photons, and electron irradiations were performed using 16 MeV electrons.

All linac-based irradiations were performed with dosimeters placed in an Easy Cube phantom (Euromechanics, Schwarzenbruck, Germany). The Easy Cube is shown in Figure

2.6. This phantom is made of RW3, a plastic that is water equivalent for photons and electrons. An adapter made of RW3 was designed by Euromechanics so the gel cylinders would fit snugly inside the Easy Cube with minimal air gaps. When held within this adapter, the distance from the base of the Cube to the base of the dosimeter was 1.5 cm and the distance from the side of the Cube to the closest side of the dosimeter was 1.3 cm. The Easy Cube measured 18 × 18 × 18 cm^3. Unless otherwise noted, the Easy Cube was always positioned such that the source-surface distance (SSD) was 100 cm.

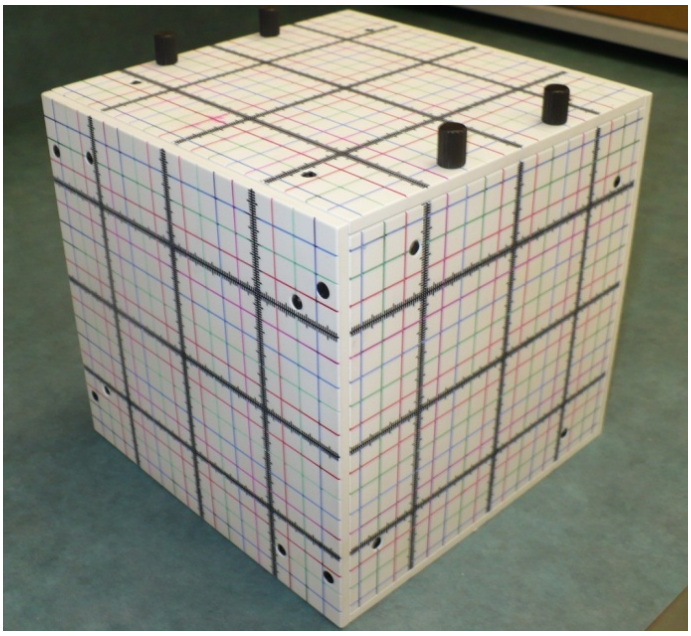

Figure 2.6: The Easy Cube phantom.

2.4.1 Monitor Unit Calculation

For all photon irradiations discussed below, the number of monitor units (MU) required to deliver a desired dose were calculated using the equation

$$MU = \frac{D}{k * PDD * FSF * OAF * BAF}$$

where D is the dose in cGy, k is the calibration in cGy/MU, PDD is the percent depth dose at the depth of interest, FSF is the field size factor, OAF is the off axis factor, and BAF is the beam attenuation factor. Irradiation conditions were selected such that OAF and BAF could be set to unity for all irradiations.

For all electron irradiations discussed below, the MUs required to deliver a desired dose were calculated using the equation

$$MU = \frac{D}{k * PDD * OF * GF}$$

where D is the dose in cGy, k is the calibration in cGy/MU, PDD is the percent depth dose at the depth of interest, GF is the gap factor and OF is the output factor. The output factor depends on the electron energy, the size of the cone, and the size of the insert. Irradiation conditions were selected so that the gap factor could be set to unity.

2.4.2 Active Region Boundaries

The determination of the boundaries of the active region required a set of simple irradiations. To assess the radial extent of the active region, a single dosimeter was used. The gel was irradiated using a 5 × 5 cm^2 photon beam directed perpendicular to the cylindrical axis of the dosimeter with 3 Gy delivered to d_{max}. To assess the vertical extent of the active region, two dosimeters were used. In the first irradiation, the Easy Cube was set on its side and irradiated using a 6 × 6 cm^2 photon beam aligned parallel to the cylindrical axis of the dosimeter, delivering 4 Gy to d_{max}. This irradiation was performed as quickly as possible to minimize the amount of time the dosimeter spent on its side, as a previous study noted instances of the gel separating from the container wall in this position [37]. Ultimately, as the response characteristics along the vertical axis of the dosimeter were found

to be of potential importance, a second irradiation was performed, this time using parallel-opposed 30 × 3 cm^2 beams that spanned the vertical extent of the dosimeter.

In total, only three gels were dedicated to the purpose of determining the boundaries of the active region of the dosimeter. However, additional data were obtained from other gels used for basic dosimeter characterization to obtain a better sense of inter-gel variability. In the end, data from a total six gels were used to characterize the boundaries of the active region (three for the radial extent, and three for the vertical extent).

2.4.3 Fractionation Effects

The general procedure used to test for fractionation effects was as follows: first, a region of the gel was irradiated to a predetermined dose in a single fraction using a 4 × 4 cm^2 photon beam. Next, the dosimeter was repositioned and the same dose was delivered to the dosimeter in four fractions. Approximately one minute was allowed to pass between each of the four fractions. The fractionated and single beam fields were positioned such that there was no direct overlap of the primary beams. Fractionation effects were assessed in two gel dosimeters. In the first, 6 Gy was delivered to d_{max}, first in a single fraction then in four fractions of 1.5 Gy. In the second, 3.5 Gy was delivered to d_{max}, first in a single fraction then in four fractions of 0.875 Gy.

2.4.4 Overlapping Fields

To test the ability of the dosimeter to render the dose distribution produced by overlapping fields, a single gel was irradiated with two photon beams. First, a dose of 1 Gy was delivered to a point along the cylindrical axis of the dosimeter using a 4 × 4 cm^2 field. The couch was then shifted down two centimeters and a dose of 2 Gy was delivered to a

point along the central axis of the dosimeter. Both beams were shot perpendicular to the cylindrical axis of the dosimeter.

2.4.5 Dose-Response Relationship and Gel Calibration

Electron irradiations were used to assess the dose-response relationship of the gel and, ultimately, for the calibration of the polymer gel dosimeters. All electron irradiations were performed using 16 MeV electron beams. A 6×6 cm^2 cone with a 6×6 cm^2 applicator was used for all irradiations. This energy and cone configuration was chosen because the resultant electron beam was penetrating enough to place most of its dose falloff in the active region of the dosimeter while maintaining a range shallow enough that additional irradiations could be performed elsewhere in the dosimeter without concerns of overlap – the depth of 80% dose and range are approximately 5.3 cm and 7.6 cm, respectively. The desired dose (i.e. the maximum dose for the calibration curve) was delivered to the depth of 80% dose distal to d_{max}. This ensured that the doses of interest were all present within the active region of the gel. An image of the Easy Cube phantom lined up for an electron irradiation is shown in Figure 2.7.

Three metrics were chosen as a basis on which to compare dose-response curves. The first was the OD of the gel in regions of zero absorbed dose, which is effectively a measurement of the change in baseline OD between the prescan and postscan. Second, the dose threshold, defined as the dose at which the measured OD is equal to the mean baseline OD plus two standard deviations of the mean baseline OD. Finally, to give a sense of the overall shape of the curve, a linear fit was applied to each curve and the slope of the fit was recorded.

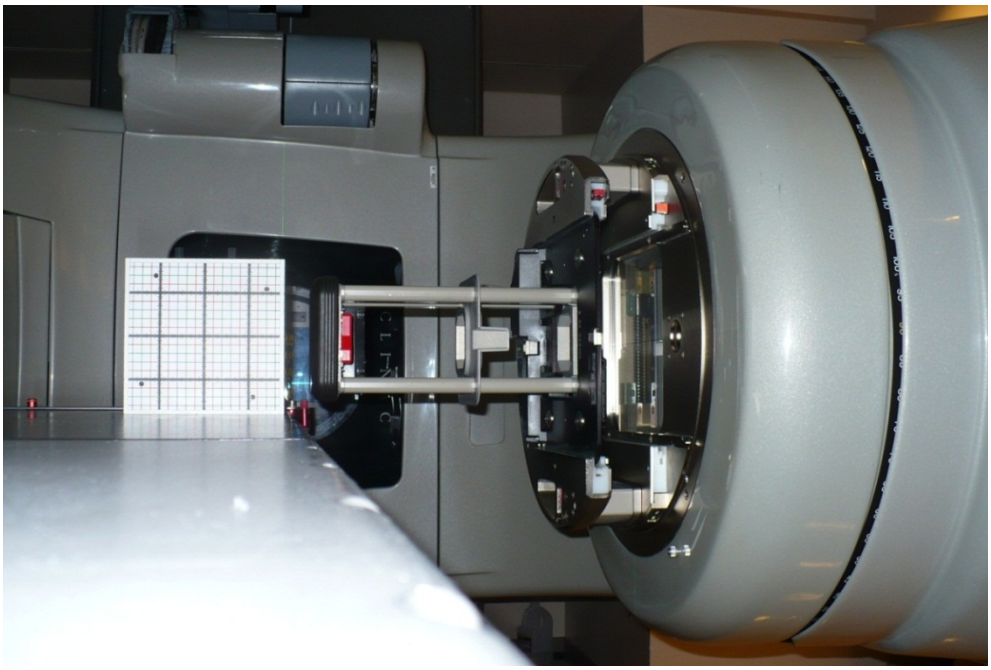

Figure 2.7: A gel in the Easy Cube phantom set up for an electron irradiation.

When a calibration curve was produced, it was assumed to be accurate only in that gel or gels produced in the same mixing sessions. As a maximum of 5 L of gel could be prepared in one session and the gel cylinders held ~2.3 L of gel, a calibration curve could, at most, be used in two gel dosimeters.

2.4.6 Data Analysis

For all irradiations discussed above, dose profiles were compared against dose data calculated using a commercial treatment planning system (Pinnacle, Philips Healthcare, Andover, MA). Treatment plans were generated based on a CT scan from a single, representative gel dosimeter. While the dosimetric characteristics may vary from batch to batch, the physical characteristics remain constant enough that a new CT scan was not required for each dosimeter. Dose distributions were exported from Pinnacle and opened in

ImageJ (Rasband, NIH), a public domain image processing program. From there, line profiles or dose planes could be extracted as needed.

To obtain dose information from the gel dosimeters, reconstructed gel volumes were exported to ImageJ. This software was then used to obtain OD profiles along the extent of the dosimeter. Similar profiles were obtained from corresponding Pinnacle plans. All data collected in ImageJ were then brought into Excel for analysis. Typically, dose distributions were compared by normalizing the OD data measured in a gel to the dose data calculated by Pinnacle at the center of the gel dosimeter. For most irradiations, the doses delivered along the central axis of the beam fell inside the linear region of the dose-response curve, justifying this type of comparison. When a comparison of absolute doses was desired, a calibration curve was produced by plotting the doses obtained from Pinnacle as a function of ODs measured in a gel for an electron irradiation. A fit was then produced and used to convert the ODs of interest to dose.

Additionally, for the measurement of overlapping fields, gamma analysis was performed using DoseLab (Mobius Medical Systems, Houston, TX). As no calibration curve had been produced for the overlapping fields dosimeter, a calibration curve produced from a different gel batch was applied. A 5% dose agreement, 3 mm distance-to-agreement (DTA) criteria was selected for this comparison. Two orthogonal planes were obtained from both the gel and Pinnacle data sets using ImageJ and were imported into DoseLab. The software was then allowed to scale the gel data such that the highest possible percent of pixels passed gamma analysis. All analyses of this sort were restricted to the active region of the dosimeter.

2.5 Proton Irradiations

2.5.1 Proton Facility

Proton irradiations were performed on a passive scattering port with a fixed gantry at the PTC-H. The facility contains four treatment rooms, three with rotating gantries and a fourth with two fixed, horizontal beamlines. One of the horizontal beamlines is used for large-field treatments while the second is intended for small-field, ocular treatments. Both fixed units and two of the rotating gantries are equipped to deliver passively scattered treatments. The final rotating gantry is capable of delivering spot scanned treatments. The major proton therapy equipment was provided by Hitachi, Ltd. (Tokyo, Japan)

For patient treatments, CT simulations are performed using an in-house CT scanner. Treatment plans are created using the Eclipse treatment planning system (Varian Medical Systems, Palo Alto, CA). As of February 2012, over 3000 patients have received treatment at the PTC-H. Patients have been treated for a broad range of conditions, including prostate, lung, and pediatric cancers.

2.5.2 Monitor Unit Calculation

For each irradiation, the MUs required to deliver a desired dose were calculated using the following equation

$$MU = \frac{D}{k * ROF * SOBPF * RSF * SOBPOCF * OCR * FSF * ISF * CPSF}$$

where D is the dose in cGy to the center of the Bragg peak, k is the calibration in cGy/MU, ROF is the relative output factor, SOBPF is the spread-out Bragg peak factor, RSF is the range shifter factor, SOBPOCF is the SOBP off center factor, OCR is the off-center ratio,

FSF is the field size factor, ISF is the inverse square factor, and CPSF is the compensator and patient scatter factor. Irradiation conditions were selected such that all correction factors besides the ROF, SOBPF, and FSF could be set to unity. This equation was developed for the PTC-H passively scattered proton beams by Sahoo et al. [15].

2.5.3 Polymer Gel Irradiations

All proton irradiations were performed on the PTC-H large-field fixed gantry. Irradiations were performed using a small snout in combination with three brass apertures that produced a 5×5 cm^2 field. All irradiations were performed using 200 MeV protons and utilized a 4 cm SOBP centered at an SAD of 270 cm.

Dosimeters were placed in a water tank with a 2 mm water-equivalent thickness window. All alignment involving the dosimeters intended for irradiation was performed in the dark aided by a red head lamp. Gross alignment of the tank and dosimeter was performed using a dummy dosimeter – an old gel that had been irradiated and read out previously. This allowed a rough alignment of both the tank and the gel to be performed under standard lighting conditions, substantially increasing the ease of setup. The large-field fixed gantry, water tank, and dummy dosimeter used in proton irradiations is shown in Figure 2.8.

Figure 2.8: The fixed gantry at the PTC-H. The water tank and a dummy dosimeter are present on the treatment couch.

2.5.3.1 Proton Dose Measurement

Initial irradiations were performed with the proton beam directed perpendicular to the cylindrical axis of the gel dosimeter, through the wall of the dosimeter. It was ultimately discovered that this geometry lead to artifacts upon reconstruction. As such, additional irradiations were performed with the beam directed through the base of the dosimeter, parallel to the cylindrical axis of the dosimeter.

For the PTC-H fixed gantry, the range for a 200 MeV proton beam was found to be 21.7 cm [15]. It was desired that the center of the 4 cm SOBP be placed at an SAD of 270 cm, the position at which the ISF mentioned in Section 2.5.2 may be set to unity. Further, the entire SOBP needed to be contained within the active region of the dosimeter. Accounting for the water equivalent thicknesses of the water tank window (~2 mm), the acrylic cylinder (~3.6 mm), and factoring in the relative stopping power of the gel, it was

determined that 138 mm of water and 80 mm of water were needed between the window and the gel cylinder for irradiations through the base and side of the dosimeter, respectively.

In total, four dosimeters were used for the purposes of proton dose measurement. Electron calibration curves were produced for the final three of these four – a calibration curve was not produced for the first irradiation as unexpected reconstruction problems were noted. Calibration curves were created using electrons either in a dosimeter mixed in the same batch as the gel used for the proton irradiation or in the dosimeter used for the proton irradiation itself. For all measurements of proton dose, a physical dose of 3 Gy was delivered to the center of the SOBP.

2.5.3.2 Proton LET Measurement

All irradiations for LET measurement were performed after reconstruction problems were noted for irradiations perpendicular to the cylindrical axis of the dosimeter. As such, all irradiations were performed through the base of the gel cylinder. Proton range was accounted for in the same way as discussed in Section 2.5.3.1. For each gel type, a dose prescription to the center of the SOBP was suggested by the manufacturer that would place the majority of the proton beam dose distribution well within the linear region of the dose-response curve. For the LET-Baseline gel, this dose was 3 Gy. For the LET-Meter gel, the recommended dose was 6 Gy.

2.5.4 Data Analysis

2.5.4.1 Proton Dose Measurement

Proton dose measurements were compared against ion chamber measurements produced by the same gantry. While the aperture used to make the ion chamber

measurements was somewhat larger than the aperture used in this study (5×5 cm^2 versus 10×10 cm^2), a previous study performed at the PTC-H found the difference in the depth dose distributions produced by these two field sizes was negligible (<2%) for 200 MeV proton beams [38]. As these ion chamber measurements were made in water, it was necessary to scale the measured depths from depths in gel to depths in water. This was done simply by multiplying the depth measured in gel by the stopping power ratio of the gel (1.085).

Additionally, gel measurements were compared against data produced by Eclipse. Dose distributions were exported from Eclipse to ImageJ. Using this software, dose planes were obtained from both the gel measurements and Eclipse plans. Dose planes were compared using DoseLab. Gamma analysis was performed using a 5% dose agreement, 3 mm DTA criteria. As before, DoseLab was allowed to scale the gel data such that the highest possible percent of pixels passed gamma analysis.

After viewing early results, it became apparent that a correction factor based on the vertical response characteristics of the gel might improve results for proton irradiations performed through the base of the dosimeter. A correction was calculated based on measurements taken while characterizing the vertical extent of the active region. This height-dependent correction factor was calculated by dividing the relative dose calculated in Pinnacle by the relative dose measured in a gel across the vertical extent of the dosimeter. A two-dimensional matrix containing this correction was created using MATLAB (The Math Works, Natick, MA) and saved as a TIFF image. Then, using the ImageJ image calculator, a pixel by pixel multiplication of the correction image and each slice of the gel volume was performed, resulting in a corrected gel image.

2.5.4.2 Proton LET Measurement

As mentioned in Section 2.1.2, this initial goal of this project was to use the LET gels to directly measure LET from a proton beam. Upon learning that the gels were not yet capable of this function, the project goal was revised to investigating the relationship between proton LET and overresponse in the LET-Meter gel relative to the LET-Baseline gel. The overresponse of the LET-Meter gel was quantified using the equation

$$\%OverResponse = \frac{LM - BL}{BL}$$

where LM is the response from the LET-Meter gel and BL is the response from the LET-Baseline gel along the central axis of the proton beam. Overresponse was calculated and plotted as a function of proton LET. As a reminder, the generic term LET is used to mean the track-average LET of the SOBP distribution, as the LETs of the individual pristine beams making up the SOBP vary along their respective ranges.

The LET of the proton beam was calculated using an analytical model developed by Wilkens et al. [39]. This model is capable of calculating the track-average LET along the central axis of a proton beam. The model calculates the LET due to primary protons only, ignoring the production of all secondary particles. A simple program was created using MATLAB in order to calculate the LET based on this analytical model. The output from this program for a 200 MeV proton beam with a 4 cm SOBP is shown in Figure 2.9.

Once calculated, LET-Meter overresponse was plotted as a function of LET. As in Section 2.5.4.1, it was necessary to scale the depths in gel to depths in water using the gel stopping power ratio of 1.085 as the analytical model output LET as a function of depth in water.

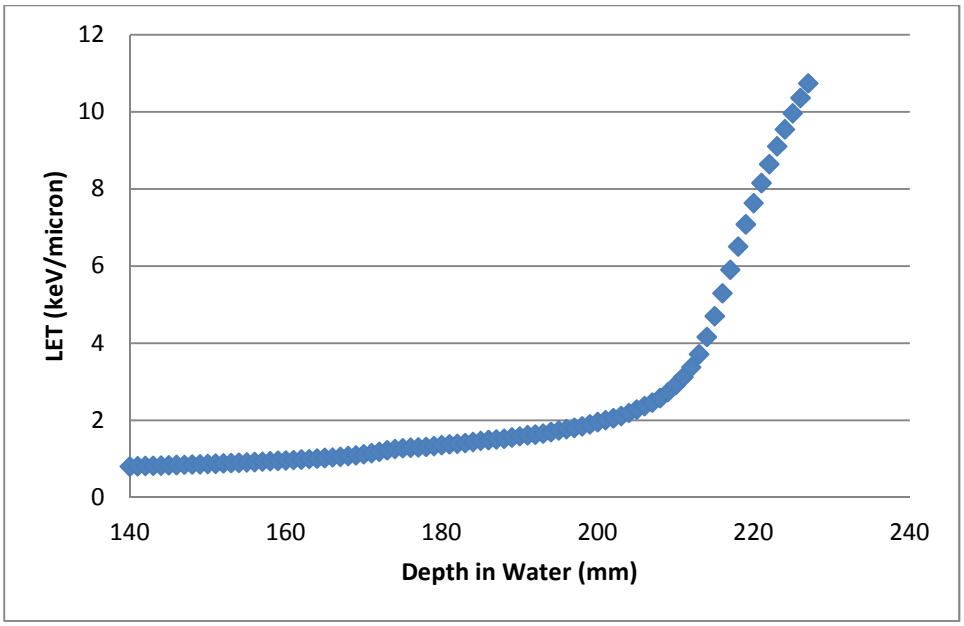

Figure 2.9: LET for a 4 cm SOBP across the range of depths relevant to this project.

Chapter 3

Results and Discussion

3.1 Dosimeter System Characterization

3.1.1 Dose-OD Relationship and Gel Calibration

The dose-response relationship of the BANG®-3-Pro-2 BANGkits™ was investigated in three gels using electron irradiations. For the OCT scanner used in this project, "response" refers to the optical density coefficient, read out in units of cm^{-1}. All dose-response curves produced from BANGkits™ are shown in Figure 3.1. For doses higher than approximately 30 cGy, these curves have the appearance of a stretched out sigmoid. Below this point, a sharp decline is noted, particularly in curves 2 and 3. This decline corresponds to the dose threshold, the dose below which no response over baseline is noted in the gel.

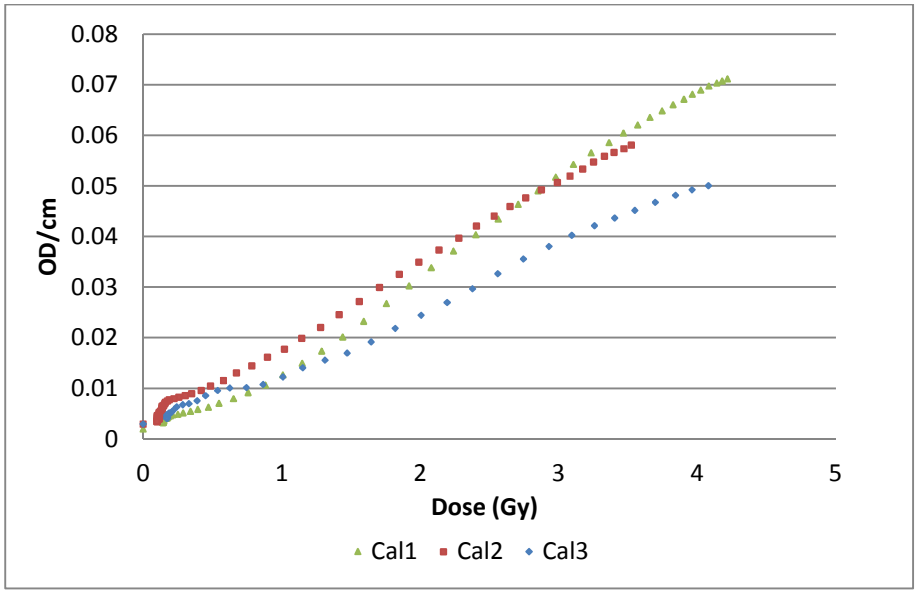

Figure 3.1: Dose-response curves for BANG®-3-Pro-2 BANGkits™.

As noted in Section 2.4.5, three characteristics were chosen for the purposes of comparing the dose-response curves. The values of these characteristics are summarized in Table 3.1.

Table 3.1: Key characteristics from BANG®-3-Pro-2 dose-response curves.

Gel	OD @ 0 Gy	Dose Threshold (cGy)	Slope of Linear Fit (OD/cm/Gy)
Cal1	0.002	15	0.0167
Cal2	0.004	13	0.0159
Cal3	0.003	18	0.0118
Average	0.003	15	0.0148

The data displayed in Figure 3.1 were also used to produce calibration curves for three of the four proton dose measurements performed as part of this study. To convert OD measurements to dose measurements, absorbed dose (as calculated by Pinnacle) was plotted as a function of OD. As the resultant curves showed substantial deviations from linearity in the low dose region, a fourth order polynomial was used to model the relationship. A sample calibration curve is shown in Figure 3.2. All other calibration curves produced in this study for both the BANGkits™ and LET gels are contained in Section 5.3.

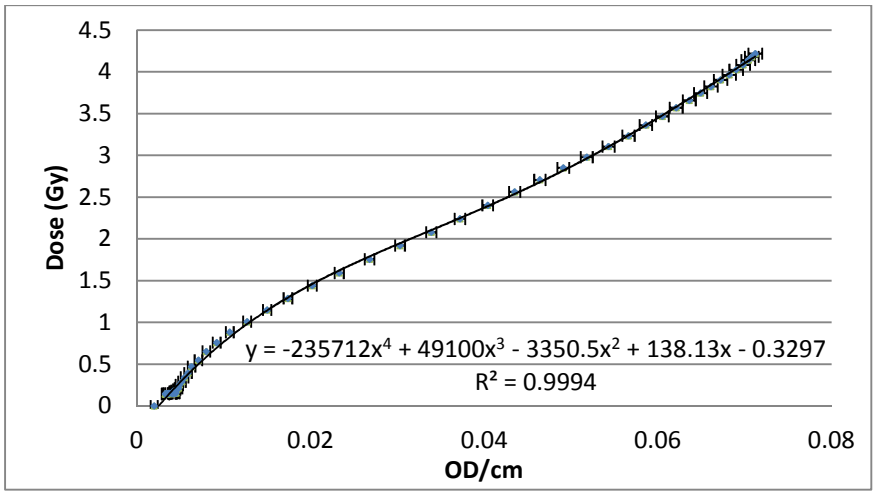

Figure 3.2: A sample calibration curve for a BANG®-3-Pro-2 BANGkit™.

Measurement uncertainty was assessed by measuring the standard deviation of OD measurements in 200 pixel ROIs. These data were collected using nearly all gels irradiated in this study to ensure the results could be consistently applied. The measured uncertainties are plotted as a function of mean ROI OD in Figure 3.3. Absolute uncertainty tended to increase as OD increased, and was thus modeled using a linear fit. The error bars in Figure 3.2 and in all other calibrations generated as part of this project came from this fit. Percent uncertainties were typically 3% or less, though this number increased substantially regions of low dose due to the extremely low ODs measured in these areas.

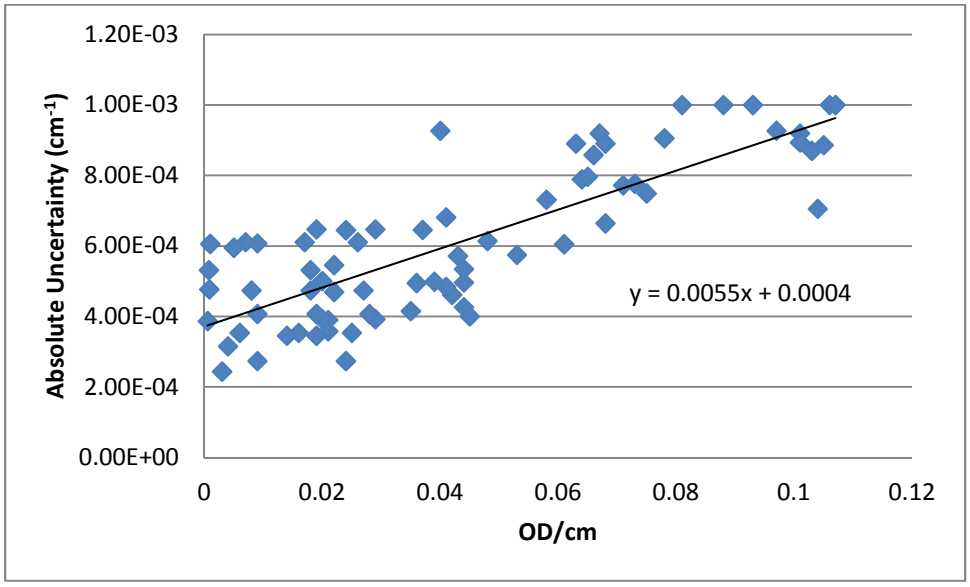

Figure 3.3: Measurement uncertainty for OD measurements.

3.1.1.1 Discussion

For a large portion of the project, calibration curves were fit in two parts as had been done in a previous BANG® study [29]. For doses below ~1.5 Gy, a quadratic fit was used, while for doses above that threshold, a linear curve was applied. Upon review of all dose-response data, it was determined that a single fourth-order polynomial would be more

convenient for the purposes of this study and for future gel dosimetrists. This fit requires only one curve and the dose level at which the quadratic fit gives way to the linear fit does not need to be determined every time. It is worth stressing that while the polynomial fit does not represent the physical phenomenon occurring in the gel, it serves as an adequate model from which optical density measurements can be converted into doses.

The non-zero baseline ODs observed after prescan subtraction were expected based on the post-irradiation handling process. After a gel was irradiated, it was allowed to sit out at room temperature for 24 hours to allow the polymerization reaction to propagate and the OD distribution to stabilize. As alluded to in Section 2.1.3, polymerization events occur spontaneously when gels are left out at room temperature, increasing the baseline OD of the gel. The absolute variation in this parameter across these gels is small and may be attributed to either inter-batch response variations or slight variations in the amount of time a gel was allowed to sit between irradiation and readout.

The dose threshold of the system was found to be 15 cGy on average. This value is slightly lower than that reported in a previous study using the same gel. Zeidan et al reported a dose threshold of approximately 35 cGy in a BANG®-3-Pro-2 dosimeter produced at MGS Research, Inc. [29]. However, the study does not make it clear how, exactly, this threshold was defined. Data in and below this dose level are absent from their published calibration curve. As such, these results do not necessarily conflict with one another.

The general shape of the dose-response curve agreed with what was observed by Zeidan et al [29]. Additionally, while the calibration scheme applied by Zeidan was somewhat different from that used in this study, the slope of the linear fit of his calibration curve falls within two standard deviations of the measurements from this study

(0.0189 cm^{-1}/Gy versus 0.0148±0.026 cm^{-1}/Gy). The discrepancies observed between the individual linear fits for the curves produced in this study were not surprising. It was communicated by MGS Research, Inc., that variations in the precise amounts of additives used, the temperature at which the kits were allowed to melt, the temperature at which additives were added, and a range of other factors all have an effect on the final response characteristics of the gel [40]. Additionally, a study by Oldham et al showed similar variations in calibration curve slopes produced in several studies by independent researchers using BANG® and BANG®-2 dosimeters [41].

3.1.2 Boundaries of Active Region

3.1.2.1 Radial Extent

The radial extent of the active region was investigated by comparing the dosimeter response to 6 MV photons against a relative dose distribution calculated in Pinnacle. The dosimeter response was normalized to the Pinnacle data at 75 mm into the gel volume – the center of the gel. A plot of these data is shown in Figure 3.4. In this figure, and in all other depth dose profiles produced by irradiations through the side of a dosimeter, the depth of zero is defined as the position of the gel pixel closest to the cylinder wall through which the beam enters. It was decided that the active region boundaries would be defined as the points of 5% agreement between the gel measurement and the Pinnacle distribution. For the dosimeter used specifically for this purpose, the distance from the wall of the beam entrance to the beginning of the active region was found to be 25 mm, and the distance from the end of the active region to the wall of the beam exit was 17 mm.

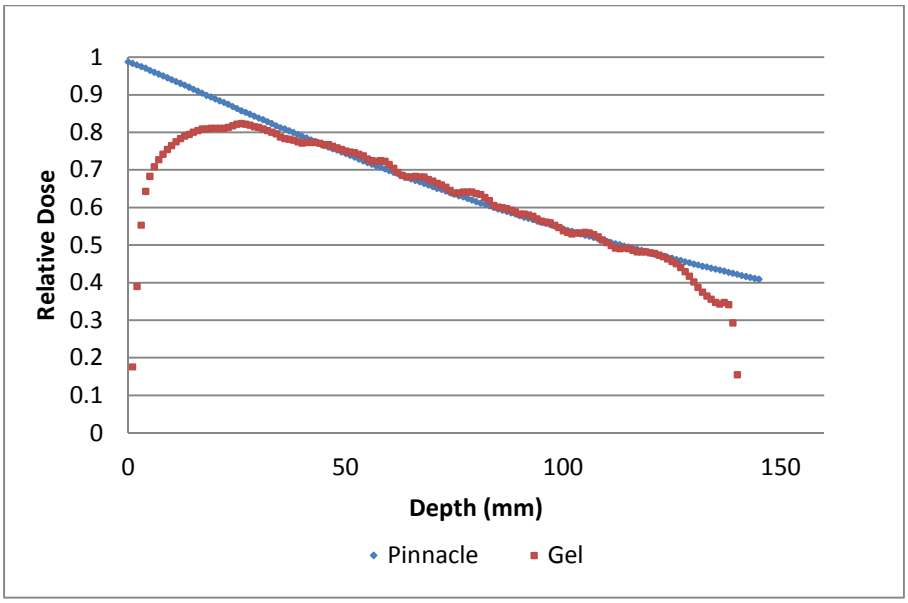

Figure 3.4: Gel and Pinnacle data used to assess the radial extent of the active region of a dosimeter.

As noted in Section 2.4.2, additional data were obtained from other gels intended for basic dosimeter characterization (fractionation effects and overlapping fields). The data from all three gels are shown in Table 3.2. The average width of the active region was found to be 99±4 mm.

Table 3.2: Data from three gels used to assess the radial extent of the active region of a dosimeter.

	Distance from cylinder edge to 5% agreement		
Gel Name	Entrance (mm)	Exit (mm)	Region Width (mm)
Gel1	25	17	104
Gel2	28	23	95
Gel3	17	30	99
Average	23	23	99

3.1.2.2 Vertical Extent

The vertical extent of the active region was investigated by comparing the dosimeter response to 6 MV photons against the relative dose calculated in Pinnacle. The gel response was normalized to the Pinnacle data at 60 mm into the gel volume – roughly the center of the most commonly used scan extent. A plot of the data obtained from one of the dosimeters used in these measurements is shown in Figure 3.5. In this figure, and in all other depth dose profiles produced from irradiations through the base of a dosimeter, the depth of zero corresponds to the plane 3 mm above the base of the dosimeter – the shallowest plane that could be reconstructed using the OCTOPUS. The beginning of the active region was defined the same way as in Section 3.1.2.1. In the first dosimeter used specifically for this purpose, the distance from the base of the dosimeter to the beginning of the active region was found to be 29 mm, and the distance from the end of the active region to the top of the dosimeter was 41 mm.

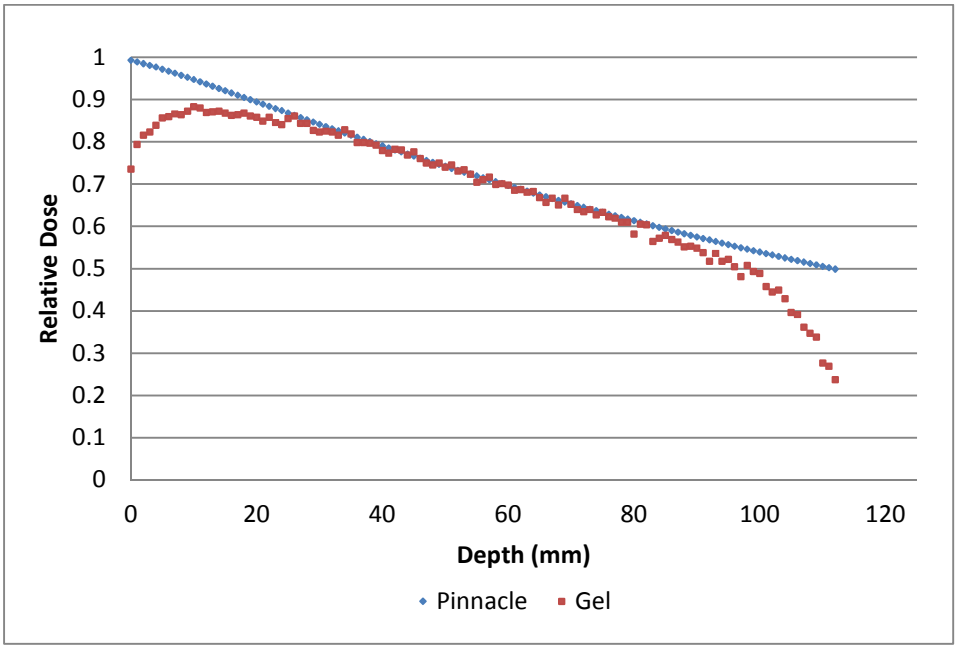

Figure 3.5: Gel and pinnacle data used to assess the vertical extent of the active region of a dosimeter.

As with the radial measurements, additional data were obtained from dosimeters used in other parts of this study. The data from all three gels are shown in table 3.3. The average height of the active region was found to be 73±2 mm.

Table 3.3: Data from three gels used to assess the vertical extent of the active region of a dosimeter.

	Distance from cylinder edge to 5% agreement		
Gel Name	Base (mm)	Top (mm)	Active Height (mm)
Gel1	29	41	71
Gel2	19	47	75
Gel3	21	48	72
Average	23	46	73

Later in this study, proton irradiations were performed through the base of several dosimeters. Response discrepancies noted in these irradiations made it appear that a correction factor based on the vertical response characteristics of the gel could be useful, especially if the correction was reproducible. The correction was calculated by dividing the response expected from Pinnacle by the response observed in the gel. A plot of the correction curves obtained from the three gels used for assessing the vertical extent of the active region is shown in Figure 3.6. This correction will be given further attention in Section 3.2.2.

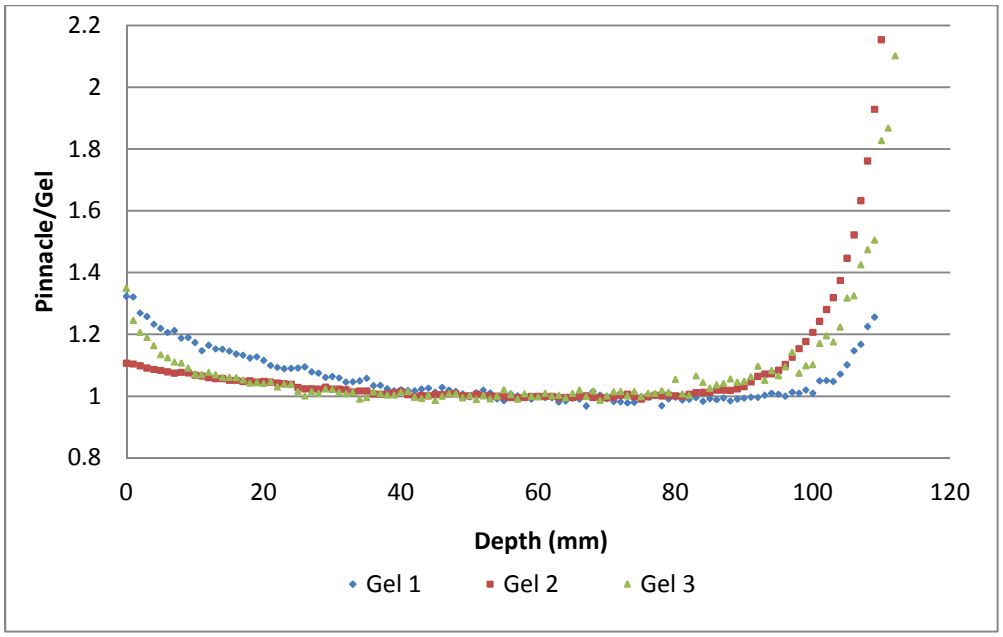

Figure 3.6: The ratio of Pinnacle calculated dose to gel measurement as a function of height in several gel dosimeters.

3.1.2.3 Discussion

The general shape of the active region was fairly unsurprising. The average distances from the walls of the cylinder to the beginning of the active region and from the base of the cylinder to the beginning of the active region were the same, as would be expected given that the base and walls are made of the same material. The average distance from the top of the cylinder to the active region was roughly twice that measured from any other boundary. This increased distance was expected based on the manufacturing process. After being poured, gel dosimeters were allowed to sit covered but not sealed for 24 hours before the lid was completely closed. While this was necessary to avoid deformation of the cylinder as the gel cooled, it left a 24 hour window for atmospheric oxygen to diffuse directly into the gel.

As is clearly shown by the data above, the active region of the dosimeter is substantially smaller than the total gel volume. One acrylic cylinder is capable of holding

approximately 2.3 L of gel. As BANGkits™ can only be purchased in units of 0.5 L, five are required to completely fill a cylinder completely. Using the average active region extents determined above, the active region produced by 2.5 L of gel has a volume of only 0.56 L – roughly 20% of the total required gel volume. In terms of the acrylic cylinder, the active region makes up approximately 24% of the total cylinder volume. To put this in a monetary perspective, with 0.5 L of gel costing at least $55, roughly $215 out of a $275 dosimeter are not contributing to the active region of the dosimeter. For a substance that is ultimately intended for clinical use, this much waste is a clear roadblock to widespread acceptance, particularly considering that other gel dosimeters can be created using commercially available chemicals for a fraction of the cost [42].

This issue could potentially be alleviated, if not completely solved, by using a substance more resistant to the diffusion of oxygen to build the cylinders. While this could potentially increase the initial cost of the cylinder, a substantial increase in the active region volume could make this worthwhile. Such material would, ideally, have an effective atomic number and electron density nearly equivalent to that of water and, perhaps more importantly, an index of refraction near that of the gel dosimeter and the OCTOPUS matching fluid to avoid any reconstruction artifacts caused by laser reflection or refraction.

3.1.3 Fractionation Effects

The effects of fractionation on gel response were investigated by comparing the dosimeter response to 6 MV photons against the relative dose measured in Pinnacle under two conditions: 100% of the prescribed dose to d_{max} given in a single beam and 100% of the prescribed dose to d_{max} given across four fractions with one minute breaks between fractions. In the first irradiation performed for this experiment, 6 Gy was delivered to d_{max} through the

side of the dosimeter. Unknown issues with this dosimeter led to poor agreement between the gel data and Pinnacle when comparing relative doses. As such, a calibration curve was not produced and these data were not used to assess the accuracy of single beam or fractionated responses. However, these data were saved to assess general differences between the fractionated and non-fractionated courses. The data from this dosimeter are shown in Figure 3.7.

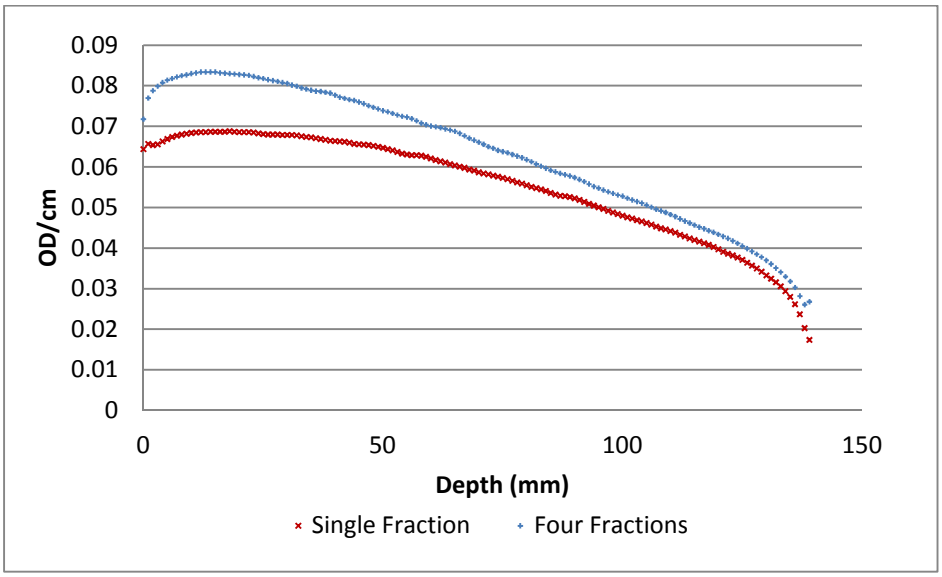

Figure 3.7: Fractionation effects in a gel with 6 Gy delivered to d_{max}.

A second dosimeter was used to test for fractionation effects, this time delivering 3.5 Gy to d_{max}. Much better results were noted in this dosimeter, with dose data from the single fraction irradiation agreeing well with Pinnacle within the active region of the gel. Data from the single fraction and multi-fraction irradiation are compared against Pinnacle in Figure 3.8.

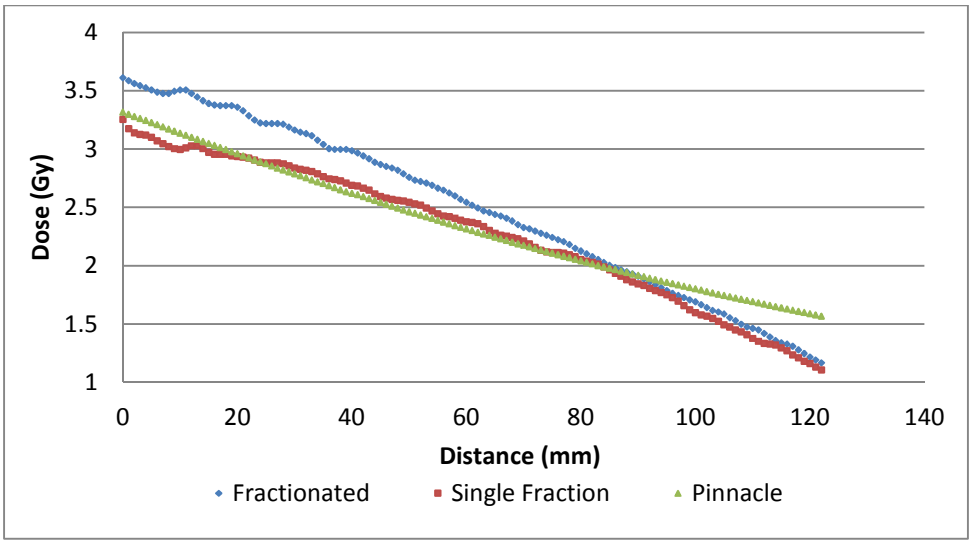

Figure 3.8: Fractionation effects in a gel with 3.5 Gy delivered to d_{max}. Dose data from Pinnacle are included for comparison.

As this effect appeared to increase at higher doses, the ratio of the multi-fraction course to the single beam course was calculated for both gels. These data are plotted as a function of dose in Figure 3.9. The response for the fractionated course ranges from 2% to 20% higher than that of the single beam irradiation over the dose range investigated (roughly 2 – 6 Gy). As shown in Figure 3.9, the difference between the single beam and multiple fraction irradiations is more pronounced at higher doses.

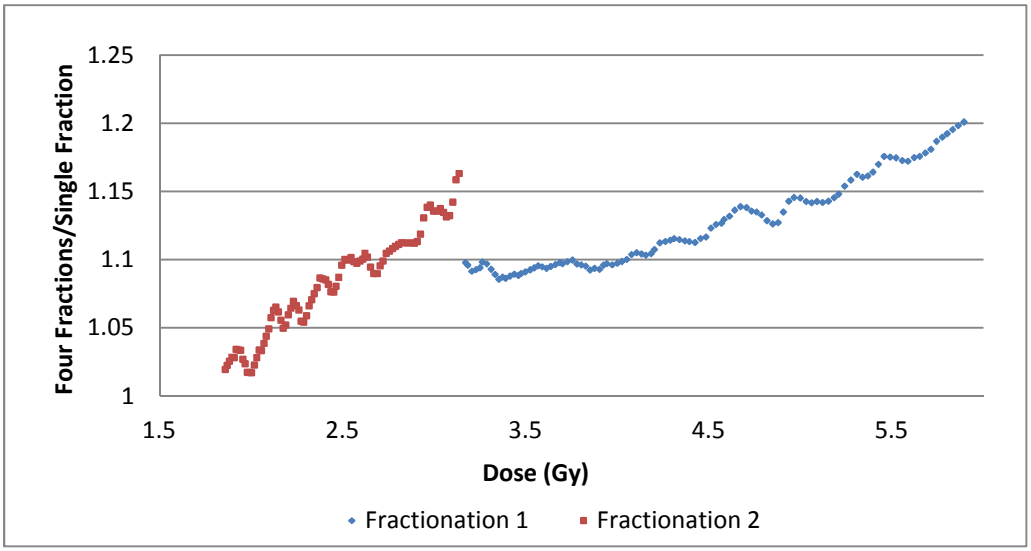

Figure 3.9: Fractionation effects as a function of dose.

3.1.3.1 Discussion

The fractionation effects observed in this project agree with data that have been reported in methacrylic acid-based gel dosimeters in past studies. In 2007, Karlsson et al. performed a study in which vials of a normoxic polymer gel using methacrylic acid monomers (nMAG) were irradiated to a range of doses using a variety of fractionation schemes. Approximately 70 seconds were allowed to pass between fractions. The gels were then read out using MRI and the R_2 values of the nMAG gels were compared. Two major effects were noted: first, for fixed total absorbed dose, the overresponse of the fractionated course increased relative to the single beam course as fraction size decreased (e.g. 4 × 1 Gy responded more than 2 × 2 Gy, which responded more than 1 × 4 Gy). Second, for fixed fraction size, higher absorbed doses produced a greater discrepancy between the fractionated and single beam courses [36]. Figure 3.9 demonstrates a third variant of these results, in which the number of fractions was fixed while the dose per fraction and total dose were varied. Clearly, substantial overresponse is noted across the range of doses investigated, with the magnitude of the overresponse increasing with increasing absorbed dose. The discrepancy in the slopes of the two curves produced by the gels is likely a result of inter-batch response variability.

The discrepancy between fractionated and single beam response is due to the difference in radical concentrations produced by the two irradiation schemes. In the single beam irradiation, a high concentration of radicals is produced and maintained for the duration of the treatment. In the fractionated treatment, radicals are produced in shorter bursts. In the minute between fractions, the radical concentration gradually decreases, yielding a lower average concentration across the treatment time. In both irradiations, approximately the

same number of total radicals is produced. As the rate of polymerization in these dosimeters increases with radical concentration and the rate of termination of the polymerization reaction increases with the square of radical concentration, the lower average radical concentration produced in the fractionated treatment reduces the termination rate more than it does the polymerization rate relative to the single beam treatment, leading to an overall increased response. In short, delivering the total dose all at once results in a lower response than that produced by a fractionated delivery [36].

This fractionation effect is a major issue if gel dosimeters are intended for use in patient specific quality assurance (QA). In 2009, Heard observed a 35% overestimate of dose in a gel dosimeter being used for IMRT QA. He cited the fractionation effect as the cause of this discrepancy [22]. As the magnitude of the discrepancy depends on the total dose delivered in a given location, comparing relative doses would not necessarily provide a fix for this problem. As was concluded by Heard, a calibration procedure utilizing a number of fractions similar to that used in treatment delivery must be developed if gels are to be used to make accurate dosimetric measurements.

3.1.4 Overlapping Fields

The ability of a gel dosimeter to render overlapping fields was tested by comparing its response against calculations from Pinnacle at the center of the gel dosimeter. Due to space constraints in the dosimeter, no calibration curve could be produced. As a result, the two distributions were compared in terms of relative dose. The gel and Pinnacle data were normalized to unity at the center of the highest dose plateau. The resultant relative dose distributions are shown in Figure 3.10. In general, good agreement was noted between the two distributions, with most measured points conforming closely to the calculated

distribution. The largest deviations occurred near the bottom of the dosimeter, where the measured dose was substantially higher than the calculated dose, and in the dose plateau nearest the top of the dosimeter, where some underresponse was noted in the measured distribution. Explanations for these effects will be addressed in the discussion section below.

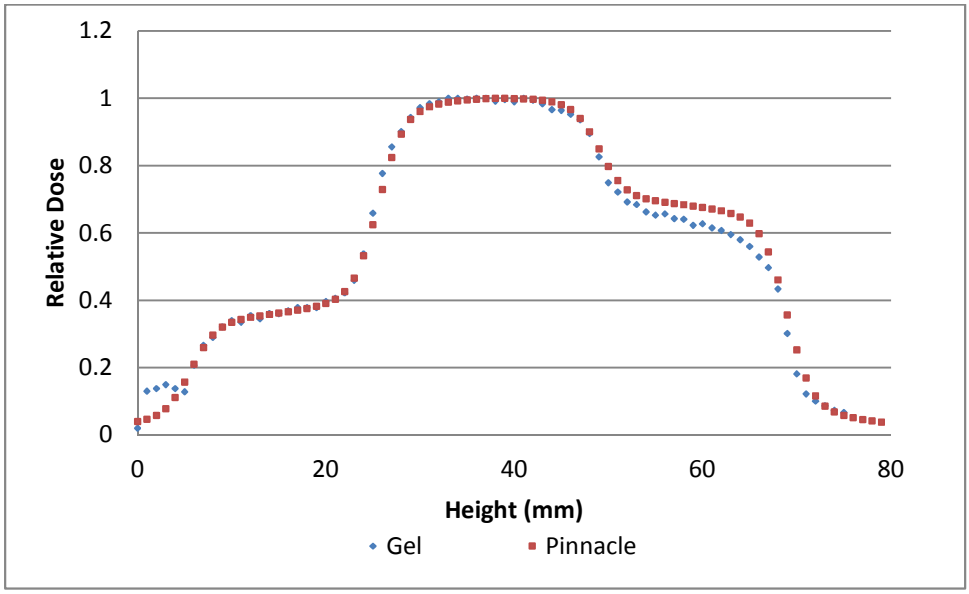

Figure 3.10: Comparison of beam profiles produced overlapping fields from Pinnacle and a gel dosimeter. The left side of plot is towards the bottom of the dosimeter.

To quantify the agreement between the calculated and measured data, gamma analysis was performed, comparing planes from the Pinnacle and gel dose distributions. As no calibration curve had been produced, a calibration curve produced in another gel was applied to the data. As a result, the gamma results provide some insight into the effect that inter-batch response variability has on dose readout. Positive results would indicate the possibility that a generic calibration curve could be appropriate in the absence of batch-specific calibration data. Gamma results from two orthogonal planes are shown in Figures 3.11 and 3.12.

Based on a 5%/3 mm gamma criterion, over 93% of points passed in both planes studied. Pass rates of 95.4% and 93.1% were observed in Figures 3.11 and 3.12, respectively. The regions of worst agreement in both images, near the bottom right of Figure 3.11 and in the bottom half of Figure 3.12, correspond to the region of underresponse noted in Figure 3.10. The application of the dose calibration reduced the effect observed on the left side of Figure 3.10, improving agreement in this region.

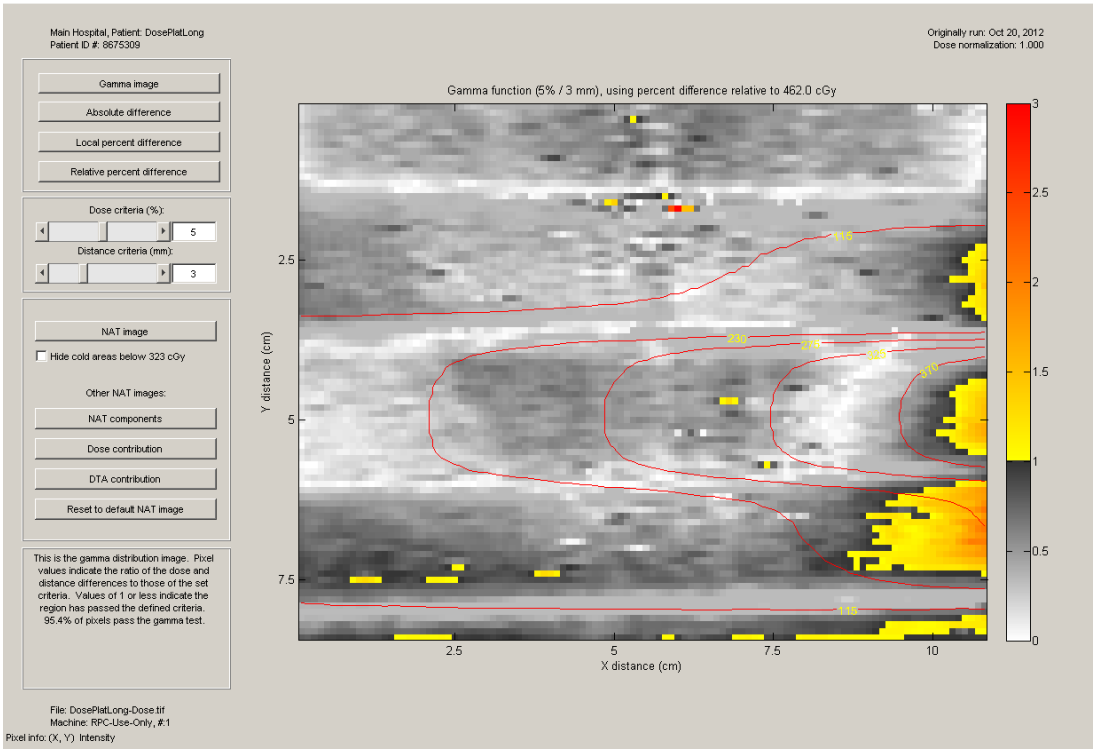

Figure 3.11: Gamma results for the dosimeter irradiated with overlapping fields. The top of the image is towards the bottom of the dosimeter and the beam enters through the right side of the image.

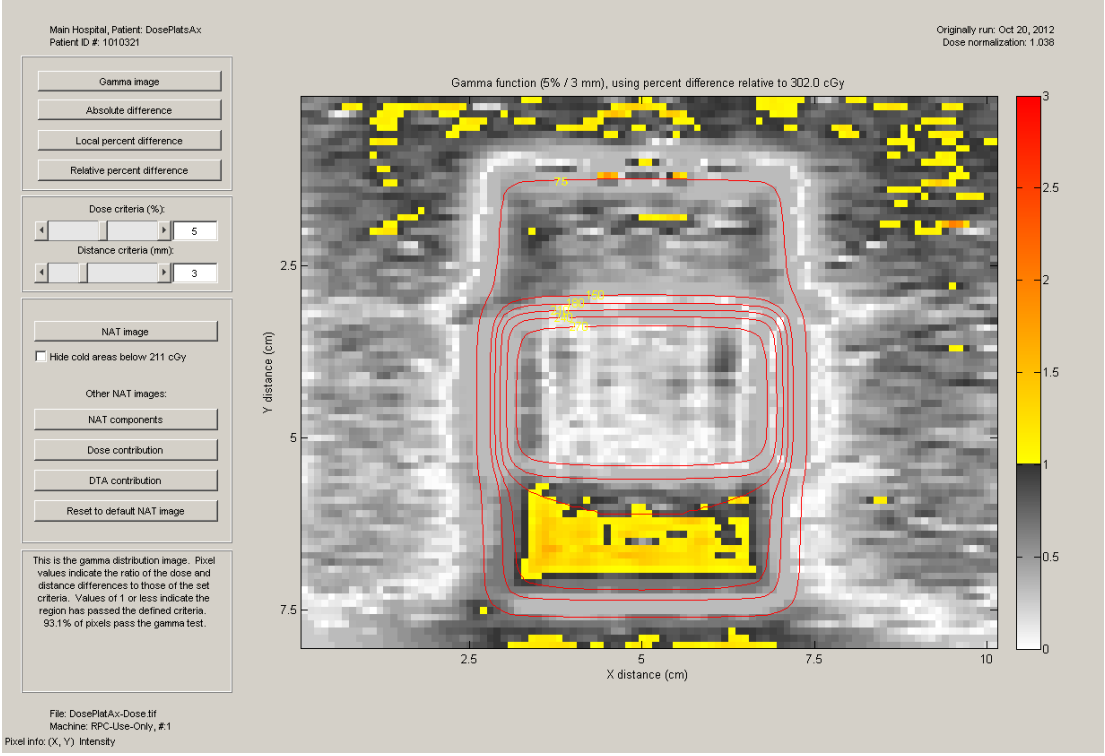

Figure 3.12: Gamma results for the central coronal plane of the dosimeter irradiated with overlapping fields. The top of the image is towards the bottom of the dosimeter and the treatment fields are traveling into the page.

3.1.4.2 Discussion

Two major discrepancies were noted in comparing the relative doses profiles produced by Pinnacle and the dosimeter. The first discrepancy was observed on the left side of Figure 3.10, where a substantial overresponse was observed in the gel data. This is a product of the fact that these data were initially analyzed without a calibration in place. As mentioned previously, between irradiation and readout, a gel dosimeter was allowed to sit out for 24 hours, during which time the baseline OD of the gel increased; thus, a region that received no dose did not typically have an OD of zero, even after the subtraction of the prescan. Without a calibration, this is not corrected for.

The second discrepancy is noted on the dose plateau on the right side of Figure 3.10. Here, gel response was somewhat lower than expected. This is a result of the positioning of

the radiation fields in the dosimeter. The fields used to produce this dose distribution were stacked vertically on top of one another with a small region of overlap between them. The higher of the two fields was closer to lid of the dosimeter and, apparently, at least partially outside the active region of the gel. As a result, partial oxygen inhibition of the gel response is noted in this region. This also explains why the overresponse observed on the left side of the image (near the bottom of the dosimeter) was not observed on the right: due to oxygen inhibition, the baseline OD outside of the active region does not appreciably increase when left at room temperature.

Gamma results were better than expected given that the calibration curve applied to the data was from a different batch of gels. Even with an inappropriate calibration applied, the final gamma passing rates were fairly strong, with 95.4% and 93.1% of pixels passing at the 5%/3 mm level. While the use of a generic calibration curve is not advised for measurements of absolute dose due to the inter-batch dose-response variations noted in Section 3.1.1 (e.g. data sets 2 and 3 in Figure 3.1), this result shows a generic gel calibration curve may be appropriate for gamma analyses where a unique calibration curve is not available.

3.2 Proton Dose Measurement

3.2.1 Irradiations Perpendicular to Cylindrical Axis

Initial proton irradiations were performed with the beam oriented perpendicular to the cylindrical axis of the dosimeter – through the side of the cylinder. A dose of 3 Gy was delivered to the center of a 4 cm SOBP using 200 MeV protons. Two BANG®-3-Pro-2 dosimeters from different batches were used to measure dose using this orientation. A calibration curve was only produced for the second dosimeter; this calibration curve is shown

in Figure 5.10. A comparison of the relative doses measured in the first gel and an ion chamber is shown in Figure 3.13. A comparison of the absolute dose measured in the second gel and ion chamber measurements scaled to 3 Gy is shown in Figure 3.14. Ion chamber measurements in these figures have been shifted so they would line up with gel measurements – zero depth is roughly 9 cm into range of the beam for these irradiations.

Substantial discrepancies are immediately obvious in both figures. In Figure 3.13, good agreement is observed across most of the range of the proton beam, with minor underresponses noted just after the beam enters into the gel and near the distal edge of the SOBP. Past the 60% dose point in the distal falloff region, major discrepancies are apparent, with substantial overresponse noted across the rest of the gel. Relative doses of just under 0.3 were measured centimeters beyond the edge of the SOBP in a region that received no dose. In Figure 3.14, a similar effect is noted, but is overshadowed by the ~85% higher than expected absolute dose measured along the SOBP. In terms of the relative dose, the gel response to the second proton irradiation again matched well with the delivered dose at depths shallower than the distal falloff of the SOBP.

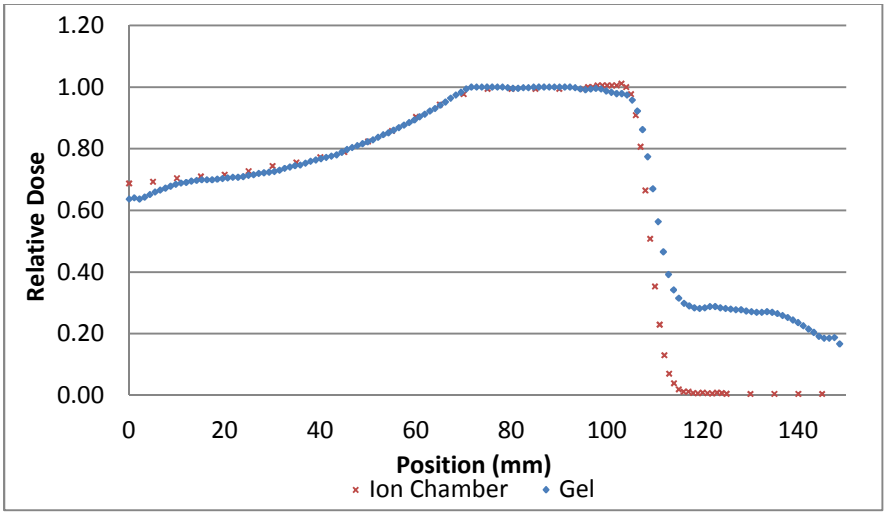

Figure 3.13: Results of the initial proton irradiation of a gel dosimeter through the side of the dosimeter.

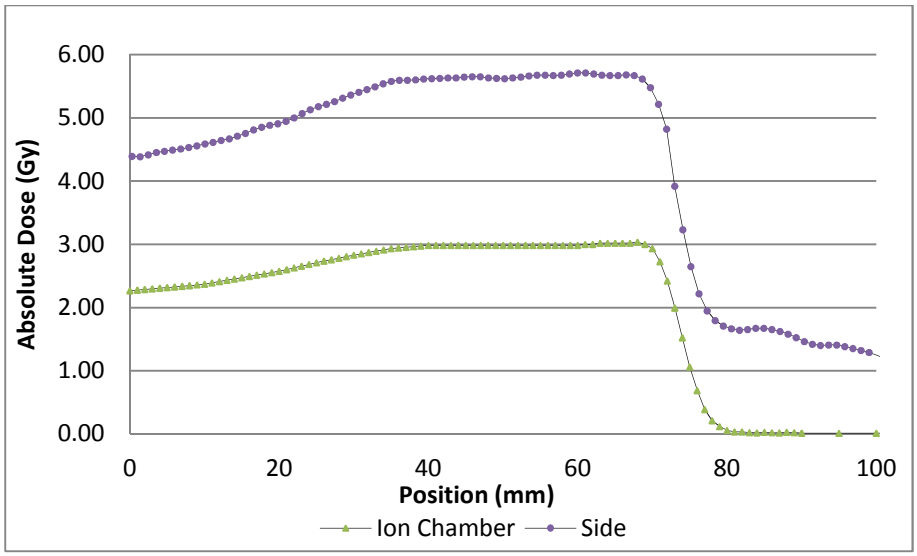

Figure 3.14: Results of the second proton irradiation of a gel dosimeter through the side of the dosimeter.

Data from the second proton irradiation were used to perform gamma analysis. Two orthogonal slices of the gel were compared against a dose distribution generated in Eclipse. A 5%/3 mm gamma criterion was selected for this comparison. The results of this analysis are shown in Figures 3.15 and 3.16. Gamma passing rates of 85.7% and 89.9% were noted in the longitudinal and axial planes respectively. The regions of worst agreement occurred in and beyond the distal falloff of the SOBP and in the beam penumbra, particularly within the slice plane.

It is worth noting that these results may have been affected by the way DoseLab handles negative doses. As is shown in Figure 3.17, the calibration curve for this dosimeter yielded doses less than zero in and just beyond the beam penumbra. DoseLab interprets these negative doses as equal to zero. As zero dose is closer to the calculated distribution than negative dose in this region, it is possible that the percents of pixels passing were slightly higher than they should have been, particularly in Figure 3.16.

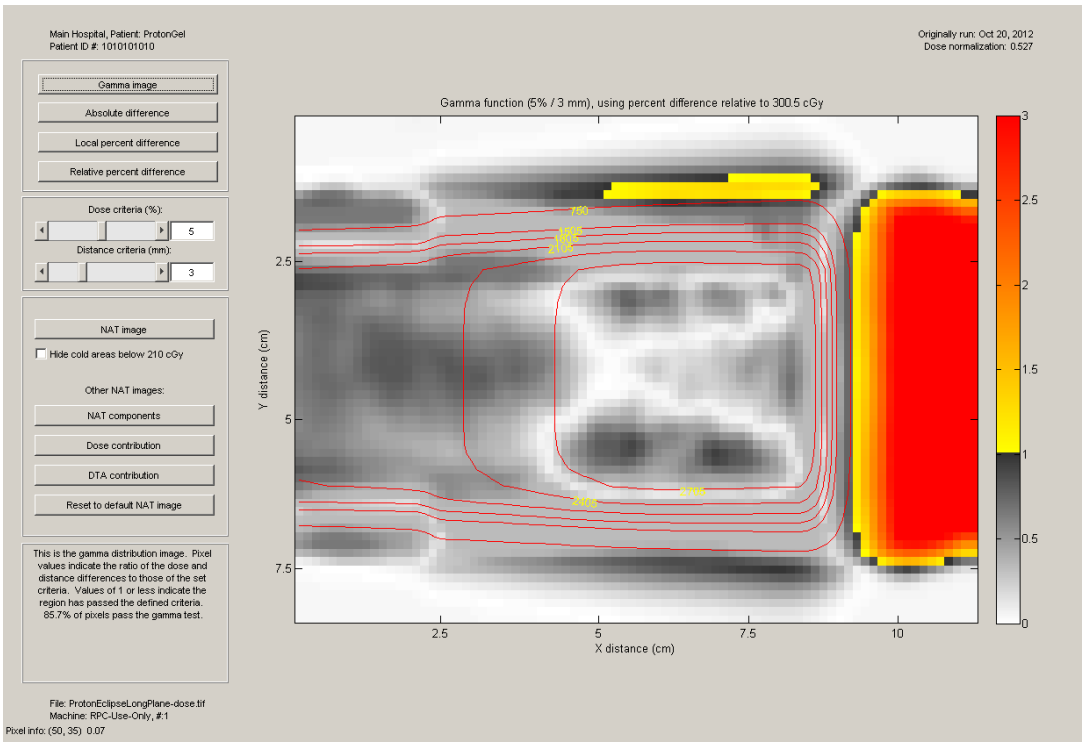

Figure 3.15: Gamma results for a proton irradiation through the side of a dosimeter. The top of the image is right from the perspective of the beam and the beam enters through the left side of the image.

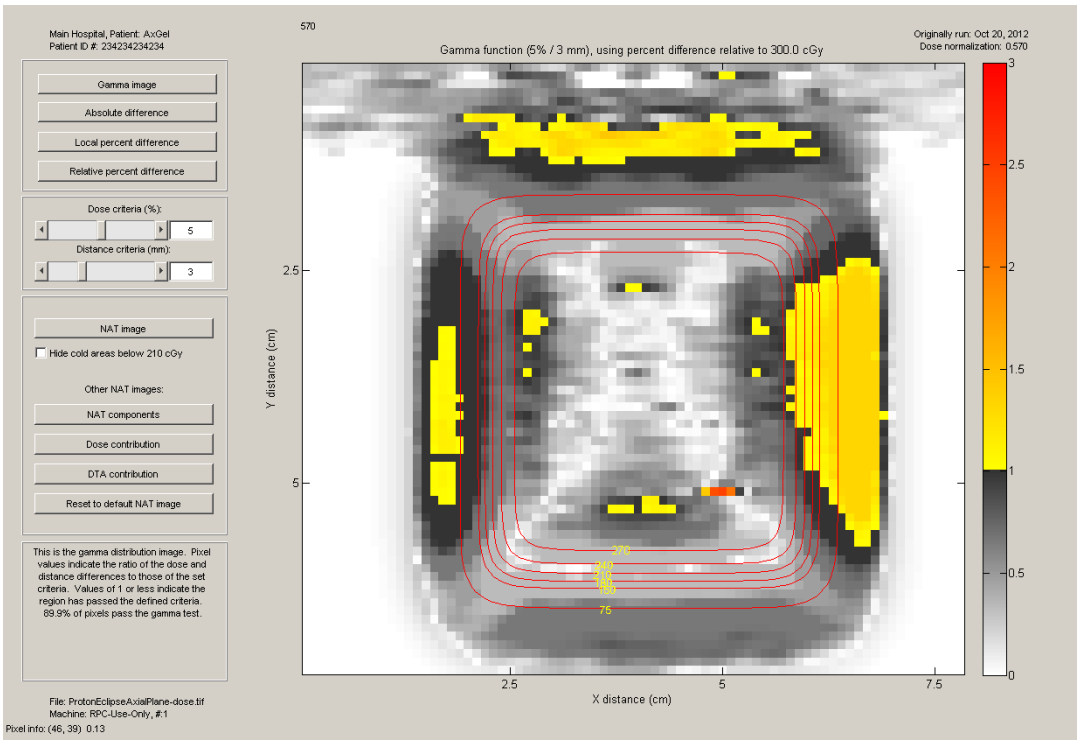

Figure 3.16: Gamma results for a proton irradiation through the side of a dosimeter. The right side of the image is to the right from the perspective of the beam and the beam is traveling into the page.

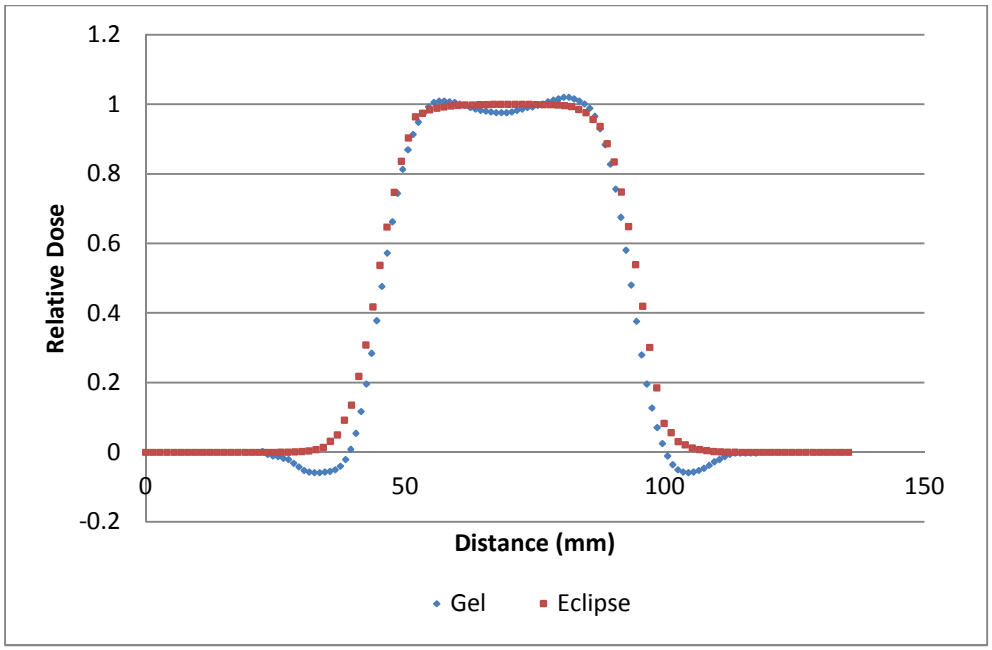

Figure 3.17: Transverse profile comparison of gel and Eclipse data for a proton irradiation through the side of a dosimeter. The profile was taken at the depth of mid-SOBP. The left side of the plot is left from the perspective of the beam.

3.2.2 Irradiations Parallel to Cylindrical Axis

In an attempt to remove the artifact noted in Section 3.2.1, additional proton irradiations were performed with the beam oriented parallel to the cylindrical axis of the dosimeter – directed through the base of the dosimeter. As before, a dose of 3 Gy was delivered to the center of a 4 cm SOBP using 200 MeV protons. Two BANG®-3-Pro-2 dosimeters from different batches were used to evaluate the gel response. A calibration curve was produced for both dosimeters; these calibration curves are shown in Figures 5.9 and 5.11. A comparison of the relative doses measured with both gels and with an ion chamber is shown in Figure 3.18. A comparison of the absolute doses measured in both gels and ion chamber measurements scaled to 3 Gy is shown in Figure 3.19. Ion chamber measurements in these figures have been shifted so they would line up correctly with gel measurements – zero depth is approximately 14 cm into the proton beam range.

Substantial discrepancies are again obvious in both figures. In Figure 3.18, underresponse is noted leading up to the SOBP and overresponse is noted near the end of the SOBP. Note that both gels were normalized to unity 1 cm into the SOBP – had they been normalized at a different location, the degree of underresponse and overresponse observed would have changed (e.g. normalizing at the beam entrance would have led to apparent overresponse throughout the dose distribution). The response in the two dosimeters appears to be fairly consistent: 2 cm and further into the dosimeter, the two gel measurements agree with one another within 3%. Additionally, the artifact observed in and beyond the distal falloff region in section 3.2.1 no longer appeared to be present.

In Figure 3.19, substantial overresponse was again observed, yielding absolute dose measurements higher than the delivered doses. At the center of the SOBP, overresponses of approximately 33% and 100% were observed for the first and second proton irradiations, respectively.

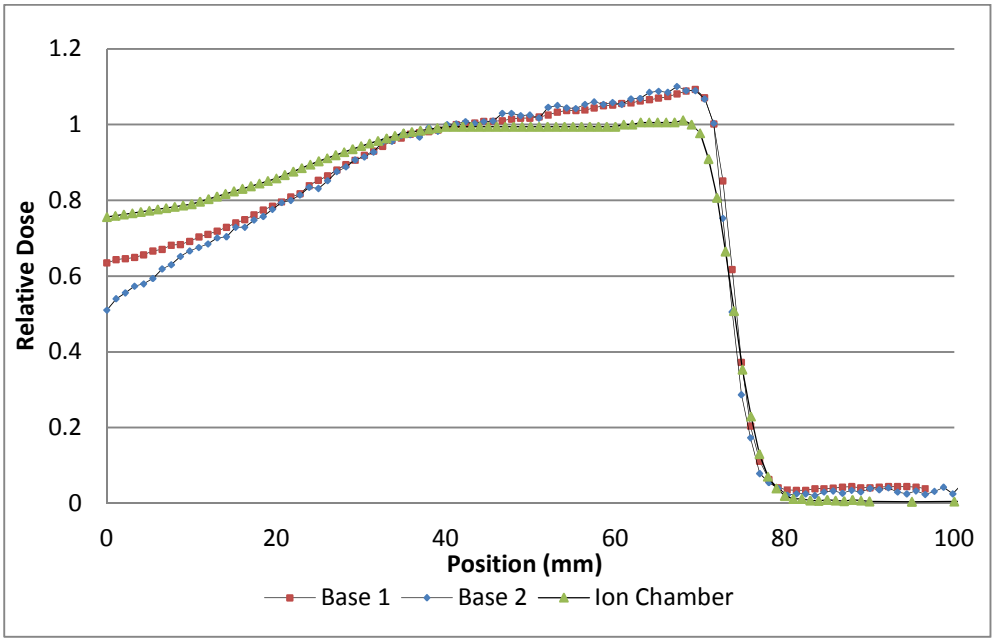

Figure 3.18: Relative dose measurements from proton irradiations through the bases of two dosimeters compared against ion chamber data.

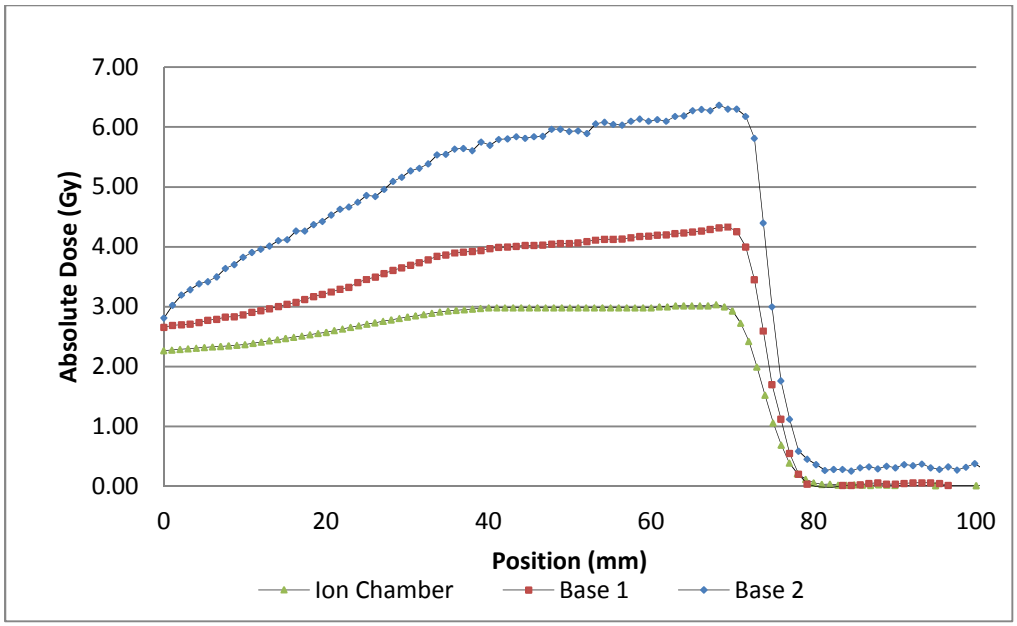

Figure 3.19: Absolute dose measurements from irradiations through the bases of two dosimeters compared against scaled ion chamber data.

As the height-dependent response discrepancies seen in these irradiation were not observed in the irradiations performed through the side of the dosimeter, it was thought that the beam orientation was somehow responsible for the discrepancy. In an attempt to address this issue, a correction curve was developed based on the vertical response data collected in Section 3.1.2.2. The average of the three curves shown in Figure 3.6 was calculated and applied to the data from the first irradiation through the base of the dosimeter. The corrected, relative dose measurement is shown in Figure 3.20. Better agreement is noted throughout the dosimeter, though overresponse in excess of 5% is still noted near the distal edge of the SOBP.

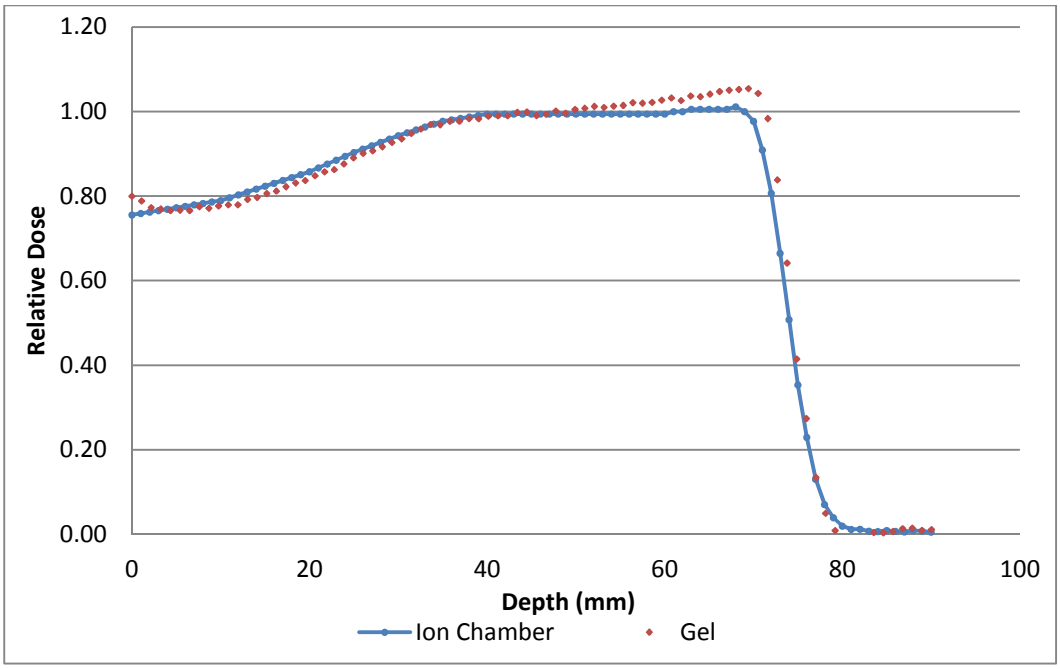

Figure 3.20: Corrected results for a proton irradiation through the base of a dosimeter.

These corrected data were used to perform gamma analysis. Two orthogonal slices of the gel were compared against a dose distribution generated in Eclipse. A 5%/3 mm gamma criterion was selected for this comparison. The results of these analyses are shown in Figures 3.21 and 3.22. Passing rates of 94.6% and 99.3% were noted for the longitudinal and axial plane comparisons, respectively.

Note that, as before, the calibration caused some slight dips into negative dose values, which DoseLab interprets as a dose of zero. However, these pixels were located outside of the field and almost certainly would have passed anyway. As such, they are expected to have little impact on the overall percentage of pixels passing. A sample profile demonstrates this in Figure 3.23, where slightly negative relative dose values are noted several centimeters beyond the penumbra region on both sides.

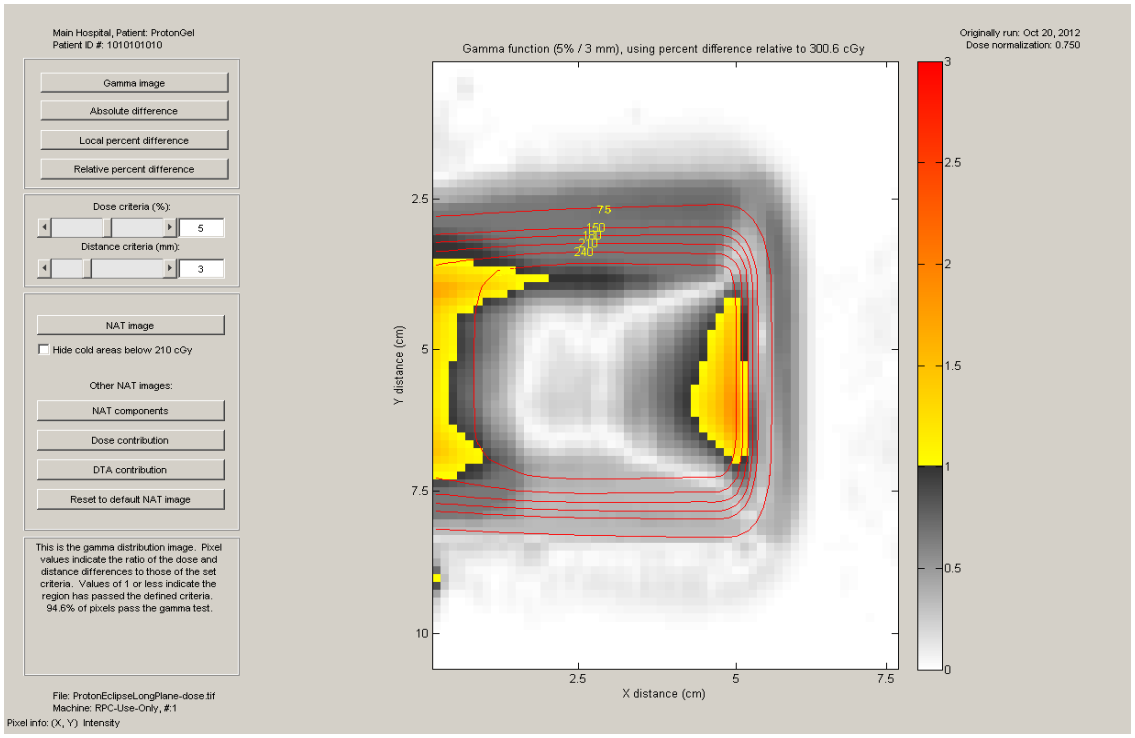

Figure 3.21: Gamma results for a proton irradiation through the base of a dosimeter. The top of the image is left from the perspective of the beam and the beam enters through the left of the image.

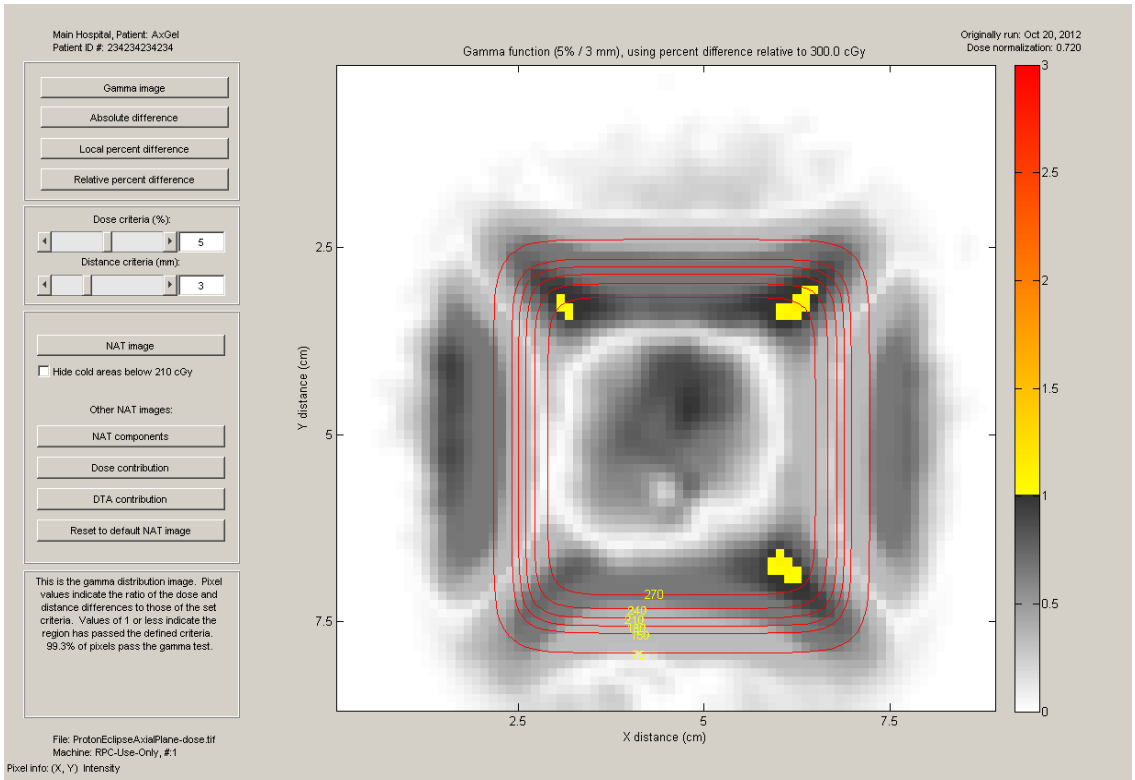

Figure 3.22: Gamma results for a proton irradiation through the base of a dosimeter. The right side of the image is to the right from the perspective of the beam and the beam is traveling into the page.

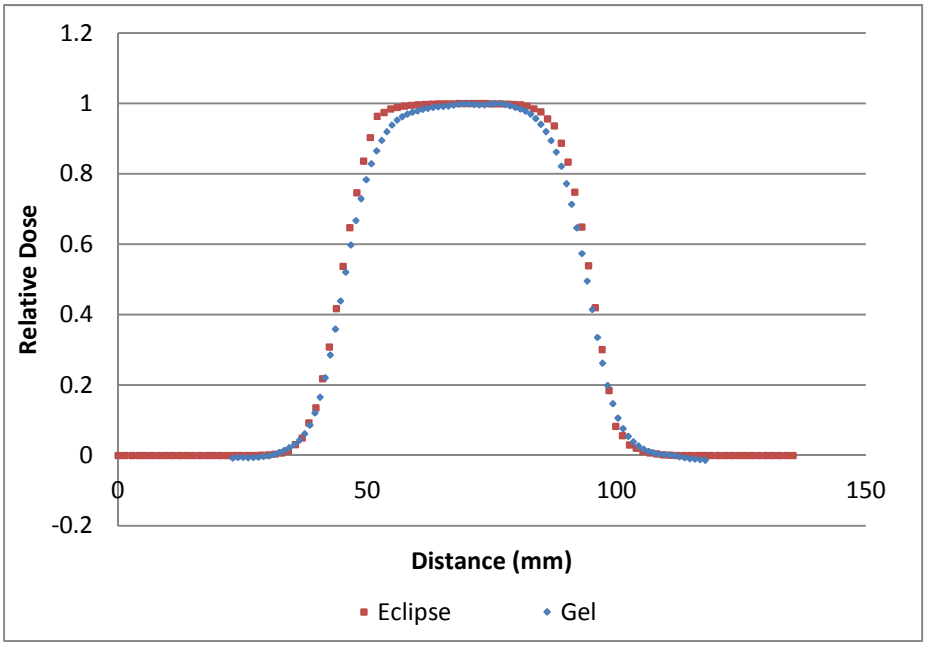

Figure 3.23: Mid-SOBP profile comparison of gel and Eclipse data for an irradiation through the base of a dosimeter. The left side of the plot is left from the perspective of the beam.

3.2.3 Discussion

3.2.3.1 Absolute Dose Measurements

Over the course of this study, a number of obstacles were encountered while attempting to measure dose from proton beams. Proton irradiations produced substantially higher ODs than were expected for the delivered dose based on the electron calibration curves produced throughout this study. These were continually used throughout the study because, after each failure, alternate explanations were conceived that provided potential explanations for the sometimes enormous response discrepancies. For example, in the second irradiation performed through the side of the dosimeter (the first for which a calibration curve was produced), the beamline had not been tuned to deliver 200 MeV protons. As a result, the dose was delivered one spill (approximately 10 - 20 MU) at a time, with many seconds passing between each spill. Based on the previously observed

fractionation effects reported in Section 3.1.3, it was deemed possible that the overresponse was due to the unintentional fractionation of the treatment delivery.

The first irradiation performed through the base of the dosimeter was the second for which a calibration curve was produced. The beamline was properly tuned prior to this irradiation. Here, a substantially smaller overresponse was noted than in the first irradiation, but dose in the SOBP was still found to be approximately 33% higher than expected. In preparing for this irradiation, four dosimeters had been warmed up together in the conditions described in Section 2.1.3. It was suggested by MGS Research, Inc., that the gels may not have reached room temperature due to the number of gels being warmed in the relative small space. Historically, some BANG® formulations gels have exhibited a temperature dependent response when scanned using MRI [24]; the colder a gel was during irradiation, the greater the response would be. As the electron calibration was performed days after the proton irradiation without a period of refrigeration in between, temperature issues could have explained the discrepancy between the electron and proton responses. However, a previous BANG® study found that the response difference between a room temperature gel and 15 °C gel (lower than a worst case scenario estimate of gel temperature for the four gels) was found to be nearly negligible for doses less than 5 Gy and the immediate predecessor of BANG®-3-Pro-2, BANG®-3-Pro-1, showed no such temperature dependence when scanned using OCT [24, 43].

To rule out temperature as a factor, a third dosimeter underwent proton irradiation and calibration. The temperature of the environment was carefully monitored for this dosimeter and over 24 hours were given for the dosimeter to warm up. This gel was observed to overrespond by approximately 100% at the center of the SOBP. As the dose

response curve was produced in a different gel from the same batch and appeared less steep than had been seen in previous batches, an alternate calibration curve was applied. An overresponse of approximately 30% was still noted at the center of the SOBP.

The response variations noted in this study were unexpected in light of previous work with BANG®-3-Pro-2 dosimeters. In a 2010 study, Zeidan et al. reported that electron beams yielded "satisfactory calibration curve[s] for a given gel batch" for irradiations with proton beams [29]. However, all analysis in Zeidan's study was performed using relative dose distributions. As will be discussed in Section 3.2.3.2, the relative measurements produced in this study were, on the whole, far more satisfactory than the absolute measurements. Historically, response differences have been observed in BANG®-3 gels irradiated to the same dose using both proton and photon beams [38].

Assuming the absolute dose measurements from Zeidan's gels did agree with his ion chamber measurements and TPS calculations, the characteristics of the proton beams used in this study may account for the calibration problems. The proton center used in the Zeidan et al. BANG®-3-Pro-2 study accelerated protons using a cyclotron. In contrast to the synchrotron-based system at the PTC-H, protons from a cyclotron are output continuously during dose delivery. The spill-based delivery produced by a synchrotron may be inducing a form of the fractionation effect reported in Section 3.1.3 even when the system is working properly. Further investigation into the response of these dosimeters to different treatment modalities and fractionation schemes, particularly on the sort of time scale observed in synchrotron-based proton therapy, is warranted.

3.2.3.2 Relative Dose Measurements

Measurements of absorbed dose aside, substantial issues were also noted for both irradiation configurations in regards to the relative dose distributions. For irradiations through the side of the dosimeter, substantial overresponse was noted past the 60% dose point in the distal falloff region. This was ultimately determined to be the result of an OCT artifact. It is believed that the high integral OD produced by the proton irradiation within the slice plane attenuated the OCTOPUS laser to such a degree that the reconstruction software misinterpreted where, precisely, the beam was being attenuated. The artifact is not unlike high-atomic number streaking artifacts observed in x-ray CT. The negative dose areas along the beam penumbra noted in Figure 3.17 are believed to be a second effect of this artifact, as they were observed only in the side irradiations. Additional discussion of this artifact is included in Section 5.2.

The apparent increase in gel response with height in the dosimeter observed in the gels irradiated through the dosimeter base is puzzling. As this was observed for only one of the gel orientations, it seems unlikely that the effect is related to the characteristics of the proton beam. Additionally, as was shown in Figure 3.18, two gels from separate batches exhibited nearly identical relative responses in the active region of the gel, seemingly indicating that the effect does not vary between gel batches. Finally, as will be shown in Figure 3.24, this effect was not observed in the LET-Baseline gel, indicating that the effect is probably not caused by the OCTOPUS. While correcting the proton measurements using the vertical response data improved the agreement with ion chamber data considerably, a gentle slope was still observed in the data, particularly in the SOBP. This residual slope may be a result of LET-induced overresponse. Two studies conducted by the University of Florida

have noted slight overresponses near the distal edge of the SOBP, with one study demonstrating a relationship between overresponse and LET [29, 35]. However, this still would not explain why the effect was not observed in the irradiations through the side of the dosimeter. Additional research should be directed towards finding the cause of this response discrepancy.

To the credit of the BANGkits™, the severe LET-induced quenching noted in earlier BANG® formulations and other gel dosimeters was not observed here [27, 44]. While slight underresponse was noted at the distal edge of the SOBP in the first side-irradiation gel, this was not reproduced in the subsequent three gels. Additionally, the results of the gamma analyses performed on these distributions are rather respectable, particularly for the corrected base irradiation. However, it must be stressed again that these results were produced by allowing DoseLab to normalize the gel data in the manner that produced the best gamma results. As was already discussed, the amount of polymerization generated by proton beams in these dosimeters was substantially greater than was expected based on the electron calibration curve.

3.3 Proton LET Measurement

The LET-Meter and LET-Baseline gels were irradiated through the bases of their cylinders with a 200 MeV proton beam utilizing a 4 cm SOBP. Based on the manufacturer's recommendations, doses 6 Gy and 3 Gy were delivered to the LET-Meter and LET-Baseline gels, respectively. After irradiation, electron calibration curves were produced in these dosimeters. The calibration curves are shown in Figures 5.12 and 5.13. However, a substantial disagreement was noted between the calibration curve produced for the LET-Meter gel and the ODs measured from the proton irradiation. At a point 1 cm into the SOBP,

before any substantial LET effects were expected, the OD measured in the LET-Meter gel was 70% higher than that expected based on the calibration curve. As such, analysis had to be restricted to the SOBP where a calibration was unnecessary as the absorbed dose was constant – any response differences could be attributed to the effects of LET. No such discrepancy was noted with the LET-Baseline gel, which showed agreement within 4% of the expected OD across the SOBP. The LET-Meter and LET-Baseline measurements were normalized 1 cm into the SOBP to allow for direct comparison. The normalized data from both gels are shown in Figure 3.24.

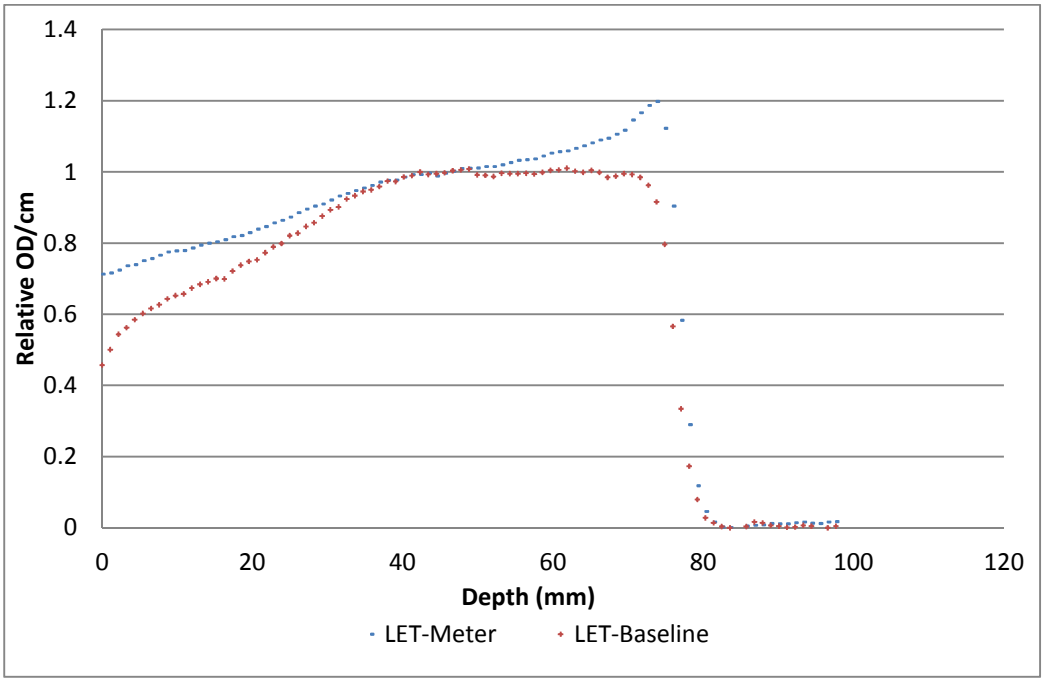

Figure 3.24: Data from the LET-Meter and LET-Baseline gels.

The overresponse of the LET-Meter gel was calculated as discussed in Section 2.5.4.2. Overresponse is plotted as a function of proton beam LET in Figure 3.25. Across the range of LETs that could be investigated (those contained within the SOBP), a linear trend was noted between LET-Meter overresponse and track-average proton LET. A threshold for

LET response was observed at ~1.5 keV/micron and the linear trend was maintained through ~3.5 keV/micron.

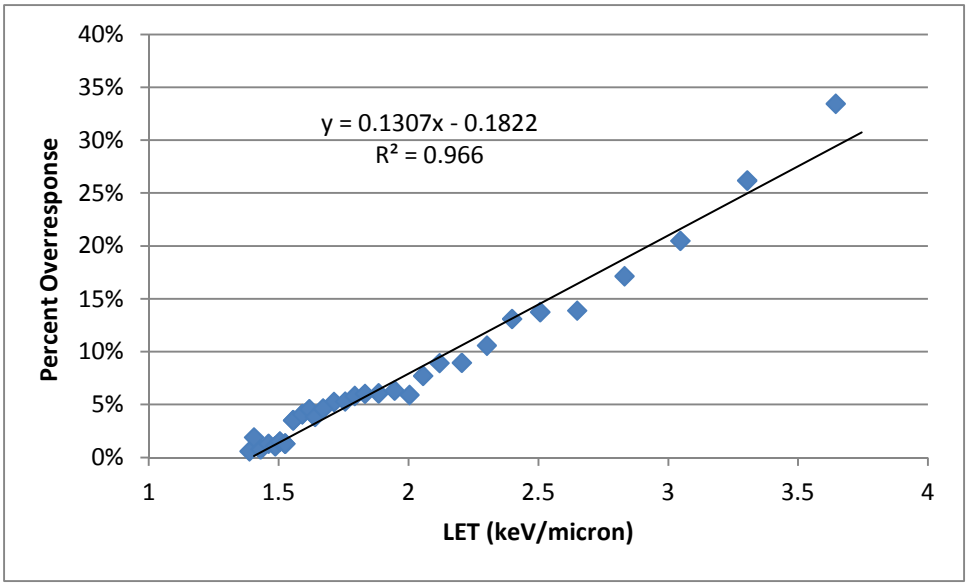

Figure 3.25: Percent overresponse of the LET-Meter gel plotted as a function of track-average proton LET.

3.3.1 Discussion

Across the range of LETs that could be investigated in this study, a linear trend between LET and overresponse was observed. This matched well with a previous study by Lopatiuk-Tirpak et al. conducted using the same gels [35]. While the same maximum LET reported in that study (nearly 5.5 keV/micron) was not observed in this study, that study investigated depths slightly beyond the distal edge of the SOBP in the dose falloff region where higher LETs are present. The LET threshold for response was the same as that reported by Lopatiuk-Tirpak et al. Further investigation into the response characteristics of the LET-Meter gel is required so a proper calibration can be performed and data collection and analysis can occur throughout the distal falloff of the SOBP, where the highest LETs are present. Once these issues are resolved, these LET gels show promise for use in measuring three-dimensional LET distributions.

While not directly relevant to the goal of LET-measurement, it is worth noting that the response observed in the LET-Baseline gel matched well with expectations in the SOBP based on the electron calibration curve. As the exact difference between these LET gels and the BANGkits™ is proprietary, it is difficult to speculate as to why this is the case. Given the calibration problems observed with the BANGkits™, further development of the LET-Baseline gel formulation would certainly be worthwhile, as neither the calibration issues nor the response variations with dosimeter height were observed in these gels.

Chapter 4

Summary and Conclusions

4.1 Summary

The goals of this project were two-fold: to evaluate the ability of BANG®-3-Pro-2 BANGkits™ to measure the dose deposited by a proton beam and evaluate the ability of BANG®-3-Pro-2 variants to measure the LET of a proton beam. These polymer gel dosimeters are capable of making measurements in three-dimensions, giving them a distinct advantage over more commonly used two-dimensional and point measurement devices. All polymer gel dosimeters used in this study were purchased from MGS Research, Inc. The gels intended for LET measurement (LET-Meter and LET-Baseline) were mixed by the manufacturer then shipped, while the BANGkits™ were mixed at the RPC after arrival. All dosimeters were scanned using the OCTOPUS™-IQ OCT scanner, also purchased from MGS Research, Inc.

Basic characteristics of the BANG®-3-Pro-2 BANGkits™ were investigated using photon and electron irradiations. The dose-response characteristics were assessed in three different gel batches using 16 MeV electrons. The dose-response relationship was found to be approximately sigmoidal, with a dose threshold for response of about 15 cGy. The exact shapes of the dose-response curves varied between gel batches due to mixing conditions and other factors. The size of the active region of the dosimeters was evaluated using data from a total of six gels. The active region was found to measure approximately 10 cm by 7 cm, with a volume 24% that of the entire cylinder. The regions of poor response were believed to be a result of oxygen inhibition. Substantial fractionation effects were observed in the dosimeters.

The gel response produced by a dose delivered in a single beam was found to be less than that produced by the same dose delivered in four fractions. The size of the discrepancy between the single beam and four fraction responses was found to increase with increasing dose. Finally, a dosimeter was used to render the dose delivered by a set of overlapping fields. Minor discrepancies between the measured and calculated doses were noted due to the placement of the treatment fields (one was slightly outside the active region) and the lack of calibration curve for this dosimeter. When a calibration curve from a different gel batch was applied to the data, gamma pass rates of 95.4% and 93.1% were observed in two planar gamma analyses.

Proton dose measurements were performed using these dosimeters with the proton beam oriented either through the side or through the base of the dosimeter. For side irradiations, artifacts were noted in and beyond the distal falloff of the SOBP, as well as in and near the beam penumbra. These artifacts provided the motivation for the second irradiation orientation. While gamma pass rates of 85.7% and 89.9% were observed from gamma analyses of two orthogonal planes measured in one of the side irradiations, the absolute dose from the same gel was found to be 85% higher than the expected dose in the SOBP. For base irradiations, a monotonic increase in the response was noted throughout the reconstructed dose distribution. While the exact cause of this behavior is unknown, it was partially corrected using a correction curve derived from the vertical response characteristics of the gel. Gamma pass rates of 94.6% and 99.3% were observed in gamma analyses of two orthogonal planes obtained from a corrected dosimeter. However, substantial overresponses were noted in measurements of absolute dose, this time 33% and 100% at the center of the SOBP. The extreme overresponses noted when measuring absolute dose were postulated to

be either a hyper-fractionation effect produced by the synchrotron-based beamline used in this study or dosimeter response differences between proton and electron radiation.

The gels intended for LET measurement were not deemed ready by MGS Research, Inc., to directly measure the LET of a proton beam. As such, it was decided that the response characteristics of the gels would be investigated. The response differences between the LET-Baseline and LET-Meter gel formulations were calculated for a proton beam irradiation. As the LET-Meter gel was found to have an overresponse issue similar to that observed in the BANGkits™, data analysis was restricted to the SOBP, where the condition of constant dose made a calibration curve unnecessary. LET-Meter overresponse was found to increase linearly with track-average proton LET across the range of LETs present in the SOBP. The threshold for LET response was noted to be 1.5 keV/micron and the linear relationship was noted through at least 3.5 keV/micron.

4.2 Conclusions

The hypothesis of this study was that, through the use of LET-dependent and -independent polymer gel dosimeters, the LET of a proton beam could be determined and the three-dimensional dose distribution of a proton beam could be obtained with an agreement of 5%/3mm between the measured and expected doses. While LET measurement could not be performed, a linear relationship was observed between LET-Meter overresponse and track-average proton LET across the SOBP of a proton beam. With additional research, it seems these gels could be capable of rendering three-dimensional LET distributions. For irradiations through the base of the gel dosimeters, gamma pass rates in excess of 90% were noted for orthogonal planes obtained from a reconstructed three-dimensional dose distribution. Thus, the results of this project support the hypothesis.

It must be stressed that, for the measurements of proton dose, the hypothesis conditions were satisfied only in the most literal reading of the hypothesis. As was clearly shown from the data collected throughout the proton irradiations, the BANGkits™ failed to accurately measure the absolute doses deposited by a proton beam, sometimes in spectacular fashion. Further research into calibration curve production and comparisons of calibration curves produced by proton beams, electron beams, and photon beams for both these gels and the LET measurement gels is recommended.

BANGkits™ are certainly not without merits. Compared to other methods of gel production (particularly those requiring nitrogenous environments), the mixing process is quite simple, although the cost is considerably greater. For photon measurements, absolute dose agreement was quite good in the subset of gels for which calibration curves were produced. Considering only photons and electrons, the major obstacle facing these kits for the time being are issues with fractionation. The fractionation effects noted in this study would certainly complicate the measurement process for treatment plans using multiple fields, but these effects can, perhaps, be quantified. Further study into these effects is recommended.

4.3 Future Work

If these dosimeters are to enter the mainstream medical physics community for use in IMRT or IMPT QA, additional research must be done. For the BANG®-3-Pro-2 BANGkits™, a more thorough understanding of the fractionation effect is integral. A study that thoroughly characterized and demonstrated a correction for fractionation effects would be extremely beneficial for this gel in particular and all polymer gel dosimeters exhibiting these effects in general. Improvements should be made to the cylindrical vessels used to hold

the dosimeters to improve the size of the active region (e.g. replacing the acrylic walls with a less permeable material like glass or Barex). For both the BANGkits™ and the LET-Meter gel, further investigations into calibration curve production should be performed so they can be more fully utilized for absolute dose measurement and LET measurement, respectively.

Additional work with the LET gels is required before they can be properly utilized as an LET measurement system. Once calibration issues are dealt with, investigations using pristine proton beams would provide data for higher LET. Future work with heavy ions would allow even higher LETs to be investigated. Additionally, further development of the LET-Baseline gel is highly recommended, as it was the only gel produced in this study observed to reproduce the absolute dose delivered to the SOBP when an electron-based calibration curve was applied.

For the field of gel dosimetry as a whole, work should continue towards the development of a dosimeter formulation that is simple to produce, relatively inexpensive, and provides reproducible results. These three characteristics are integral to the wide-spread adoption of gel dosimeters into a clinical setting.

Chapter 5

Appendix

5.1 Scanner Operation

The purpose of this section is to guide new users through the use of the OCTOPUS-IQ optical CT scanner. This section contains step-by-step instructions for scanning, reconstructing images from, and viewing images from a gel cylinder. Additionally, a concise operational checklist for the readout procedure is included. It is recommended that the latter item be used as a guideline for each scan, as missing certain steps can have detrimental effects on the output images, potentially necessitating a time-consuming rescan.

Optical Computed Tomography Scanning Procedures

OCTOPUS-IQ Model

MGS Research, Inc.

Scan Preparation

1. Turn on the motor controllers (master, then slave), laser (turn key to "ON"), and photodetector (check the batteries before each use of the system – flip the power switch to "BATT CHK" and check that the green light activates).
2. Clean the external windows of the tank with a lint-free wipe and 70% isopropyl rubbing alcohol. If any visible dust has collected on the collimating or collecting lenses, use canned air to clean the lens.

From this point forward, the gel cylinder will need to be out in the open. Turn off or cover all sources of lights. A red lamp may be used to light the room.

3. Affix the attachment claw to the square lid of the gel cylinder. An attachment convention should be chosen so pre- and post-irradiation scans may be performed using the same configuration (e.g. the two movable arms of the claw are always on the front and left sides of the lid). Ensure that the claw is securely fastened – there should be little to no room for the cylinder to move (there may be some vertical wiggle-room, but the claw should not move left, right, forward, or backward)
4. Place the gel on the scanning turntable. As before, follow a convention (e.g. white block towards the user) to ensure the pre- and post-irradiation scans are as similar as possible.

5. Clean the internal windows of the tank with the squeegee. Make sure no bubbles will be in the way of the scanning laser.
6. Mount the rotary motor to the top of the sample tank, making sure to tightly secure the clamp at the front of the tank (it should not be possible to move the mechanism without moving the sample tank as well). Connect the motor to the gel canister using the descending bar and tighten the knob. Close the shutters to prevent dust from getting into the tank. Connect the motor's cable to the adapter labeled "3".
7. Close the outer shell of the device to protect the gel from stray light in the scanning room.

Data Acquisition

1. Turn on the laptop (password: OCTOPUS). From the desktop, double-click the icon entitled "OCTIQ13RSCOM3" to open the data acquisition program.
2. Select the appropriate parameters to perform a prescan. Typically, A/D voltage range should be set to 5.0 V, the number of prescan projections set to 1, and the number of motor steps set to 100. For "Direction of First…", "positive" is to the right as viewed by the photodetector – prescan back to "positive" (do **NOT** just change the setting to positive) before performing the full scan. The layout is shown below in Figure 5.1.
3. Click "Prescan" to produce a single projection. Check for gross errors (anything in the way of the laser path, photodetector not on, etc). Perform a prescan with "full slice acquisition" checked to produce projections for an entire slice. Ensure that the gel is rotating properly. The "full slice acquisition" box should remain checked for the full scan.

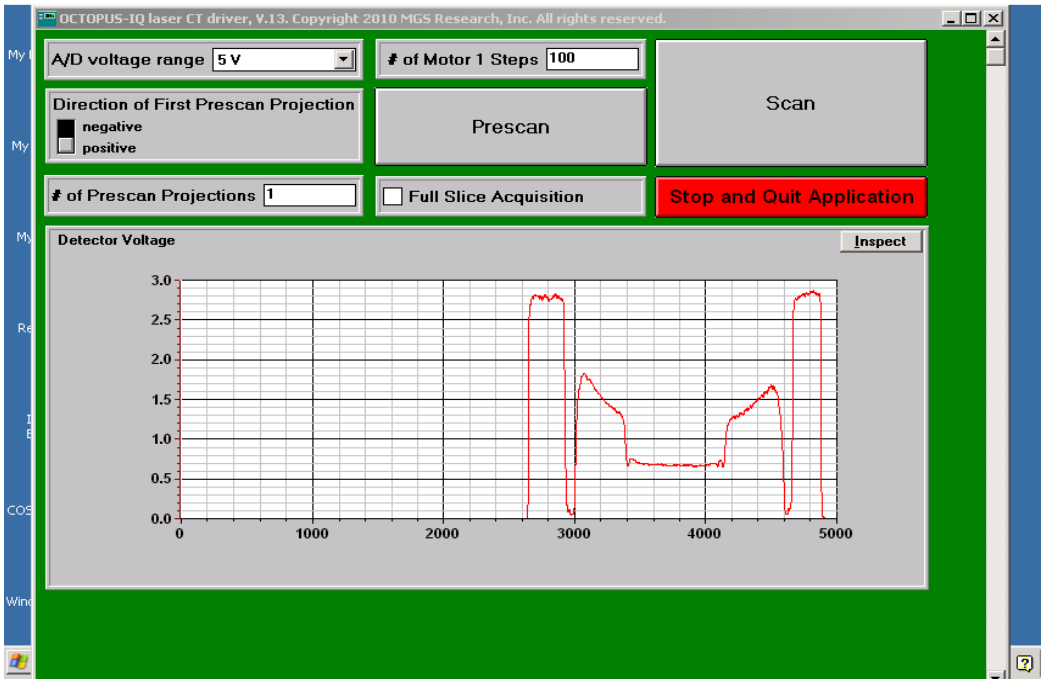

Figure 5.1: Layout of the pre-scanning interface for the OCTOPUS-IQ.

4. Once satisfied with the prescan, click “Scan”. The window shown in Figure 5.2 will appear. Select an appropriate output destination (preferably a flash drive for ease of data transportation) and name for the gel being scanned. The scan direction should be set to “Up” and the number of slices and slice spacing should be chosen based on the user’s needs. Setting a delay of ~20 seconds gives an appropriate amount of time for the user to exit the room before scanning begins.
5. When ready to exit the room, click start scan. Promptly exit the room. The scanner takes ~25 seconds to scan one slice, so plan your return accordingly.
6. When the scan is complete, follow the gel placement directions in reverse to remove the gel from the scanner. Be sure to protect the cylinder from light before turning the lights on.

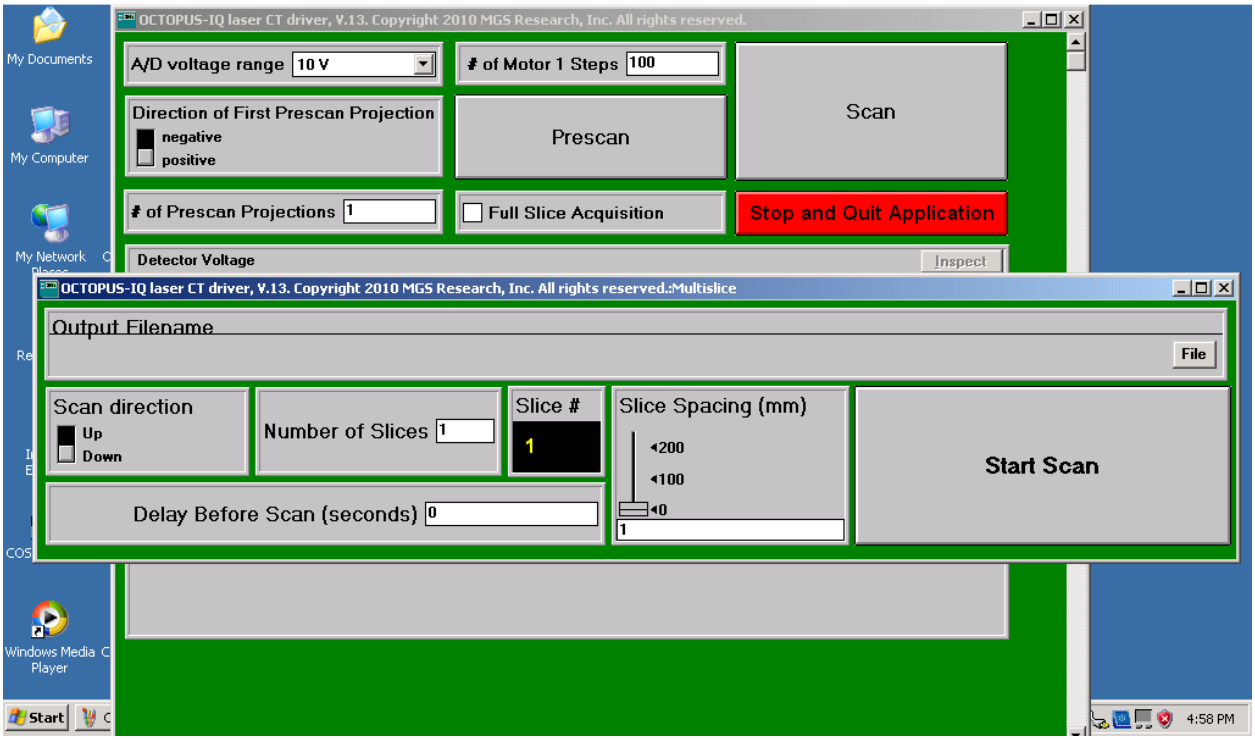

Figure 5.2: Layout of the scanning interface for the OCTOPUS-IQ.

Image Reconstruction

1. Open the image reconstruction program (named reconIQ360v4 as of 5/22/12).

Note: All reconstructions performed in this thesis were done using evaluation versions of the reconstruction software. These trials continue to work past the nominal ends of the trial periods if the date of the computer they are being run on is set to a date contained in the trial period. If necessary, set the computer date back to such a date prior to attempting to open the program.

2. Click the "Select one slice…" button to inspect the raw data and the sinogram from a single slice of the gel volume. Set the system's field of view to 200 mm and click "OK." Select a slice of the gel to be reconstructed. The final result of this operation should be the production of "Figure 4: Re-binned Sinogram."
3. To determine if the gel is properly centered, click the cursor at the top upper left corner of the gel container wall on the upper left corner of the sinogram and record the x-coordinate. Do the same thing for the right edge at projection number 200 (y = 200). Subtract the mean of these two numbers from 100 to obtain the centering shift.
4. Return to the main menu and click the "Build a volume…" button. Select the slice chosen in step two as both the first and last slice in the stack. Choose not to use default settings and fill out the appropriate image reconstruction parameters when prompted (typical parameters are shown in Figure 5.3). Fill in the centering shift calculated in Step 3 and select "No Reference" for the reference file, then click "OK" both at this prompt and the next prompt. Assess the sharpness of the produced image. Repeat this step twice, adding and subtracting 1 from the centering shift and compare the results. Choose the centering shift that produces the sharpest images.

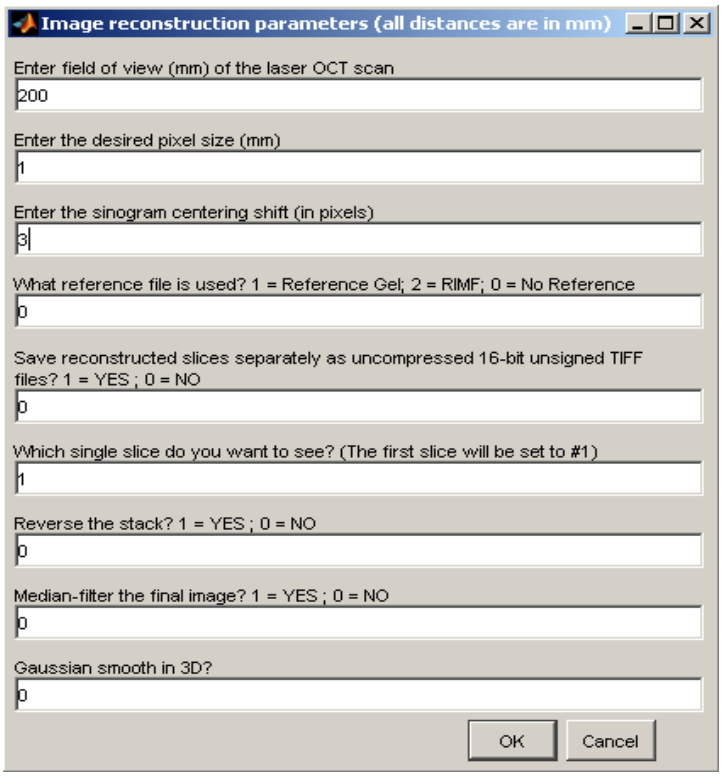

Figure 5.3: Typical image reconstruction parameters for the OCTOPUS-IQ reconstruction program.

5. When satisfied with the centering shift, click the "Build a volume…" button and select the first and last slices of the gel volume. If this is a reference (pre-irradiation) gel, select "No Reference" for the reference file. If the gel has already been irradiated, select "Reference Gel" for the reference file and select the first and last slices of the reference gel volume when prompted. If desired, the median-filtering or Gaussian smoothing may be performed during the reconstruction – this will reduce the noise in the image but may also degrade high-contrast resolution, vital in accurately imaging sharp gradients in dose distribution. Click "OK" several times to begin reconstruction.

6. When reconstruction is complete, a file entitled "filename_float32" will appear either in the folder containing the gel data or, if a reference scan was used, the folder containing the reference gel data. This file may be opened in ImageJ for analysis using the

Import>Raw command under the file menu and selecting the parameter shown in Figure 5.4. “Number of images” should be set to the number of slices scanned; all other parameters should be unchanged.

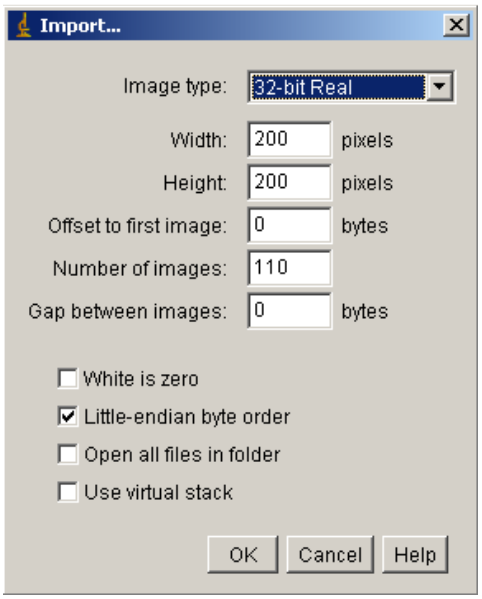

Figure 5.4: Parameters for importing gel volumes into ImageJ.

Operational Checklist

- ☐ Turn motors, laser, and photodetector on
- ☐ Clean lenses (if needed) and outside of sample tank
- ☐ Affix attachment claw to the gel

  → Leave little to no wiggle room

  → Use an attachment convention (e.g. knobs positioned on front and left)
- ☐ Place gel on scanning turntable

  → Use a placement convention (e.g. white block towards viewing window)
- ☐ Clean inside of sample tank with squeegee
- ☐ Affix the rotary motor to the top of the sample tank; tighten knob
- ☐ Connect the gel canister to the rotary motor with the descending bar; tighten knob
- ☐ Plug in the rotary motor
- ☐ Close the outer casing
- ☐ Power up the laptop (Password: OCTOPUS)
- ☐ A/D Voltage = 5V; # of Prescan Projections = 1; # of Motor Steps = 100;
- ☐ Prescan to check for gross errors
- ☐ Select “Full Slice Acquisition;” prescan to ensure gel is rotating
- ☐ Select “Scan”
- ☐ Scan direction – up; Select other settings appropriately
- ☐ Begin scan when ready

  → Close laptop

5.2 Artifacts and Other Issues

Over the course of this study, a number of OCT artifacts and other OCTOPUS-IQ related issues were encountered. This section will briefly describe the issues and suggest possible solutions where appropriate. Additional information on OCT artifacts, including many not encountered during this work, was published by Oldham and Kim in 2004 [45].

Artifact/Issue: Ring Artifact

Appearance: A straight, vertical line running through the sinogram of one or a few subsequent images causing a ring to appear in one or several subsequent slices of the OCT image. Figure 5.5 shows an example of this artifact.

Cause: As the extent of the ring is limited to a few slices, this is likely due to a scratch or debris on the device's collecting lens or on the sample tank.

Solution: If the cause is debris, cleaning the lens or tank should solve the problem. As noted in Section 5.1, the tank should be cleaned on the outside with a lint-free wipe and rubbing alcohol and on the inside with a squeegee before every scan. For the lens, using compressed air should be sufficient for dust and most other small debris. If this fails, the lens can be *carefully* cleaned using deionized water and a little soap. If the blemish is on the grooved side of the lens, the lens will need to be left to dry in a dust-free environment (wrap the lens with coffee filters). On the flat side, the lens may be gently wiped dry with coffee filters. If either the lens or the tank is scratched, the only real solution is replacement. In the interim, it would be wise to avoid placing dose distributions in regions that would be disrupted by the ring.

Artifact/Issue: Tube Artifact

Appearance: A straight, vertical line running through the sinograms of each image in a data set, causing a ring to appear in each slice of the OCT image.

Cause: As the tube extends throughout the gel volume, this is likely due to a scratch or debris on the device's collimating lens.

Solution: Same as for the ring artifact, with the collimating lens rather than the collecting lens. As the tube appears throughout the entire gel volume, promptly solving the problem is integral as it will almost certainly interfere with dosimeter readout.

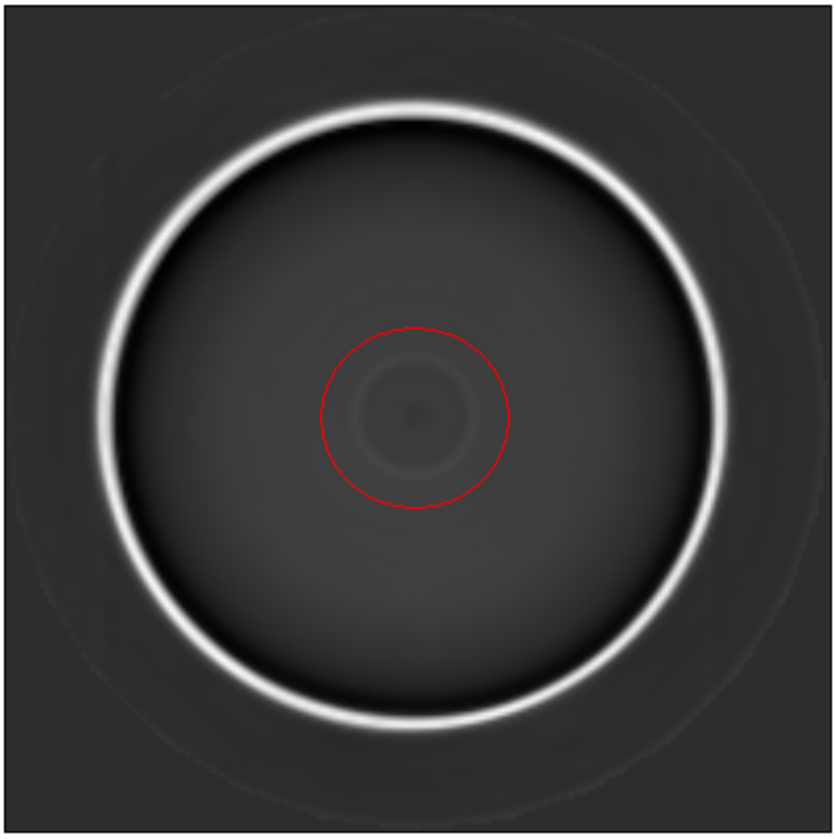

Figure 5.5: An optical CT ring artifact.

Artifact/Issue: Fogging

Appearance: A light haze around the outer radius of the reconstructed gel cylinder that grows lighter over time. Dose data in the center of the cylinder will be blurred. Before and after shots are shown in Figure 5.6.

Cause: Cause unknown. The effect occurred in one set of cylinders provided by the manufacturer.

Solution: No known solution - as the effect occurs inside the cylinder, manual cleaning is required. Cylinders demonstrating this effect, as well as any cylinders that arrived in the same order, should be set aside and not used for any studies requiring OCT scanning. Unused cylinders could be tested by warming up a used dosimeter and pouring it into the unused cylinder – the fogging reaction should be visible within a week or so. As the effect seems to occur only at the acrylic-gel interface, the cylinders may still be appropriate for MRI readout.

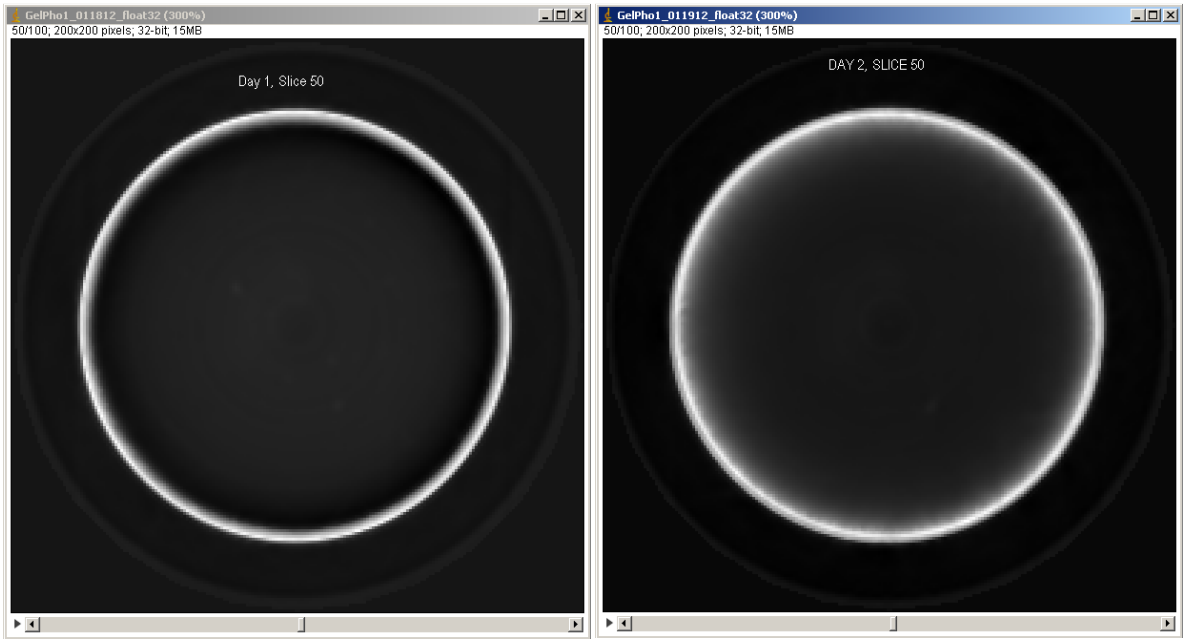

Figure 5.6: Before (left) and after (right) OCT images of a gel cylinder exhibiting fogging.

Artifact/Issue: Over Attenuation

Appearance: A region (or regions) of inaccurate OD. Occurs in the slice plane.

Cause: This artifact is roughly equivalent to beam starvation artifacts in x-ray CT – the extreme attenuation of the laser causes the reconstruction algorithm to believe the dosimeter and the matching fluid along the beam path are more optically dense than they are in reality. Additionally, the regions on the left and right side of the beam (above and below in Figure 5.7) are artificially lowered.

Solution: As the artifact occurs only within the slice plane, shooting from the bottom of the dosimeter and, thus, lowering the integral OD in the slice plane should alleviate the problem. Otherwise, in cases when this may not be an option, lowering the delivered dose will reduce the OD in the dosimeter, minimally reducing the magnitude of the problem. As this is an issue with the reconstruction program itself, a true solution would require edits to the program's code.

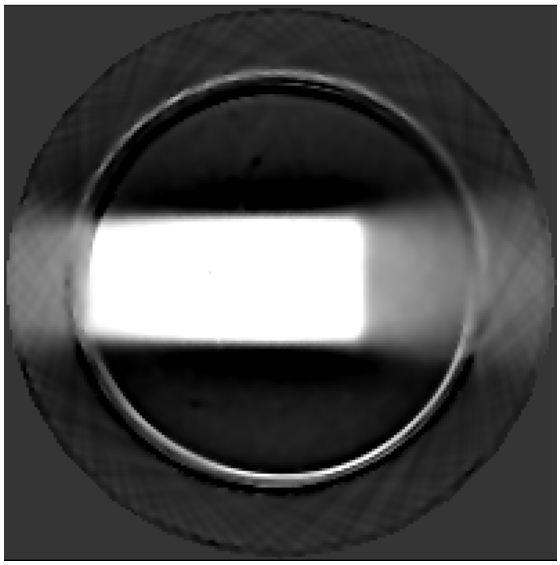

Figure 5.7: The optical density is inaccurately high both proximal and distal to the proton dose distribution along the path of the highest integral optical density. Darkening is observed on both sides of the dose distribution.

Artifact/Issue: Air Bubbles

Appearance: Bright points in the gel reconstruction, sometimes visible by visually inspecting the gel.

Cause: Some bubbles are produced during gel mixture when transferring from the flask to the cylinder – these can be minimized, but some are inevitable. Others can move from the top to the side of the gel cylinder if it is allowed to remain on its side for too long.

Solution: In pouring, bubbles can be minimized by pouring the gel slowly along the inner wall of the cylinder. For bubbles produced when the gel is left on its side, these are due to air trapped between the lid and gel. These can be reduced by ensuring that the cylinder is filled enough that there is no room for air once the lid is sealed but not so high that the cylinder cannot be sealed tightly. Of course, alternately, the gel could be kept upright to avoid the problem completely.

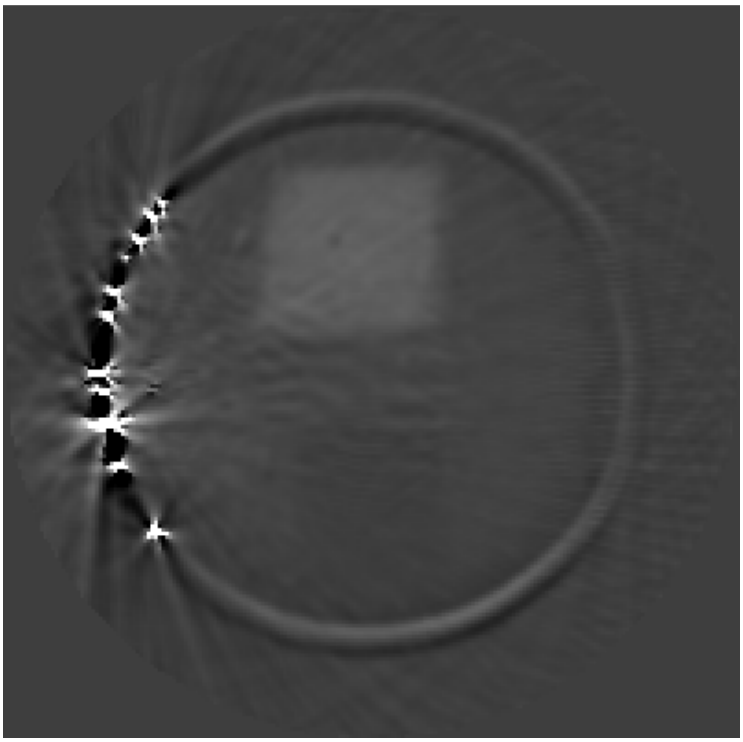

Figure 5.8: The effect of air bubbles on gel readout.

5.3 Calibration Curves

This section contains the calibration curves produced throughout this study.

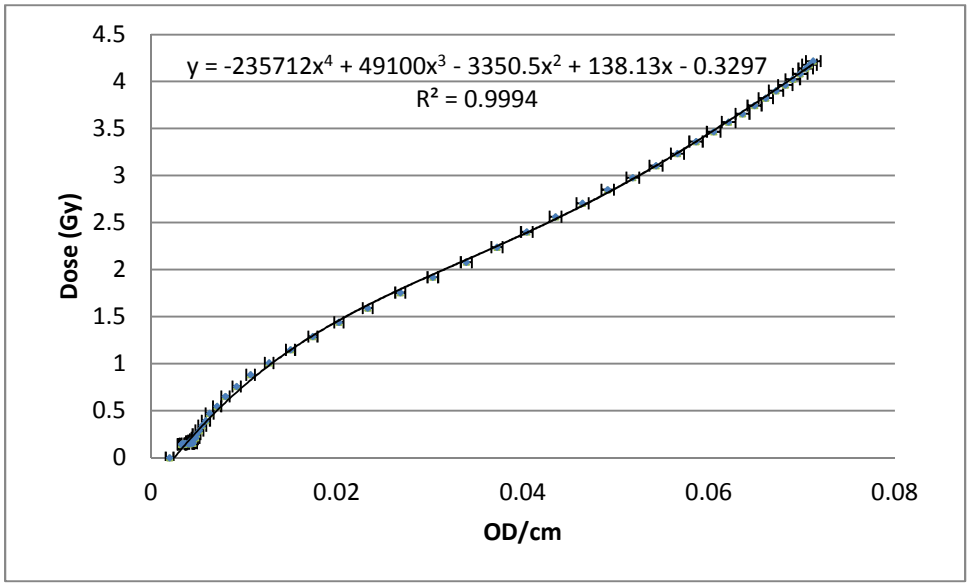

Figure 5.9: Calibration curve for the first proton irradiation through the base of a cylinder.

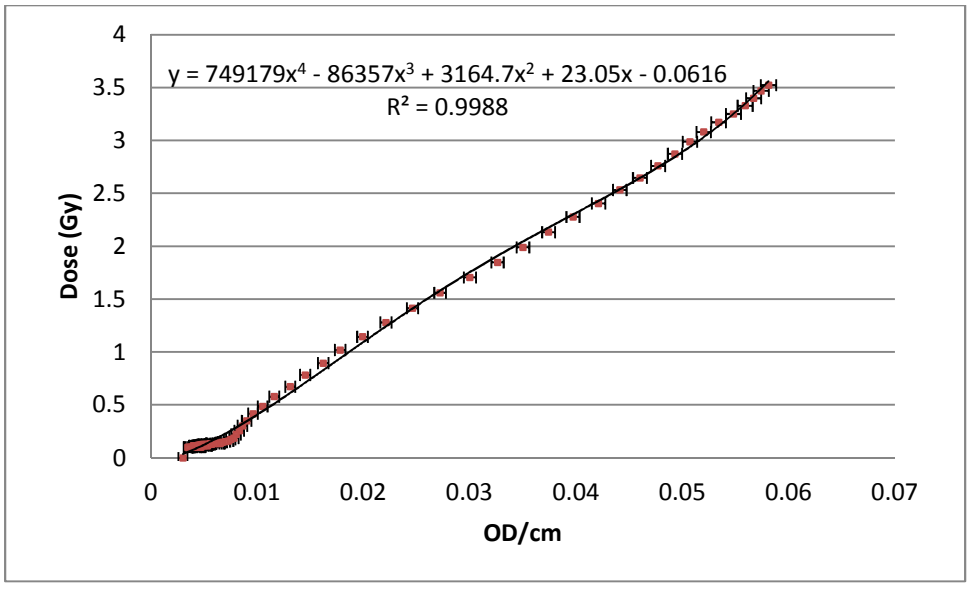

Figure 5.10: Calibration curve for the second proton irradiation through the side of a cylinder.

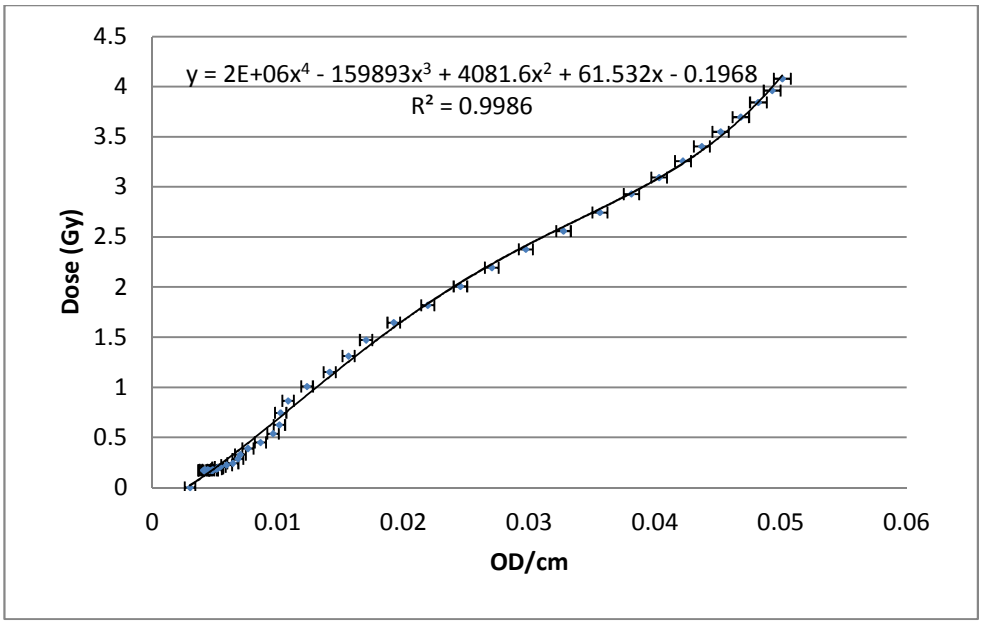

Figure 5.11: Calibration curve for the second proton irradiation through the base of a cylinder.

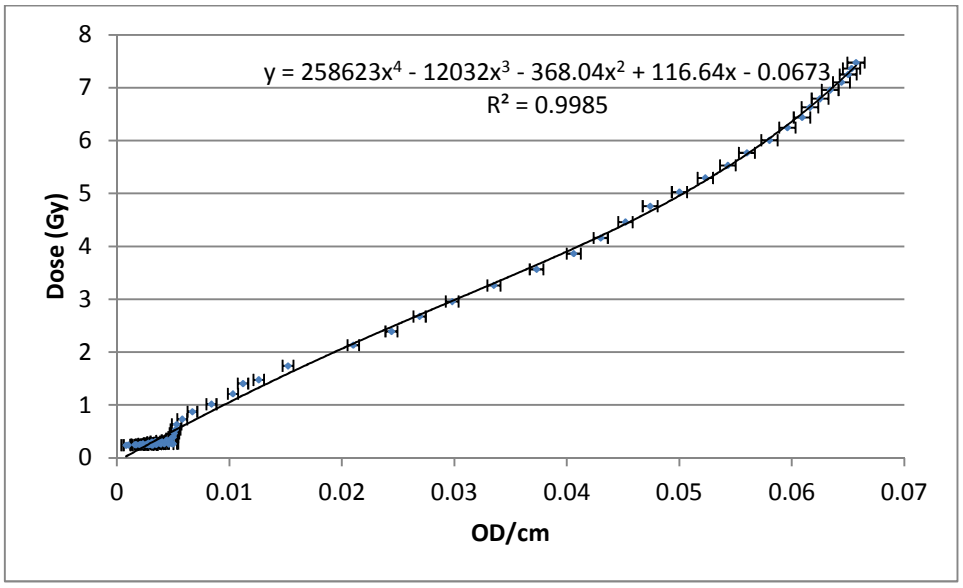

Figure 5.12: Calibration curve for the LET-Meter dosimeter.

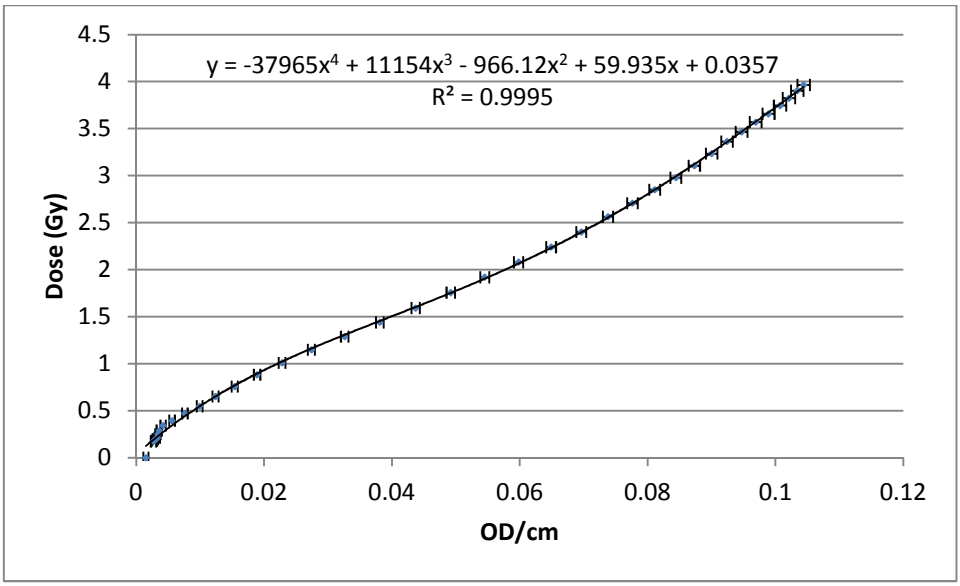

Figure 5.13: Calibration curve for the LET-Baseline dosimeter.

References

1. Peeler, C., D. Mirkovic, D. Grosshans, and R. Mohan, *TH-C-213AB-05: Correlating Areas of Radiation Toxicity with Relative Biological Effectiveness-Weighted Dose Distributions in Proton Radiotherapy* Med. Phys., 2012. **39**(6): p. 1.

2. Wilson, R.R., *Radiological use of fast protons.* Radiology, 1946. **47**(5): p. 487-91.

3. Tobias, C.A., J.H. Lawrence, J.L. Born, C.R. Mc, J.E. Roberts, H.O. Anger, B.V. Low-Beer, and C.B. Huggins, *Pituitary irradiation with high-energy proton beams: a preliminary report.* Cancer Res, 1958. **18**(2): p. 121-34.

4. Kjellberg, R.N., W.H. Sweet, W.M. Preston, and A.M. Koehler, *The Bragg peak of a proton beam in intracranial therapy of tumors.* Trans Am Neurol Assoc, 1962. **87**: p. 216-8.

5. Smith, A. and H. Paganetti. *Proton Therapy*. in *The 49th AAPM Annual Meeting*. 2007. Minneapolis, Minnesota.

6. PTCOG. *Particle therapy facilities in operation (incl. patient statistics).* 2012 June 26, 2012; Available from: http://ptcog.web.psi.ch/ptcentres.html.

7. ICRU, *Stopping Powers and Ranges for Protons and Alpha Particles.* ICRU Report 49, 1993.

8. Hall, E.J. and A.J. Giaccia, *Radiobiology for the radiologist*. 6th ed. 2006, Philadelphia: Lippincott Williams & Wilkins. ix, 546 p.

9. Boag, J.W., *The relative biological efficiency of different ionizing radiations*. Vol. NBS Report 2946. 1953, Washington: National Bureau of Standards.

10. ICRU, *PRESCRIBING, RECORDING, AND REPORTING PROTON-BEAM THERAPY.* Journal of the ICRU, 2007. **7**(2): p. NP.

11. Paganetti, H., A. Niemierko, M. Ancukiewicz, L.E. Gerweck, M. Goitein, J.S. Loeffler, and H.D. Suit, *Relative biological effectiveness (RBE) values for proton beam therapy.* Int J Radiat Oncol Biol Phys, 2002. **53**(2): p. 407-21.

12. Paganetti, H. and M. Goitein, *Radiobiological significance of beamline dependent proton energy distributions in a spread-out Bragg peak.* Med Phys, 2000. **27**(5): p. 1119-26.

13. Smith, A., M. Gillin, M. Bues, X.R. Zhu, K. Suzuki, R. Mohan, S. Woo, A. Lee, R. Komaki, J. Cox, K. Hiramoto, H. Akiyama, T. Ishida, T. Sasaki, and K. Matsuda, *The M. D. Anderson proton therapy system.* Med Phys, 2009. **36**(9): p. 4068-83.

14. Gillin, M.T., N. Sahoo, M. Bues, G. Ciangaru, G. Sawakuchi, F. Poenisch, B. Arjomandy, C. Martin, U. Titt, K. Suzuki, A.R. Smith, and X.R. Zhu, *Commissioning of the discrete spot scanning proton beam delivery system at the University of Texas M.D. Anderson Cancer Center, Proton Therapy Center, Houston.* Med Phys, 2010. **37**(1): p. 154-63.

15. Sahoo, N., X.R. Zhu, B. Arjomandy, G. Ciangaru, M. Lii, R. Amos, R. Wu, and M.T. Gillin, *A procedure for calculation of monitor units for passively scattered proton radiotherapy beams.* Med Phys, 2008. **35**(11): p. 5088-97.

16. Alexander, P., A. Charlesby, and M. Ross, *The Degradation of Solid Polymethylmethacrylate by Ionizing Radiation.* Proceedings of the Royal Society of London. Series A. Mathematical and Physical Sciences, 1954. **223**(1154): p. 392-404.

17. Maryanski, M.J., J.C. Gore, R.P. Kennan, and R.J. Schulz, *NMR relaxation enhancement in gels polymerized and cross-linked by ionizing radiation: a new approach to 3D dosimetry by MRI.* Magn Reson Imaging, 1993. **11**(2): p. 253-8.

18. Gore, J.C., Y.S. Kang, and R.J. Schulz, *Measurement of radiation dose distributions by nuclear magnetic resonance (NMR) imaging.* Phys Med Biol, 1984. **29**(10): p. 1189-97.

19. Baldock, C., Y. De Deene, S. Doran, G. Ibbott, A. Jirasek, M. Lepage, K.B. McAuley, M. Oldham, and L.J. Schreiner, *Polymer gel dosimetry.* Phys Med Biol, 2010. **55**(5): p. R1-63.

20. Maryanski, M.J., R.J. Schulz, G.S. Ibbott, J.C. Gatenby, J. Xie, D. Horton, and J.C. Gore, *Magnetic resonance imaging of radiation dose distributions using a polymer-gel dosimeter.* Phys Med Biol, 1994. **39**(9): p. 1437-55.

21. Maryanski, M.J., G.S. Ibbott, P. Eastman, R.J. Schulz, and J.C. Gore, *Radiation therapy dosimetry using magnetic resonance imaging of polymer gels.* Med Phys, 1996. **23**(5): p. 699-705.

22. Heard, M., *Identification and Characterization of an Optimal Three-Dimensional Dosimetry Stystem for Remote Auditing by the RPC*. 2009, University of Texas Graduate School of Biomedical Sciences at Houston.

23. Fong, P.M., D.C. Keil, M.D. Does, and J.C. Gore, *Polymer gels for magnetic resonance imaging of radiation dose distributions at normal room atmosphere.* Phys Med Biol, 2001. **46**(12): p. 3105-13.

24. Murakami, Y., T. Nakashima, Y. Watanabe, T. Akimitsu, K. Matsuura, M. Kenjo, Y. Kaneyasu, K. Wadasaki, Y. Hirokawa, and K. Ito, *Evaluation of the basic properties of the BANGkit gel dosimeter.* Phys Med Biol, 2007. **52**(8): p. 2301-11.

25. Ibbott, G.S., M.J. Maryanski, P. Eastman, S.D. Holcomb, Y. Zhang, R.G. Avison, M. Sanders, and J.C. Gore, *Three-dimensional visualization and measurement of conformal dose distributions using magnetic resonance imaging of BANG polymer gel dosimeters.* Int J Radiat Oncol Biol Phys, 1997. **38**(5): p. 1097-103.

26. Gustavsson, H., A. Karlsson, S.A. Back, L.E. Olsson, P. Haraldsson, P. Engstrom, and H. Nystrom, *MAGIC-type polymer gel for three-dimensional dosimetry: intensity-modulated radiation therapy verification.* Med Phys, 2003. **30**(6): p. 1264-71.

27. Heufelder, J., S. Stiefel, M. Pfaender, L. Ludemann, G. Grebe, and J. Heese, *Use of BANG® polymer gel for dose measurements in a 68 MeV proton beam.* Medical Physics, 2003. **30**(6): p. 1235-1240.

28. Lopatiuk-Tirpak, O., K. Langen, S. Meeks, P. Kupelian, M. Maryanski, W. Hsi, J. Palta, and O. Zeidan. *SU-GG-T-270: Evaluation of a Novel 3-D Polymer Gel Dosimetry System for Proton Radiotherapy*. 2008: AAPM.

29. Zeidan, O.A., S.I. Sriprisan, O. Lopatiuk-Tirpak, P.A. Kupelian, S.L. Meeks, W.C. Hsi, Z. Li, J.R. Palta, and M.J. Maryanski, *Dosimetric evaluation of a novel polymer gel dosimeter for proton therapy.* Med Phys, 2010. **37**(5): p. 2145-52.

30. Pantelis, E., A.K. Karlis, M. Kozicki, P. Papagiannis, L. Sakelliou, and J.M. Rosiak, *Polymer gel water equivalence and relative energy response with emphasis on low photon energy dosimetry in brachytherapy.* Physics in Medicine and Biology, 2004. **49**(15): p. 3495.

31. Maryanski, M. *Radiation-sensitive polymer gels: properties and manufacturing*. in *Proc. DOSGEL'99, 1st Int. Workshop on Radiation Therapy Gel Dosimetry (Lexington, KY)*. 1999.

32. Jirasek, A., *Alternative imaging modalities for polymer gel dosimetry.* Journal of Physics: Conference Series, 2010. **250**(1): p. 012070.

33. Gore, J.C., M. Ranade, M.J. Maryanski, and R.J. Schulz, *Radiation dose distributions in three dimensions from tomographic optical density scanning of polymer gels: I. Development of an optical scanner.* Phys Med Biol, 1996. **41**(12): p. 2695-704.

34. Maryanski, M.J., Y.Z. Zastavker, and J.C. Gore, *Radiation dose distributions in three dimensions from tomographic optical density scanning of polymer gels: II. Optical properties of the BANG polymer gel.* Phys Med Biol, 1996. **41**(12): p. 2705-17.

35. Lopatiuk-Tirpak, O., Z. Su, Z. Li, O.A. Zeidan, S.L. Meeks, and M.J. Maryanski, *Direct Response to Proton Beam Linear Energy Transfer (LET) in a Novel Polymer Gel Dosimeter Formulation.* Technol Cancer Res Treat, 2012.

36. Karlsson, A., H. Gustavsson, S. Mansson, K.B. McAuley, and S.A. Back, *Dose integration characteristics in normoxic polymer gel dosimetry investigated using sequential beam irradiation.* Phys Med Biol, 2007. **52**(15): p. 4697-706.

37. Lopatiuk-Tirpak, O., K.M. Langen, S.L. Meeks, P.A. Kupelian, O.A. Zeidan, and M.J. Maryanski, *Performance evaluation of an improved optical computed tomography polymer gel dosimeter system for 3D dose verification of static and dynamic phantom deliveries.* Med Phys, 2008. **35**(9): p. 3847-59.

38. Warren, W., *Evaluation of BANG(R) Polymer Gel Dosimeters in Proton Beams*. 2007, Univerisity of Texas Graduate School of Biomedical Sciences at Houston: Houston.

39. Wilkens, J.J. and U. Oelfke, *Analytical linear energy transfer calculations for proton therapy.* Med Phys, 2003. **30**(5): p. 806-15.

40. Maryanski, M., *Personal Conversation*. 2011.

41. Oldham, M., M. McJury, I.B. Baustert, S. Webb, and M.O. Leach, *Improving calibration accuracy in gel dosimetry.* Phys Med Biol, 1998. **43**(10): p. 2709-20.

42. Roed, Y., *Personal Email*. 2012.

43. Massillon, J.G., R. Minniti, C.G. Soares, M.J. Maryanski, and S. Robertson, *Characteristics of a new polymer gel for high-dose gradient dosimetry using a micro optical CT scanner.* Appl Radiat Isot, 2010. **68**(1): p. 144-54.

44. Gustavsson, H., S.A. Back, J. Medin, E. Grusell, and L.E. Olsson, *Linear energy transfer dependence of a normoxic polymer gel dosimeter investigated using proton beam absorbed dose measurements.* Phys Med Biol, 2004. **49**(17): p. 3847-55.

45. Oldham, M. and L. Kim, *Optical-CT gel-dosimetry. II: Optical artifacts and geometrical distortion.* Med Phys, 2004. **31**(5): p. 1093-104.

Vita

Kevin Michael Vredevoogd was born in Warren, Michigan on September 16, 1988, the son of Michael and Kathleen Vredevoogd. After completing his high school education at Anchor Bay High School in Fair Haven, Michigan in 2006, he entered Michigan State University in East Lansing, Michigan. In May 2010, he graduated from Michigan State University with high honors and received the degree of Bachelor of Science with a major in Physics. In August of 2010, he entered the University of Texas Health Science Center at Houston Graduate School of Biomedical Sciences.